AD-A051 169 UTAH STATE UNIV LOGAN ELECTRO-DYNAMICS LAB F/G 4/1
BLACK BRANT 18.219-1 INSTRUMENTATION FOR ICECAP 74A,(U)
JUN 75 D A BURT F19628-73-C-0048
UNCLASSIFIED SCIENTIFIC-3 AFGL-TR-76-0058 NL

1 OF 2
AD
A051169



AD A051169

AFGL-TR-76-0058
HAES Report No. 66

BLACK BRANT 18.219-1 INSTRUMENTATION FOR ICECAP 74A

David A. Burt

Space Science Laboratory
Utah State University
Logan, Utah 84322

AD No. ____
DDC FILE COPY

Scientific Report No. 3

June 1975

DDC
RECEIVED
MAR 14 1978
B

Approved for public release; distribution unlimited.

This research was sponsored by the Defense Nuclear Agency under Subtask K11BAXHX534, Work Unit 07, entitled "Infrared Instrument Development and Certification."

AIR FORCE GEOPHYSICS LABORATORY
AIR FORCE SYSTEMS COMMAND
UNITED STATES AIR FORCE
HANSCOM AFB, MASSACHUSETTS 01731

Qualified requestors may obtain additional copies from the Defense Documentation Center. All others should apply to the National Technical Information Service.

Unclassified

SECURITY CLASSIFICATION OF THIS PAGE (When Data Entered)

14 Scientific-3

REPORT DOCUMENTATION PAGE

READ INSTRUCTIONS BEFORE COMPLETING FORM

1. REPORT NUMBER: AFGL-TR-76-0058
2. GOVT ACCESSION NO.
3. RECIPIENT'S CATALOG NUMBER

4. TITLE (and Subtitle): 6 BLACK BRANT 18.219-1 INSTRUMENTATION FOR ICECAP 74A
5. TYPE OF REPORT & PERIOD COVERED: Scientific Report No. 3
6. PERFORMING ORG. REPORT NUMBER: HAES Report No. 66

7. AUTHOR(s): 10 David A. Burt
8. CONTRACT OR GRANT NUMBER(s): 15 F19628-73-C-0048

9. PERFORMING ORGANIZATION NAME AND ADDRESS: use per contract + chart in doc
Electro-Dynamics Laboratories
Utah State University
Logan, Utah 84322
10. PROGRAM ELEMENT, PROJECT, TASK AREA & WORK UNIT NUMBERS: 62710H 78701006

11. CONTROLLING OFFICE NAME AND ADDRESS
Air Force Geophysics Laboratory
Hanscom AFB, Massachusetts 01731
Monitor/A.T. Stair, Jr./OPR
12. REPORT DATE: 11 June 1975
13. NUMBER OF PAGES: 12 156

14. MONITORING AGENCY NAME & ADDRESS (if different from Controlling Office): 18 AFGL, DNA
19 TR-76-0058 HAES-66
15. SECURITY CLASS. (of this report): Unclassified
15a. DECLASSIFICATION/DOWNGRADING SCHEDULE

16. DISTRIBUTION STATEMENT (of this Report)
16 7670, K11BAXH
Approved for public release; distribution unlimited.
17 10, X534

DDC RECEIVED MAR 14 1978 B

17. DISTRIBUTION STATEMENT (of the abstract entered in Block 20, if different from Report)

18. SUPPLEMENTARY NOTES
This research was sponsored by the Defense Nuclear Agency under Subtask K11BAXHX534, Work Unit 07, entitled "Infrared Instrument Development and Certification."

19. KEY WORDS (Continue on reverse side if necessary and identify by block number)
Rocketborne instrumentation
ICECAP 74A
Atmospheric measurements
Auroral measurements
Atmospheric infrared emissions measurements

20. ABSTRACT (Continue on reverse side if necessary and identify by block number)
On February 25, 1974 at 0738 GMT, Black Brant 18.219-1 was launched from Poker Flat Research Range, Alaska to measure auroral parameters. This was the second time this payload had been flown. It was first flown from Poker Flat in March 1973 as Black Brant 18.205-1. It was subsequently recovered and refurbished for use in the ICECAP 74 auroral measurements program. → next page

DD FORM 1 JAN 73 1473 EDITION OF 1 NOV 65 IS OBSOLETE

Unclassified

SECURITY CLASSIFICATION OF THIS PAGE (When Data Entered)

123 870 JOB

cont.

Successful simultaneous measurements were made of near infrared emissions (1.6 - 5.4 micrometers), selected visible and ultraviolet emissions, auroral electron fluxes, ion and neutral composition, and ionospheric electron and ion densities and temperatures. Special emphasis was placed on making measurements of infrared emissions in order to increase the knowledge of auroral chemistry and physics.

The Black Brant 18.219-1 payload was successfully recovered and will be refurbished and flown as part of the ICECAP 75 auroral measurements program.

LISTS OF CONTRIBUTORS -- SCIENTISTS AND ENGINEERS

D.J. Baker -- Principal Investigator

K.D. Baker
D.A. Burt
D.G. Frodsham
L.C. Howlett
L.L. Jensen
C.R. Jones
J.C. Kemp
G.K. LeBaron
E.F. Pound
C.L. Wyatt

ACCESSION for		
NTIS	White Section	☑
DDC	Buff Section	☐
UNANNOUNCED		☐
JUSTIFICATION		
BY		
DISTRIBUTION/AVAILABILITY CODES		
Dist.	AVAIL. and/or SPECIAL	
A		

RELATED CONTRACTS AND PUBLICATIONS

F19628-70-C-0302
F19628-69-C-0007
AF19(628)-4995
F19628-72-C-0255

Burt, D. A. and C. L. Davis, Rocket instrumentation for ICECAP 73A auroral measurements program - Black Brant 18.205-1, *USU Scientific Report No. 3, HAES Report No. 3, AFCRL-TR-74-0195,* 147 pp., Contract F19628-72-C-0255, Space Science Laboratory, Utah State University, Logan, 1974.

Burt, D. A., J. C. Kemp, L. C. Howlett, E. F. Pound, G. K. LeBaron, and G. D. Allred, ICECAP 72, A rocket measurements program for the investigation of auroral infrared emissions - Black Brant 17.110-3, *USU Scientific Report No. 5, HAES Report No. 7, AFCRL-TR-75-0001,* 160 pp., Contract F19628-72-C-0255, Space Science Laboratory, Utah State University, Logan, September 1974.

Burt, D. A. and G. D. Allred, Rocket instrumentation for auroral measurements - Aerobee 3.756 and 3.759, *UARL Final Report, AFCRL 70-0658,* 193 pp., Contract F19628-69-C-0007, Upper Air Research Laboratory, University of Utah, Salt Lake City, November, 1970.

Preceding Page BLANK - NOT FILMED

PREFACE

At Utah State University a number of individuals had specific reponsibilities for various phases of this project:

Principal Investigator	D.J. Baker
Project Scientist	K.D. Baker
Project Engineer	D.A. Burt
Electron Spectrometer	D.A. Burt P. Neal
Particle Counter and Energy Deposition Scintillator	L.C. Howlett
Plasma Frequency Probe	E.F. Pound
Langmuir Probe	D.A. Burt
Infrared Spectrometer and Radiometers	D.J. Baker C.L. Wyatt D.G. Frodsham J.C. Kemp C.R. Jones
Photometers	L.L. Jensen G.K. LeBaron
Payload Integration	D.A. Burt F.J. Riebeek
Field Operations	K.D. Baker D.J. Baker D.A. Burt F.J. Riebeek
Documentation	R.J. Bell C. Lewis

Preceding Page BLANK - NOT FILMED

TABLE OF CONTENTS

	Page
List of Contributors	iii
Related Contracts and Publications	iii
Preface	v
Table of Contents	vii
List of Illustrations	ix
List of Tables	xv
INTRODUCTION	1
PAYLOAD EXPERIMENTS	3
PAYLOAD MECHANICAL CONFIGURATION	7
Ionizing Sources	15
Electrostatic Analyzer	15
Particle Counter	17
Electron Spectrometer	20
Energy Deposition Scintillator	21
Retarding Potential Analyzer	23
Degree of Ionization	27
Mass Spectrometer	27
Plasma Frequency Probe	28
Langmuir Probe	31
Electromagnetic Emissions	35
Radiometers	35
Infrared Spectrometer	39
Photometers	41
GROUND SUPPORT SYSTEMS	43
FLIGHT RESULTS	47
REFERENCES	49
APPENDIX A - INSTRUMENT TECHNICAL DATA	A-1
APPENDIX B - PAYLOAD TELEMETRY AND TRAJECTORY TECHNICAL DATA	B-1
APPENDIX C - DISTRIBUTION LIST	C-1

Preceding Page BLANK - NOT FILMED

LIST OF ILLUSTRATIONS

Figure		Page
1	Labeled photograph of Black Brant 18.219-1 payload	8
2	Labeled photograph of Black Brant 18.219-1 payload	9
3	Black Brant 18.219-1 payload configuration.	10
4	Black Brant 18.219-1 instrument and sensor orientations and centerlines	11
5	Illustration of the in-flight sequence of events of Black Brant 18.219-1	13
6	Electrostatic analyzer block diagram.	16
7	Particle counter block diagram.	18
8	Electron spectrometer block diagram	20
9	Energy deposition scintillator block diagram	22
10	Energy deposition scintillator calibration geometry.	24
11	Retarding potential analyzer block diagram.	24
12	RPA retarding grid waveform.	26
13	Plasma frequency probe block diagram.	29
14	Langmuir probe characteristic voltage-current curve.	32
15	Langmuir probe block diagram	33
16	Langmuir probe electrode geometry.	34
17	Langmuir probe function generator and sweep monitor waveforms.	34
18	SWIR dual-channel radiometer cutaway view	37
19	SWIR dual-channel radiometer block diagram.	38
20	CVF spectrometer block diagram.	40
21	Photometer block diagram.	42

LIST OF ILLUSTRATIONS (cont.)

Figure		Page
A-1	Flasher electronics schematic diagram.	A-3
A-2	ESA logarithmic amplifier calibration.	A-4
A-3	ESA high voltage sweep monitor calibration	A-5
A-4	ESA electron energy vs. sweep time (t > 25 ms).	A-6
A-5	ESA electron energy vs. sweep time (t < 25 ms).	A-7
A-6	ESA post accelerator high voltage monitor calibration . .	A-8
A-7	ESA +28 VDC monitor calibration.	A-9
A-8	ESA $\pm$ 15 VDC monitor calibration	A-9
A-9	ESA photomultiplier high voltage monitor calibration. . .	A-10
A-10	Particle counter window locations	A-14
A-11	Particle counter count rate calibration	A-15
A-12	Particle counter count rate calibration	A-16
A-13	Particle counter count rate calibration	A-17
A-14	Particle counter count rate calibration	A-18
A-15	Particle counter count rate calibration	A-19
A-16	Particle counter count rate calibration	A-20
A-17	Particle counter channeltron board schematic diagram. . .	A-22
A-18	Particle counter geiger tube board schematic diagram. . .	A-22
A-19	Particle counter logarithmic integrator board schematic diagram	A-23
A-20	Particle counter power supply schematic diagram	A-24
A-21	Particle counter 16 segment commutator schematic diagram	A-25
A-22	Electron spectrometer energy calibration.	A-26

LIST OF ILLUSTRATIONS (cont.)

Figure		Page
A-23	Electron spectrometer log rate calibration.	A-27
A-24	Electron spectrometer schematic diagram.	A-28
A-25	Electron spectrometer DC-DC convertor	A-29
A-26	Energy deposition scintillator responsivity	A-30
A-27	Energy deposition scintillator schematic diagram . .	A-31
A-28	Retarding potential analyzer electrometer sensitivity .	A-32
A-29	Plasma frequency probe schematic diagram	A-33
A-30	Plasma frequency probe series mode output format. . .	A-35
A-31	Plasma frequency probe parallel mode output format . .	A-36
A-32	Langmuir probe schematic diagram	A-37
A-33	Langmuir probe amplifier calibration - electron output.	A-38
A-34	SWIR dual-channel radiometer signal conditioning electronics schematic diagram	A-39
A-35	SWIR dual-channel radiometer motor regulator and drive schematic diagram	A-40
A-36	SWIR dual-channel radiometer inverter-regulator schematic diagram.	A-41
A-37	SWIR dual-channel radiometer electrical interface . .	A-42
A-38	Radiometer and spectrometer orientation for field of view measurements	A-43
A-39	SWIR dual-channel radiometer field of view - NR-3B-6B	A-44
A-40	SWIR dual-channel radiometer bandpass filter transmittance - NR-3B-6B	A-45
A-41	SWIR dual-channel radiometer high gain responsivity - channel 1, NR-3B-6B	A-48

LIST OF ILLUSTRATIONS (cont.)

Figure		Page
A-42	SWIR dual-channel radiometer high gain responsivity - channel 2, NR-3B-6B	A-49
A-43	SWIR dual-channel radiometer field of view - NR-3B-7B	A-50
A-44	SWIR dual-channel radiometer bandpass filter transmittance - NR-3B-7B	A-51
A-45	SWIR dual-channel radiometer high gain responsivity - channel 1, NR-3B-7B	A-54
A-46	SWIR dual channel radiometer high gain responsivity - channel 2, NR-3B-7B	A-55
A-47	CVF spectrometer timing and signal conditioning electronics schematic diagram	A-56
A-48	CVF spectrometer inverter, regulators and motor drive schematic diagram	A-57
A-49	CVF spectrometer electrical interface	A-58
A-50	CVF spectrometer ortho-normal field of view	A-59
A-51	CVF spectrometer polar field of view	A-60
A-52	CVF spectrometer absolute spectral scan position	A-62
A-53	CVF spectrometer optical resolution	A-64
A-54	CVF spectrometer 4.3 μm extended source calibration	A-65
A-55	CVF spectrometer absolute inverse spectral radiant responsivity	A-66
A-56	Photometer field of view - PM-1-7	A-68
A-57	Photometer bandpass filter transmittance - PM-1-7	A-68
A-58	Photometer responsivity - PM-1-7	A-69
A-59	Photometer field of view - PM-1-24	A-70
A-60	Photometer bandpass filter transmittance - PM-1-24	A-70
A-61	Photometer responsivity - PM-1-24.	A-71

LIST OF ILLUSTRATIONS (cont.)

Figure		Page
A-62	Photometer field of view - PM-1-25	A-72
A-63	Photometer bandpass filter transmittance - PM-1-25. . .	A-72
A-64	Photometer responsivity - PM-1-25	A-73
A-65	Photometer field of view - PM-1-26	A-74
A-66	Photometer bandpass filter transmittance - PM-1-26. . .	A-74
A-67	Photometer responsivity - PM-1-26	A-75
A-68	Photometer field of view - PM-1-28	A-76
A-69	Photometer bandpass filter transmittance - PM-1-28. . .	A-76
A-70	Photometer responsivity - PM-1-28	A-77
A-71	Photometer field of view - PM-1-30	A-78
A-72	Photometer bandpass filter transmittance - PM-1-30. . .	A-78
A-73	Photometer responsivity - PM-1-30	A-79
B-1	Black Brant 18.219-1 trajectory	B-16

Preceding Page BLANK - NOT FILMED

LIST OF TABLES

TABLE		Page
1	Black Brant 18.219-1 payload instrumentation	4
2	Black Brant 18.219-1 instrument orientations and fields of view	12
3	Timer settings, Black Brant 18.219-1.	14
4	Electrostatic analyzer specifications	16
5	Particle counter specifications (PC 72B-2A.	17
6	PC72B-2A commutator segment assignments.	19
7	Electron spectrometer specifications.	20
8	Energy deposition scintillator specifications (EDS 72A-1A).	22
9	RPA operating parameters.	25
10	Detectable signal levels for cooled radiometers	36
11	Photometer specifications	42
12	Scientific ground support, Black Brant 18.219-1	44
A-1	ESA log amplifier calibration	A-11
A-2	ESA sweep monitor calibration	A-11
A-3	ESA electron energy vs. sweep time	A-11
A-4	ESA post accelerator HV calibration	A-12
A-5	ESA photomultiplier HV calibration	A-12
A-6	ESA +28 VDC monitor calibration	A-13
A-7	ESA $\pm$15 VDC monitor calibration	A-13
A-8	Particle counter commutator segment assignments	A-14
A-9	Particle counter count rate calibration points	A-21

LIST OF TABLES (cont.)

TABLE		Page
A-10	SWIR dual-channel radiometer relative spectral response - Channel 1, NR-3B-6B	A-46
A-11	SWIR dual-channel radiometer relative spectral response - Channel 2, MR-3B-6B	A-47
A-12	SWIR dual-channel radiometer relative spectral response - Channel 1, NR-3B-7B	A-52
A-13	SWIR dual-channel radiometer relative spectral response - Channel 2, NR-3B-7B	A-53
A-14	CVF spectrometer position reference, wavelength and percent scan ϕ	A-61
A-15	Circular variable filter spectral data report	A-63
A-16	Black Brant 18.219-1 photometer specifications	A-67
B-1	Black Brant 18.219-1 telemetry technical data, link 1	B-3
B-2	Black Brant 18.219-1 telemetry technical data, link 2	B-4
B-3	Black Brant 18.219-1 1 x 60 commutator assignments	B-5
B-4	Additional tracking and recovery systems - Black Brant 18.219-1	B-7
B-5	Magnetic aspect sensor calibration data	B-8
B-6	Black Brant 18.219-1 trajectory listing	B-10

INTRODUCTION

On 25 February 1974 at 0738:30.3 GMT (24 February 1974, 10:38 p.m. Alaskan daylight time) Black Brant 18.219-1 was successfully launched from Pad 2 at Poker Flat Research Range, Alaska, into an aurorally excited atmosphere. This rocket was part of the ICECAP 74A research program conducted at Poker Flat by DNA and AFCRL. Black Brant 18.219-1 was complexly instrumented with an array of instruments to measure energetic particles (ionizing sources), ionization levels and composition, and emissions of infrared, visible and ultraviolet.

This successful flight of the Black Brant payload marks its second application to auroral research. It was initially flown during March 1973 (Black Brant 18.205-1), was recovered, refurbished and reflown in this program. Since this payload is the refurbished BB18.205-1 payload, the descriptions in that report [*Burt & Davis*, 1974] still are valid and only the exact instrument calibrations may change. For convenience; however, there will be many things duplicated in this report to make it complete alone. If more detail is required on some items, the reader is referred to the BB18.205-1 report.

Preceding Page BLANK - FILMED

PAYLOAD EXPERIMENTS

The payload of Black Brant 18.219-1 included two classes of instrumentation: the primary instrumentation and the support instrumentation. Those instruments within the primary instrumentation category may be further sub-categorized into the following groups: 1) Instrumentation for the measurement of ionizing sources; 2) instrumentation for measurement of ionization levels and composition; and 3) instrumentation for measurement of ultraviolet, visible and infrared radiations. Table 1 lists the various instruments within each category and sub-category, giving the model/serial number and the measurement or function performed by each instrument.

The several instruments within the primary instrumentation category were designed to monitor with redundancy the total electron ionizing fluxes ranging from hyperthermal electrons to those with energies of 200 keV. Measurements of ionization levels due to the electron and proton fluxes were also made and were comprised of measurements of positive ion density and electron density and temperature. These measurements were supplemented by measurements of positive ion and neutral composition. Electro-magnetic radiations from the excited atmosphere were also monitored with measurements in the ultraviolet, visible and infrared ranges.

The prime look directions for the instruments were selected to yield as much information as possible with regard to atmospheric structure and profiles. Two areas were viewed, i.e., a common volume forward and a common volume 80° from forward. The forward-looking instruments provide information on profiles which are elaborated on by the side-looking instruments which essentially provide scans as the rocket rotates during flight.

TABLE 1

BLACK BRANT 18.219-1 PAYLOAD INSTRUMENTATION

Instrument (Experimenter/Manufacturer)	Model/SN	Measurement/Function
Energetic Particle Measurements		
Electrostatic Analyzer	SER 201A (Visidyne)	Primary Electron Spectra 3-30 keV
Particle Counters	PC 72B-2A (USU)	Primary Electron Flux E> 4.5 keV E> 9.0 keV E>17.0 keV E>28.0 keV E>42.0 keV E>86.0 keV
Electron Spectrometer	ES 73-1A (USU)	Secondary Electron Flux 100-1500 eV
Energy Deposition Scintillator	EDS 72A-1A (USU)	Electrons 4-200 keV Protons 3-2600 keV
Retarding Potential Analyzer	(Tricon)	Positive Ion Density Hyperthermal Electrons 0-100 eV (low energy cutoff)
Ionospheric Measurements		
Mass Spectrometer	(AFCRL/LKD)	Positive Ion and Neutral Composition
Plasma Frequency Probe	PFP 72-2 (USU)	Electron Density
Langmuir Probe	LP 72-2 (USU)	Electron Density, Temperature
Infrared Emissions		
Spectrometer (CVF)	NS-1B-7 (USU)	Emission Spectra 1.6 - 5.7 μm
Dual Channel Radiometer	NR-3B-6B (USU)	5.3 μm (vertical) 4.3 μm (vertical)
Dual Channel Radiometer	NR-3B-7B (USU)	4.3 μm (80° from vertical) 2.8 μm (80° from vertical)

TABLE 1 (cont.)

Instrument	Model/SN (Experimenter/Manufacturer)	Measurement/Function
Visible/Ultraviolet Emissions		
Photometer (wideband)	PM-1-7 (USU)	5200 A (80° from vertical)
Photometer (narrow band)	PM-1-24 (USU)	5200 A (80° from vertical)
Photometer	PM-1-28 (USU)	5577 A (80° from vertical)
Photometer	PM-1-25 (USU)	3466 A (80° from vertical)
Photometer	PM-1-26 (USU)	3914 A (80° from vertical)
Photometer	PM-1-30 (USU)	3914 A (vertical via mirror)
Support Instrumentation		
Despin Mechanism	(AFCRL/LCR)	Despin to 2 rps
Attitude Control System	10390 (Space Vector)	Control and Monitor Payload Attitude
Magnetic Aspect Sensor	RAM5C-SER 4497 (Schonstedt)	Magnetic Pitch Angle
Radar Beacon	Vega Model 312-S	Rocket Trajectory
Flashing Lights	LF 73-1 (USU)	Payload Position with Respect to Aurora
S-Band Telemetry Systems (2 Links)	(AFCRL/CRE)	Data Recovery
Beacon	Vega Model 312-S (AFCRL/CRE)	Payload Tracking
L-Band Transponder	Bendix ATC Model TR-641-A (AFCRL/CRE)	Payload Recovery
X-Band Beacon	Motorola Model SST-181X-E	Payload Recovery

TABLE 1 (cont.)

Instrument	Model/SN (Experimenter/Manufacturer)	Measurement/Function
Range Receiver	(AFCRL/CRE)	Payload Tracking
Parachute and Deployment Mechanism	(AFCRL/LCR)	Soft Land Payload

PAYLOAD MECHANICAL CONFIGURATION

The positions, fields of view, etc. of all the instruments on the Black Brant payload are best shown pictorially and in Tables. These are shown in Figures 1, 2, 3, 4, and in Table 2.

The sequence of events that occurred during the flight is shown in Figure 5 and the actual timer settings are given in Table 3. A despin mechanism was included in the payload which reduced the spin rate to approximately 2 rps. This was done to increase the measurements resolution from the side-looking instruments and to insure payload integrity as other instruments were extended from the payload. An attitude control system oriented the payload with its longitudinal axis normal to the surface of the earth. This was done to insure the proper forward-looking and side scanning measurements profiles. The parachute deployment was controlled by a barometric switch which closed at 20,000 feet.

During flight, the rocket is tracked by means of a radio beacon, radar, and flashing lights on the payload. The flashing lights consist of three Xenon flash tubes mounted in reflector assemblies which direct the light downward. The three lights are positioned at 120° intervals around the circumference of the payload, permitting television cameras on the ground to simultaneously record the position of the payload and the auroral forms. Also included in the payload was a magnetic aspect sensor to provide information on the payload orientation relative to the earth's magnetic field. The magnetometer was positioned in the payload at a 45° angle as shown in Figures 1 and 4.

The body of the text that follows describes the fundamentals of operation particular to each instrument included in the rocket payload.

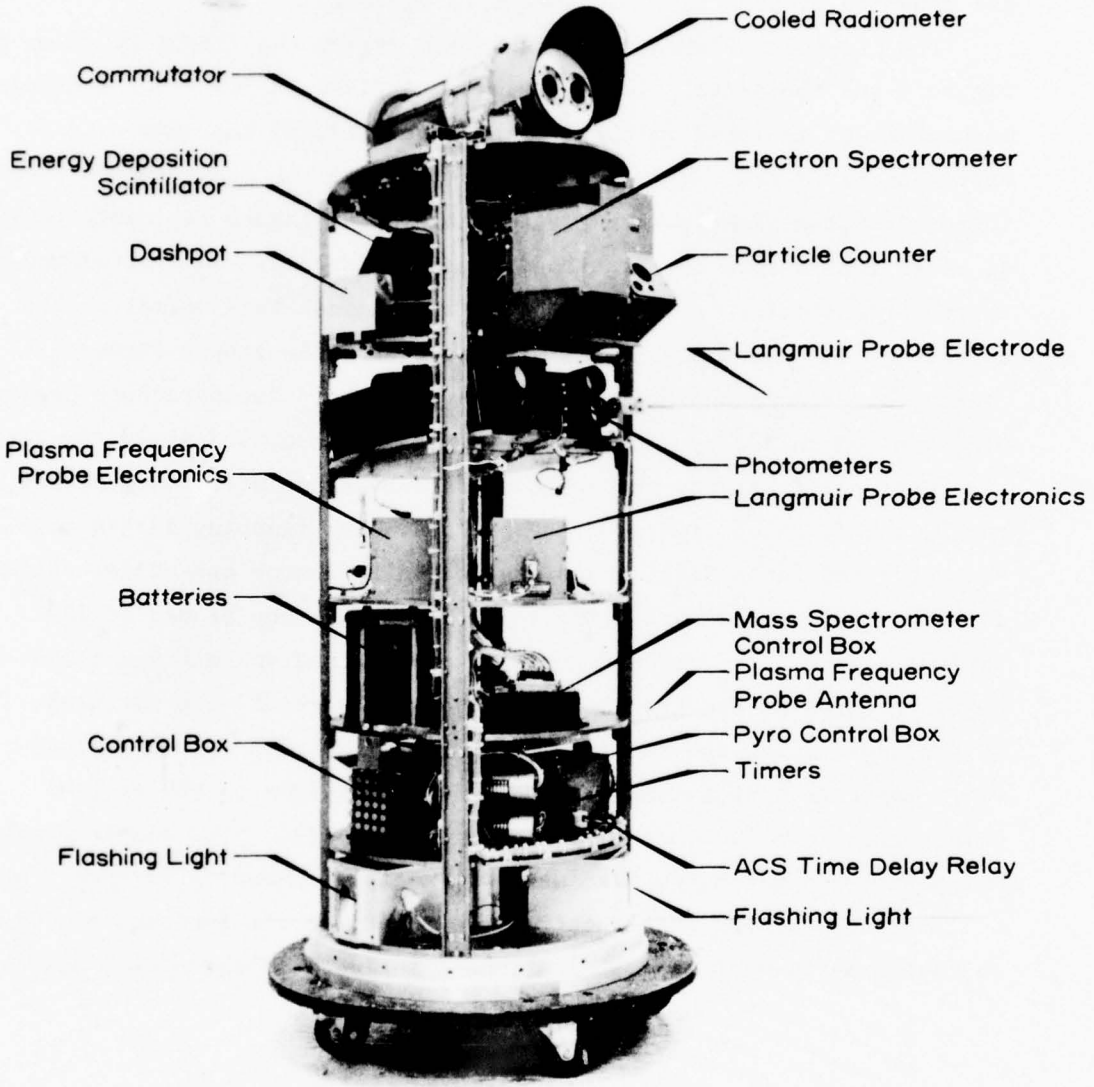


Figure 1. Labeled photograph of Black Brant 18.219-1 payload.

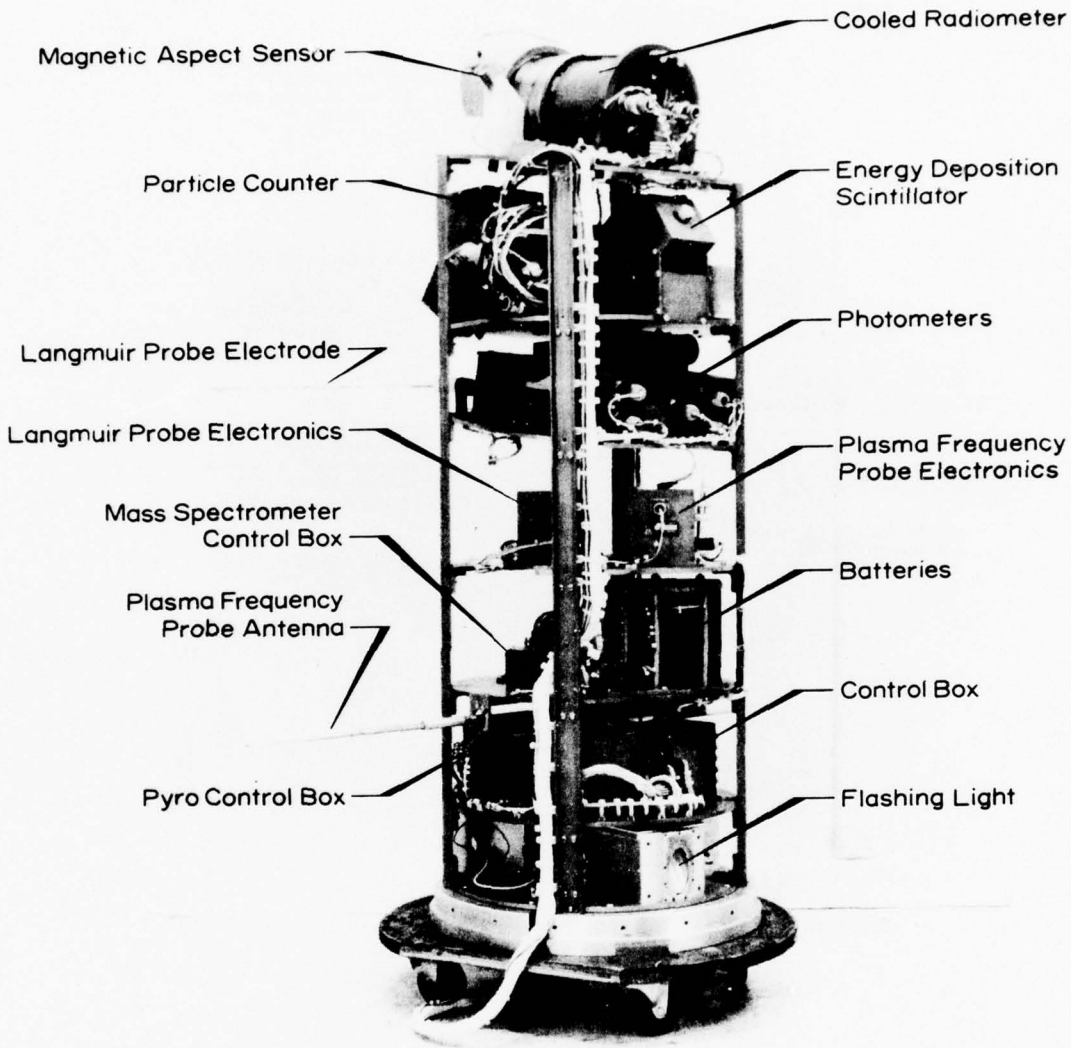


Figure 2. Labeled photograph of Black Brant 18.219-1 payload.

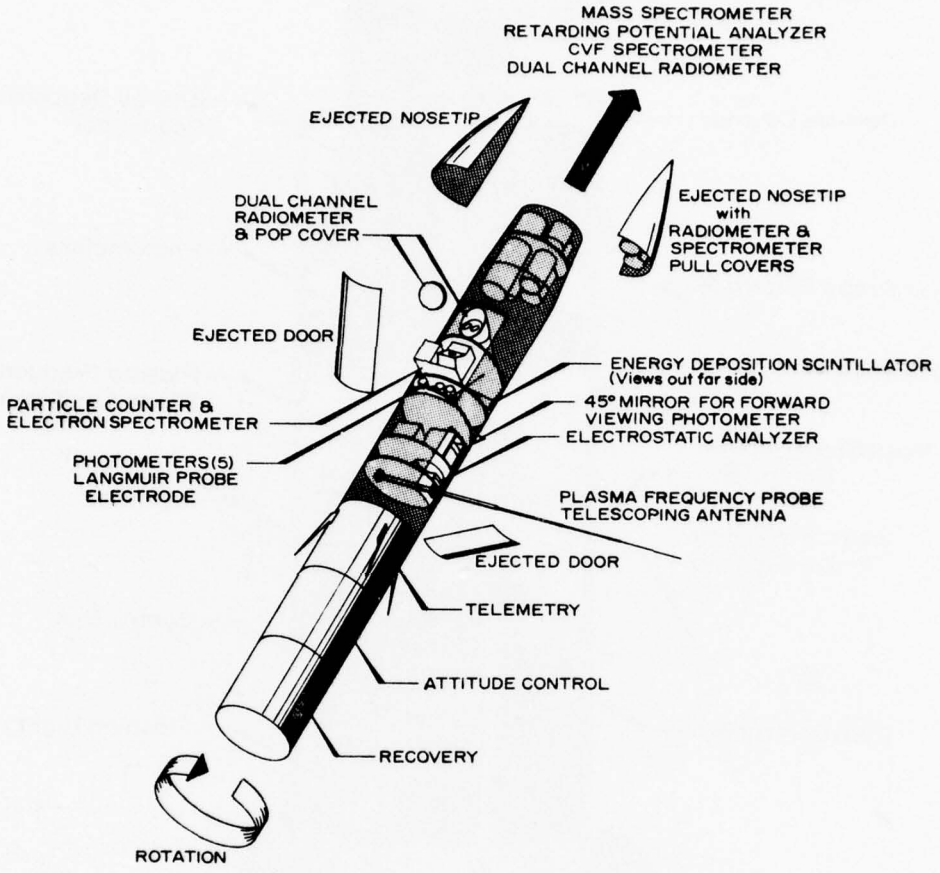


Figure 3. Black Brant 18.219-1 payload configuration.

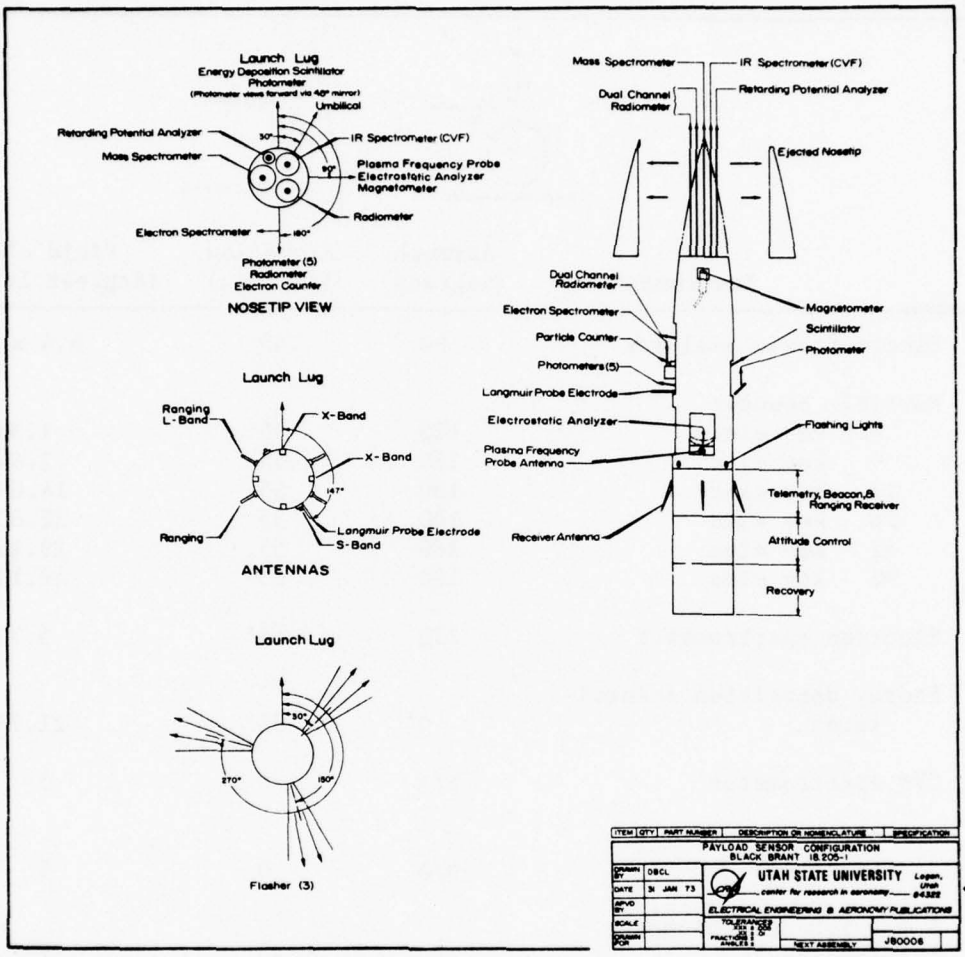
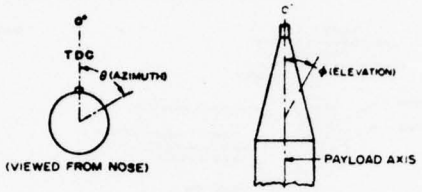


Figure 4. Black Brant 18.219-1 instrument and sensor orientation and centerlines.

TABLE 2

BLACK BRANT 18.219-1 INSTRUMENT ORIENTATIONS

AND FIELDS OF VIEW



Instrument	Azimuth (degrees)	Elevation (degrees)	Field of view (degrees full angle)
Electrostatic analyzer	90	45	6.4 x 16
Particle counter			
4.5 kev elec	180	55	1.36
9 kev elec	180	55	2.44
17 kev elec	180	55	14.88
28 kev elec	180	55	22.80
42 kev elec	180	55	19.16
90 kev elec	180	55	42.10
Electron spectrometer	270	45°	5.72
Energy deposition scintillator	0°	55°	21.73
CVF spectrometer	N/A	0	5
5.3 & 4.3 μm Radiometer (NR-3B-6)	N/A	0	5
5.3 & 2.8 μm Radiometer (NR-3B-7)	180	80	5
Photometers PM-1-7, 24, 25, 26 and 28	180	80	5
Photometer PM-1-30	N/A	0	5
Mass spectrometer	N/A	0	5

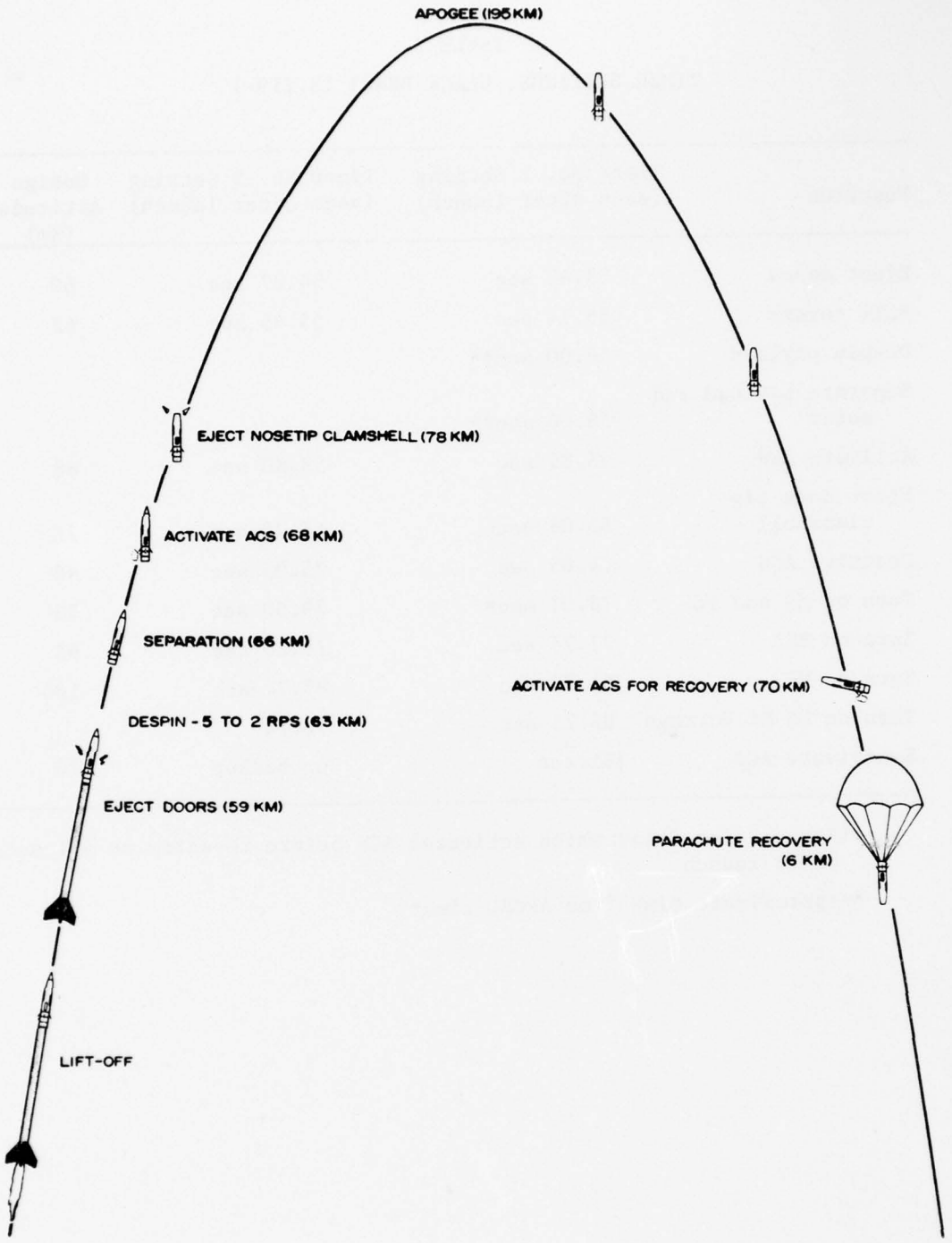


Figure 5. Illustration of the in-flight sequence of events of Black Brant 18.219-1.

TABLE 3

TIMER SETTINGS, BLACK BRANT 18.219-1

Function	Timer No. 1 Setting (secs after launch)	Timer No. 2 Setting (secs after launch)	Design Altitude (km)
Eject doors	53.45 sec	54.87 sec	60
Pull covers	55.14 sec	55.45 sec	62
Despin payload	56.00 sec**		
Separate payload and motor	58.00 sec**		
Activate ACS	58.09 sec	58.80 sec	68
Eject nose tip clamshell	65.08 sec	65.75 sec	78
Deactive ACS	74.05 sec	75.05 sec	90
Turn on ES and PC	78.01 sec*	79.30 sec	95
Turn on ESA	77.75 sec	79.20 sec	95
Turn on MS	84.73 sec	85.74 sec	105
Turn on MS Hi Voltage	89.75 sec	90.74	
Reactivate ACS	381.sec	no backup	70

*Starts time delay which activates ACS before re-entry at 381 secs after launch

**Approximate time from AFCRL timer

EXPERIMENT DESCRIPTIONS

The experiments are divided into 3 different categories:

1. Those that measure input energy or ionizing sources;
2. Those that measure the degree of ionization;
3. Those that measure electromagnetic emissions.

The calibrations of each individual instrument are given in Appendix A.

Ionizing Sources

The electrostatic analyzer, particle counter, electron spectometer, energy deposition scintillator, and retarding potential analyzer measure flux and energy spectra of energetic electrons over several energy ranges. The electron spectrometer measures low energy secondary electrons. The particle counters and the electrostatic analyzer measure primary electron flux and spectra respectively. The energy deposition scintillator measures total electron energy flux for energies greater than its threshold of approximately 3.5 keV and the retarding potential analyzer measures hyperthermal electrons. Through these measurements the total electron energy range from hyperthermal to 200 keV is monitored with redundancy provided in many cases. The energy deposition scintillator also measures proton flux with energy between 30 keV and 26 MeV.

Electrostatic Analyzer

The electrostatic analyzer (ESA) [*Visidyne, Inc.*, 1973], used on Black Brant 18.219-1, measures primary electron spectra. Table 4 gives the ESA specifications.

Figure 6 is a block diagram of the ESA. Energetic electrons entering the instrument pass between two concentric, spherical octant plates. The inner plate is grounded and a 1 kHz square wave with amplitude exponentially decreasing from -4 keV to -50 eV is applied to the outer plate. Energetic electrons entering the space between the plates are accelerated toward the inner plate by the electric field between the plates. Only electrons with a certain kinetic energy pass between

TABLE 4

ELECTROSTATIC ANALYZER SPECIFICATIONS

Parameter	Value
Serial No.	201A
Energy range	3-32 kev
Half power energy resolution	11%
Sweep period	510 ms
Field of view	6.4° x 16°
Geometric factor	9.3×10^{-2} cm^2 sr
Electron pitch angles sampled as rocket spins (with respect to instrument viewing centerline)	13° - 67°

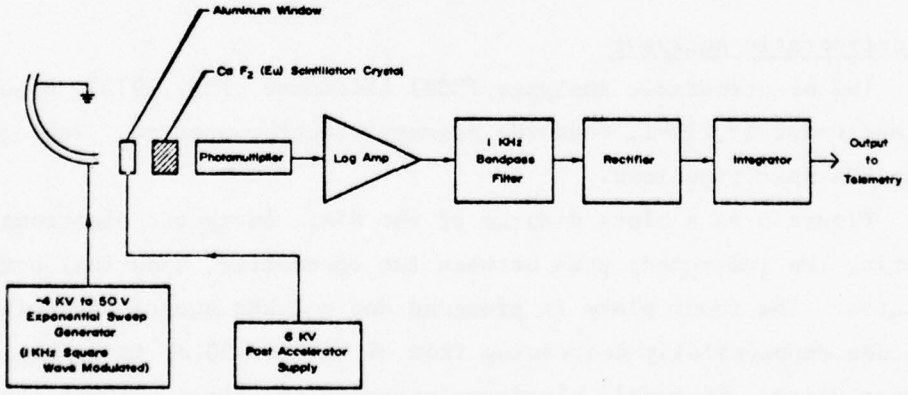


Figure 6. Electrostatic analyzer block diagram.

the plates without colliding with one of them. The electron energy required for passage between the plates is determined by the amplitude of the voltage on the outer plate.

After the electrons pass between the plates, they are post-accelerated toward an aluminum coating (on a C_aF_2(Eu) phosphor) which is 1450 A thick and is at a +6 kV potential. As the phosphor is bombarded, the light emitted by the phosphor is detected by a photomultiplier tube. The output of the photomultiplier is amplified by a logarithmic amplifier, passed through a 1 kHz bandpass filter, rectified, and integrated. The conditioned signal is then sent to the payload telemetry system.

Particle Counter

The particle counter is designed to provide quantity and low resolution energy measurements of energetic electrons within a predetermined field of view. It has six channels with each detector pointing in the same direction, and measures the number of electrons entering each channel. Each channel responds to a different minimum energy level through the use of entrance windows of varying thickness. Specifications for PC 72B-2A are shown in Table 5.

TABLE 5

PARTICLE COUNTER SPECIFICATIONS (PC 72B-2A)

Channel	Half Power Energy Level (Kev) (Protons/Electrons)	Detector Type*	Detector S/N	Geometric Factor (cm^2 sr)	Half Angle Field of View	Window Type	Window Thickness/cm^2
1	4.5	CCM 4010C	9086012	$.335 \times 10^{-5}$	.682°	Poly-propylene (Sigmatron)	76 μgm/cm^2
2	9.0	CCM 4010C	9086018	$.112 \times 10^{-4}$	1.22°	Poly-propylene (Sigmatron)	156 μgm/cm^2
3	17.0	GM 705	28451	$.216 \times 10^{-2}$	7.44°	Mica	.35 mg/cm^2
4	28.0	GM 705	9325	$.509 \times 10^{-2}$	11.4°	Mica	.75 mg/cm^2
5	42.0	GM 711	211100	$.622 \times 10^{-1}$	9.58°	Mica	1.8 mg/cm^2
6	86.0	GM 711	211101	.296	21.05°	Mica plus aluminum	1.8 mg/cm^2 (Mica) 4.8 mg/cm^2 (Al)

*CCM's are Bendix, GM's are LND

Figure 7 is a block diagram of the particle counter. Each channel has an entrance window which is opaque to electrons with energies below a prescribed level. Channeltrons are used as detectors for the two low energy channels and geiger tubes are used as detectors in the four high energy channels. The output pulses from the detectors are fed into logarithmic integrators that provide analog voltages proportional to the log of the count rate in each channel. The analog outputs of the logarithmic integrators are fed into a 16 segment, 20 frames per second electronic commutator. The commutated signal is then sent to the rocket telemetry system. The pin assignments to the commutator are given in Table 6.

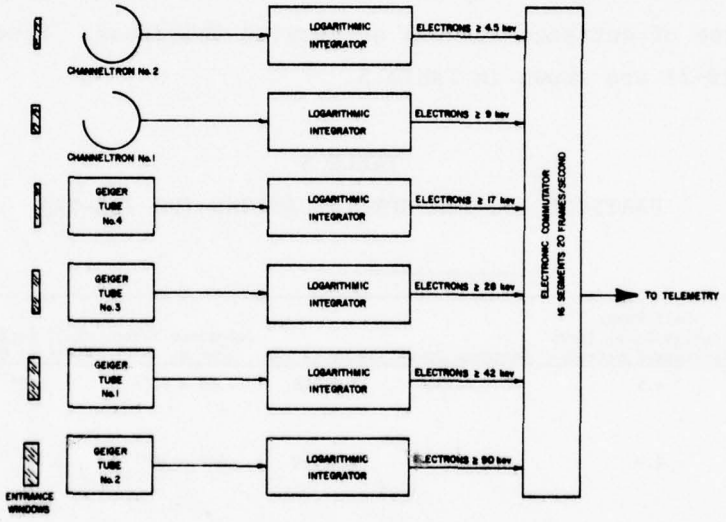


Figure 7. Particle counter block diagram.

TABLE 6

PC 72B-2A COMMUTATOR SEGMENT ASSIGNMENTS

Segment No.	Assignment
1	28 keV electrons
2	90 keV electrons
3	17 keV electrons
4	42 keV electrons
5	9 keV electrons
6	4.5 keV electrons
7	28 keV electrons
8	90 keV electrons
9	17 keV electrons
10	42 keV electrons
11	9 keV electrons
12	0 volts
13	+5 volts
14	+5 volts
15	+5 volts
16	0 volts

Electron Spectrometer

The electron spectrometer measures electron spectra in the energy range from 100 to 1500 eV at count rates of 20 to 13,000 per second, [*Neal, 1974*]. Table 7 is a complete listing of the electron spectrometer specifications. Figure 8 is a block diagram of the electron spectrometer.

TABLE 7

ELECTRON SPECTROMETER SPECIFICATIONS (ES 73-1A)

Parameter	Value
Energy range	100 to 1500 eV
Half-power energy resolution (approximate)	40%
Count rate	20 to 13,000 per second
Aperture radius	0.15 cm
Detector radius	0.15 cm
Separation distance	3.0 cm
Geometric factor (approximate)	1.08×10^{-3} cm^2 ster
Field of view (approximate)	8° (full angle)

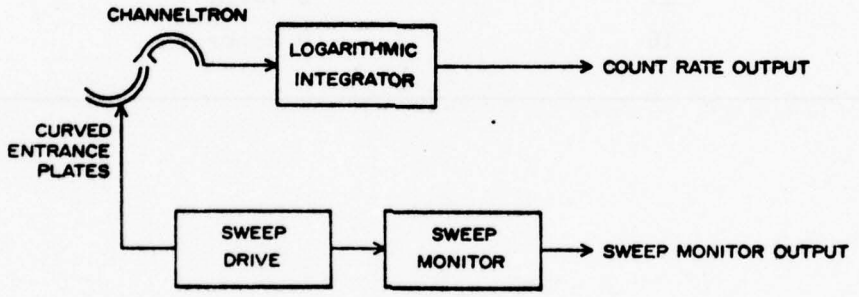


Figure 8. Electron spectrometer block diagram.

As shown on the block diagram, electrons entering the instrument's aperture have their trajectories modified in an electric field created by applying a swept voltage across two curved parallel plates. To obtain the electric field, a positive voltage is applied to one plate and a negative voltage to the other. The potential difference is varied

exponentially between 366 volts and 24 volts with a repetition time of 1 second. The plates are 5 mm apart, giving an electric field which varies between 73.2 kilovolts/meter and 4.8 kilovolts/meter. The electrons travel a distance of 3 cm between the plates. As the field strength is changed, electrons of various energies are detected by a channeltron detector placed at the end of the plates. A sweep monitor is provided which has an output voltage proportional to the electric field strength and, therefore, proportional to the energy of the electrons which are detected. The half power energy resolution is approximately 40% at any given point on the sweep.

Energy Deposition Scintillator

The energy deposition scintillator (EDS) is designed to measure, within defined limits, the total power density of energetic electrons and protons impinging on the atmosphere. As shown in Figure 9, the instrument basically consists of a scintillation phosphor viewed by a photomultiplier. The output of the photomultiplier is amplified by four cascaded saturating amplifiers. The instrument output consists of the summation of the outputs of these amplifiers to provide data compression which can be described over four ranges by linear mathematical functions. This output signal is a measurement of the rate of energy input due to particles having energies above a predetermined threshold which is determined by a thin layer of aluminum covering the exposed surface of the scintillation phosphor. Additionally, the aluminum serves to prevent ambient light from directly entering the phototube. The maximum energy which can be measured by the instrument is contingent upon the type and thickness of the scintillation phosphor. A pilot B plastic scintillation phosphor .035" thick is used in this instrument. Minimum and maximum energy levels and other characteristics of the instrument are listed in Table 8.

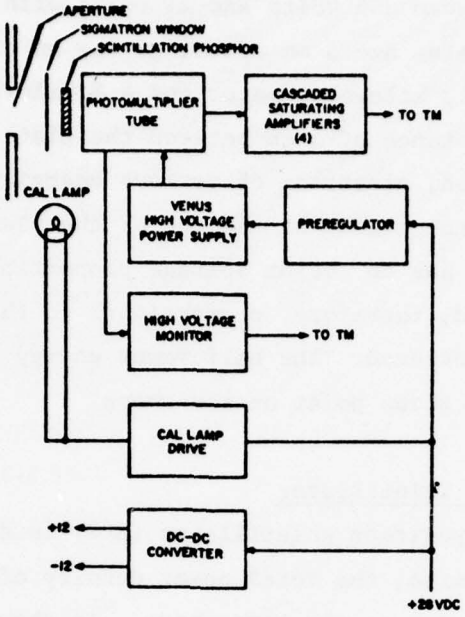


Figure 9. Energy deposition scintillator block diagram.

TABLE 8

ENERGY DEPOSITION SCINTILLATOR SPECIFICATIONS (EDS 72A-1A)

Parameter	Value
Aluminum window thickness	1600 A
Minimum energy	
Electrons	3.8 keV
Protons	33 keV
Maximum energy	
Electrons	200 keV
Protons	26 keV
Aperture radius	.63 cm
Detector radius	.63 cm
Separation distance	3.03 cm
Geometric factor	.1404 cm^2 ster
Proportionality constant	2.18 x 10^7 ergs $(cm^2$ sec sr amp$)^{-1}$

Two monitor circuits have been included in the energy deposition scintillator to check the operation of the instrument. A calibration lamp illuminates the phototube once each minute for approximately 250 ms providing an output pulse of 5.25 volts. A high voltage monitor is provided to check the operation of the high voltage power supply. The EDS 72A-1A was calibrated with a monitor voltage of 3.18 volts. The photomultiplier high voltage is approximately 396 times the monitor voltage.

Calibration of the energy deposition scintillator is accomplished using a Ni-63 source with an output which appears to the instrument as .1153 ergs cm^{-2} sec^{-1} $ster^{-1}$. The calibration geometry is shown in Figure 10. This known input is used as a reference point from which to calibrate the instrument. With the Ni-63 source in place, the current from the photomultiplier tube into the cascaded saturating amplifiers is measured. The value of the current is divided into .1153 ergs cm^{-2} sec^{-1} $ster^{-1}$ to yield a proportionality constant between amplifier input current and instrument input flux density. The data compression amplifier is calibrated by introducing known input currents into the amplifier in place of the signal currents, thereby yielding a current vs. voltage curve for the instrument. The power density vs. voltage curve is then obtained by multiplying the current vs. voltage curve by the proportionality constant.

Retarding Potential Analyzer

The retarding potential analyzer (RPA), flown aboard Black Brant 18.219-1, operates in two, time-sharing modes. In the ion mode, thermal positive ion density is measured. In the electron mode, electron temperature and hyperthermal electron density is measured.

Figure 11 is a block diagram of the RPA. The RPA sensor consists of four planar elements parallel to each other and spaced 0.2 inches apart. The aperture is a one-inch diameter double grid set in an aperture plane two inches in diameter. The double grid is used to minimize electrostatic punch-through to the external plasma when the RPA is operated in the high energy electron mode. The next element is the

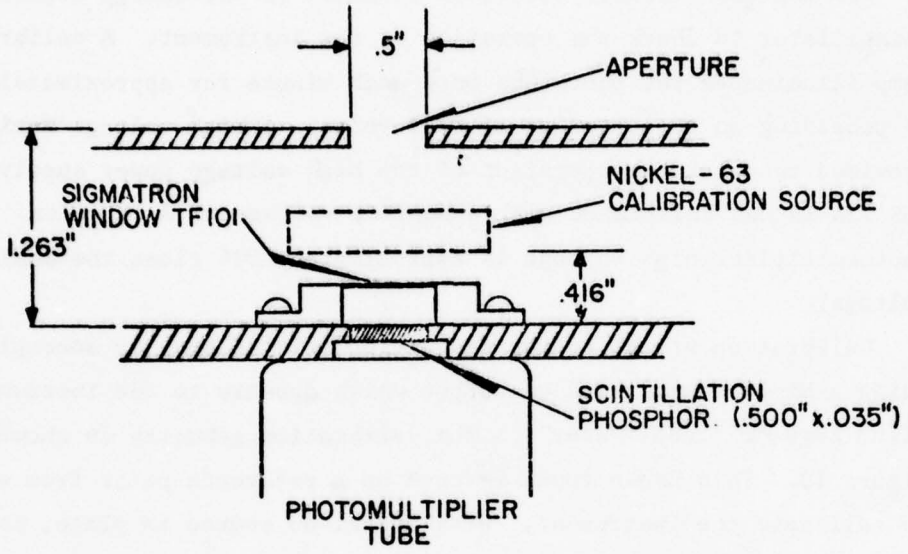


Figure 10. Energy deposition scintillator calibration geometry.

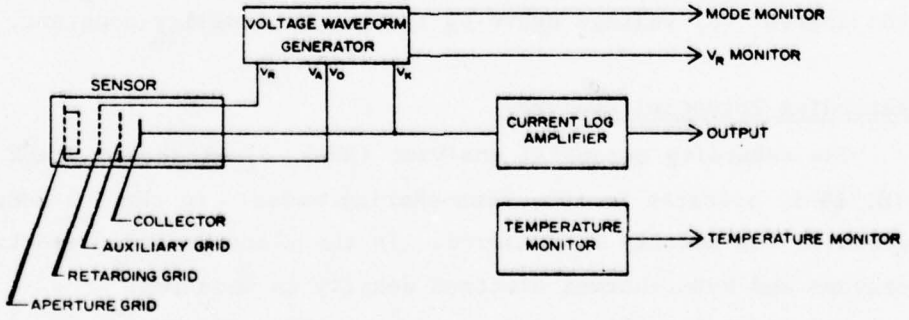


Figure 11. Retarding potential analyzer block diagram.

retarding grid which is 1.5 inches in diameter. The next element is the auxiliary grid used to reduce the capacitance between the regarding grid and collector, thereby minimizing the displacement current problem. All the grids are .001-inch, gold-plated tungsten mesh with approximately 90% optical transmission. The final element is the two-inch diameter gold plated collector.

In both operating modes the aperture and auxiliary grids were electrically connected. Table 9 describes the voltages applied for the ion and electron modes. A mode indicating output is provided to telemetry with a zero output level indicating the electron mode of operation and +4 volts indicating the positive ion mode. Figure 12 illustrates the waveform applied to the retarding grid.

TABLE 9

RPA OPERATING PARAMETERS

Element	Ion Mode	Electron Mode
Aperture and auxiliary grids	+.15 volts	+3.0 volts
Retarding grid	-.75 to +4.5 volts	-78 to +4.1 volts
Collector	-15 volts	+18 volts
Current sensitivity	5×10^{-12} to 10^{-7} amps	5×10^{-12} to 10^{-5} amps

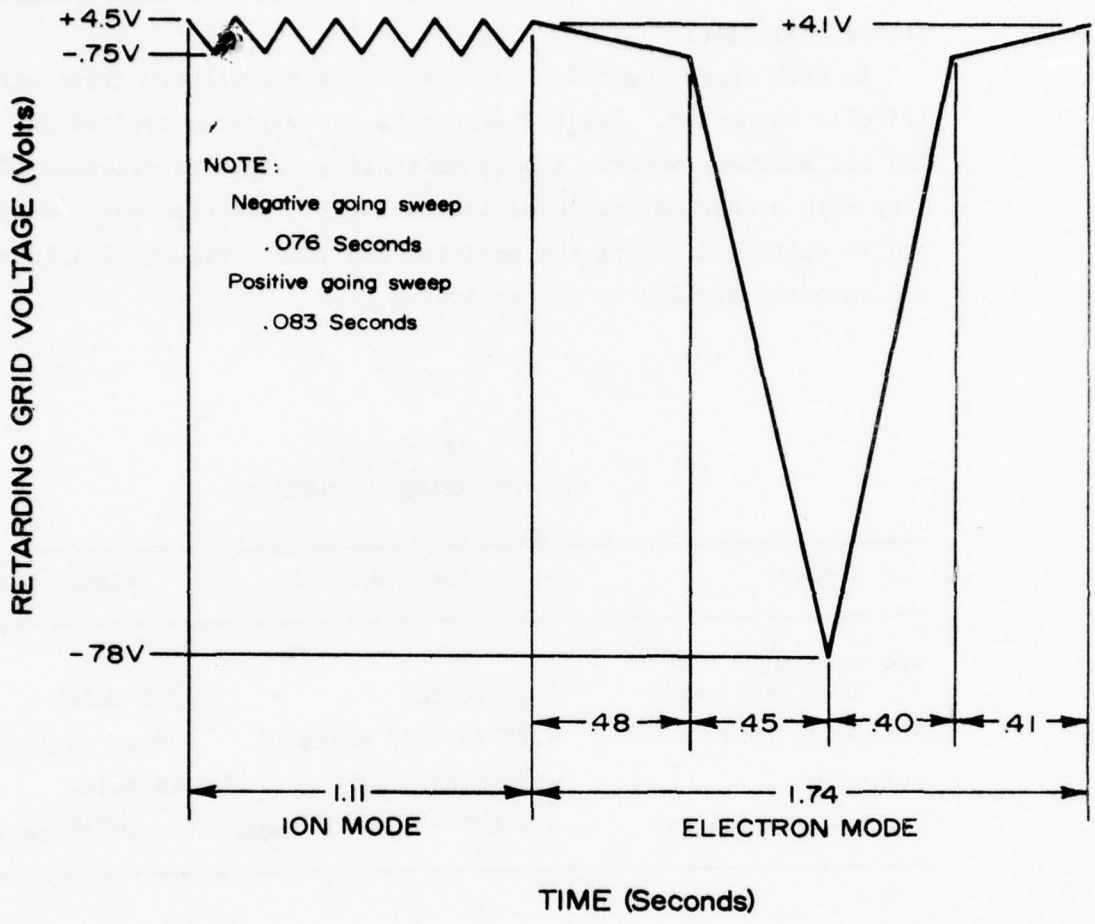


Figure 12. RPA retarding grid waveform.

Degree of Ionization

The ionization level measurements made by Black Brant 18.219-1 were positive ion composition and density, neutral composition, and electron density and temperature. The mass spectrometer and retarding potential analyzer measured positive ion and neutral composition and density, and the plasma frequency probe and Langmuir probe measured electron density and temperature.

These measurements provide data to further the understanding of the various processes and energy balance operative in the upper atmosphere. Through interpretation of the data inputs updated predictive computer codes and atmospheric models are obtained. This section of the report describes the mass spectrometer, plasma frequency probe, and Langmuir probe. The retarding potential analyzer, which measures positive ion composition, was discussed in the previous section.

Mass Spectrometer

The mass spectrometer was built by the Aeronomy Laboratory (LKD) of Air Force Cambridge Research Laboratories. It is a switched quadrupole instrument capable of measuring both positive ions and neutrals. The ambient positive ion mode scans 1 through 5 and 14 through 38 atomic mass units in approximately 1 second, and the neutral mode scans 12 through 48 atomic mass units in 1 second. Neutrals are ionized with nominally 55 volt electrons from a hot filament. Predicted sensitivity ranges were 10^{-9} to 10^{-4} torr from N_2 in the neutral mode, and 20 to 2×10^6 ions per cm^3 for N_2^+ in the ion mode.

The mass spectrometer is the same basic design as that used in the ICECAP 72 program [*Burt, et al.*, 1972; *Narcisi* and *Bailey* 1965] for D- and E-region measurements; however, since measurements were not required in this case below 90 km, the vacuum pump normally utilized was not employed. The mass spectrometer was mounted in the top portion of the payload with its orifice looking forward when the nose tip was ejected as illustrated in Figures 3 and 4. The quadrupole functions by utilizing a superimposed electric field applied to four rods having

RF and dc components which are adjusted so that of the entering beam, only those ions with a preselected mass-to-charge ratio have the bounded oscillatory trajectories necessary to traverse the length of the rods to an electron multiplier where they are counted. The mass spectrum is scanned by varying the amplitudes of the RF and dc voltages exponentially while maintaining a constant voltage ratio between the two components. Further description of the quadrupole instrument has been presented by *Narcisi* [1971].

Plasma Frequency Probe

A plasma frequency probe was flown on the Black Brant 18.219-1 rocket to measure electron density and temperature in the E and lower F regions of the ionosphere. The instrument consists of a 36-inch telescoping antenna which is immersed in the ionospheric plasma, and an electronics box aboard the rocket. The series and parallel resonant frequencies of the antenna are measured [*Pound* and *Baker*, 1971] and electron density and temperature are found as a function of the resonant frequencies.

Basically, the plasma frequency probe operates by applying a sweeping RF signal (12 MHz to 1 MHz) to the antenna and monitoring the antenna current and voltage relationship. During alternate frequency sweeps, the sweep is stopped at the series or parallel resonant points and the frequency is measured by a digital counter.

Figure 13 is a block diagram of the plasma frequency probe. The RF frequency sweep to the antenna is controlled by a ramp function from the sweep generator and is initiated by a reset pulse from the clock. As the ramp increases, the output frequency sweeps from 12 MHz to 1 MHz. As can be seen from the block diagram, an antenna current indication and a phase reference current are each fed to separate mixer circuits.

The two mixers are also fed by a second frequency which is a sweeping RF signal whose frequency is exactly 100 kHz lower than the signal applied to the antenna and reference capacitor. The difference frequency outputs from the mixers are, therefore, always 100 kHz and the relative amplitude and phase angle are coherent with the antenna current and reference signal inputs to the mixers. By use of this superheterodyne technique, the

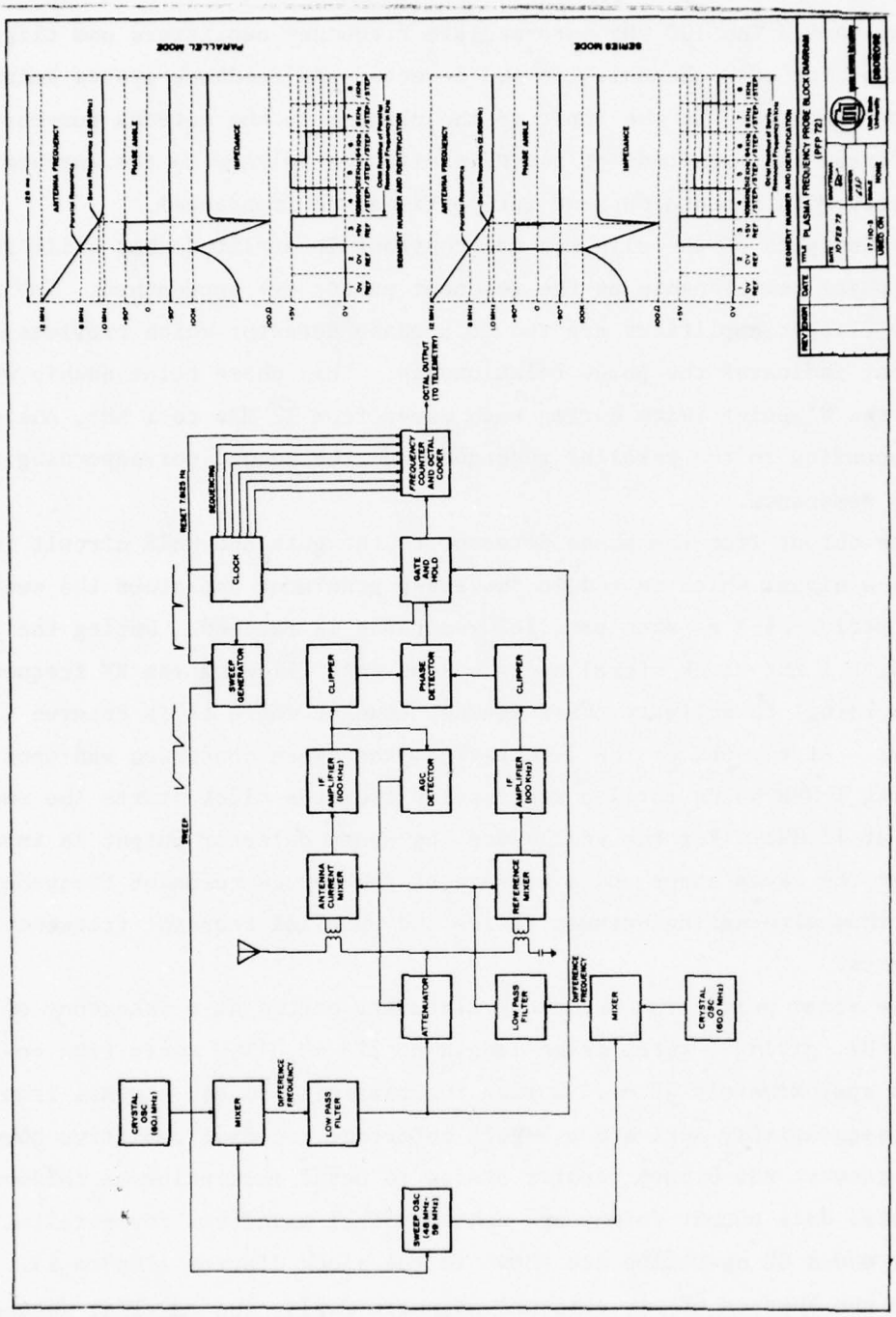


Figure 13. Plasma frequency probe block diagram.

following amplifiers, clippers, and phase detector are not required to be wide-band systems. The 100 kHz intermediate frequency amplifiers and clippers are identical for each channel. An AGC detector and feedback system maintains constant amplitude at the input to the clipper in the antenna current channel. This forces the magnitude of the RF excitation voltage to the antenna to vary inversely with antenna current (proportional to impedance).

The outputs of the clippers are constant in amplitude but shift in their phase relationship as the resonant points are approached. The outputs of the clipper amplifiers are fed to a phase detector which provides an output that indicates the phase relationship. This phase relationship will cross the 0° point twice during each sweep from 12 MHz to 1 MHz, one point corresponding to the parallel resonance and the second corresponding to the series resonance.

The output from the phase detector to the gate and hold circuit initiates a signal which is fed to the sweep generator and stops the sweep for a period of 3 ms when parallel resonance is reached. During the 3-ms period, a 1 kHz clock signal opens a 1-ms gate allowing the RF frequency (now holding) to activate the frequency counter where it is counted (in binary). At the end of the 3-ms period, the sweep continues and upon reaching 1 MHz holds until a reset pulse from the clock starts the sweep again at 12 MHz. For the next sweep the phase detector output is inverted so that the sweep stops and a measure of the series resonant frequency is taken thus alternating between series and parallel resonant frequency measurements.

The reset pulse from the clock circuitry occurs at a frequency of 7.8125 Hz, giving a total frame length of 128 ms. The sweep time requires approximately 48 ms. During the remaining 80 ms, signals from the clock sequentially activate a 5-volt reference and five resistive summers which convert the binary counter states to octal form prior to telemetry. The octal data output format and other typical waveforms for parallel and series modes of operation are shown in the block diagram (Figure 13).

In the absence of any external magnetic field, the parallel resonant frequency would correspond exactly with the plasma frequency of the medium. The presence of the earth's magnetic field, however, causes the parallel

resonant frequency to be shifted to a higher frequency known as the upper hybrid resonant frequency (fm), which is related to the plasma frequency (f_N), and the electron gyro frequency (f_H) as follows:

$$f_m^2 = f_N^2 + f_H^2$$

where $$f_N^2 = \frac{Ne^2}{4\pi^2 m \varepsilon_o}$$

and $$f_H = \frac{e}{m\beta}$$

Therefore by knowing the earth's magnetic field strength and the resonant frequency, the electron density corresponding to each octal output may be easily determined.

Langmuir Probe

The Langmuir probe described here is a rocketborne instrument used to measure the following ionospheric parameters:

1) Electron density
2) Electron temperature
3) Vehicle to plasma potential

The electron density measurement is the primary measurement of this Langmuir probe model.

The Langmuir probe consists of an electrode of known geometry which is immersed in the ionospheric plasma, and an electronics box which applies a voltage waveform to the probe and monitors the voltage-current relationship. The desired parameters can then be calculated from the voltage-current curve such as the one shown in Figure 14 as follows:

1) Electron density is proportional to the electrode current in the electron accelerating region.

2) Electron temperature can be found from the expression describing the curve in the exponential part of the electron retarding region. The expression describing this region is $i = I_o \exp \frac{eV}{kT}$ where

V = negative electrode to plasma voltage

I_o = electron current when the electrode is at space potential (point of inflection)

e = electronic charge

k = Boltzmann's constant

T = electron temperature

By taking the logarithm of the above expression, electron temperature is found to be $T = \frac{e}{K} \frac{V}{\ell n(i/I_o)}$

3) Vehicle to plasma potential is given by the voltage at the point of inflection in the voltage-current curve.

During ascent, the Langmuir probe electrode is mounted on a pivot parallel to the length of the rocket and is held against a door by a spring. When the rocket reaches altitude, the door ejects, allowing the electrode to pivot 90° so that it is perpendicular to the rocket major axis and is immersed in the ionospheric plasma.

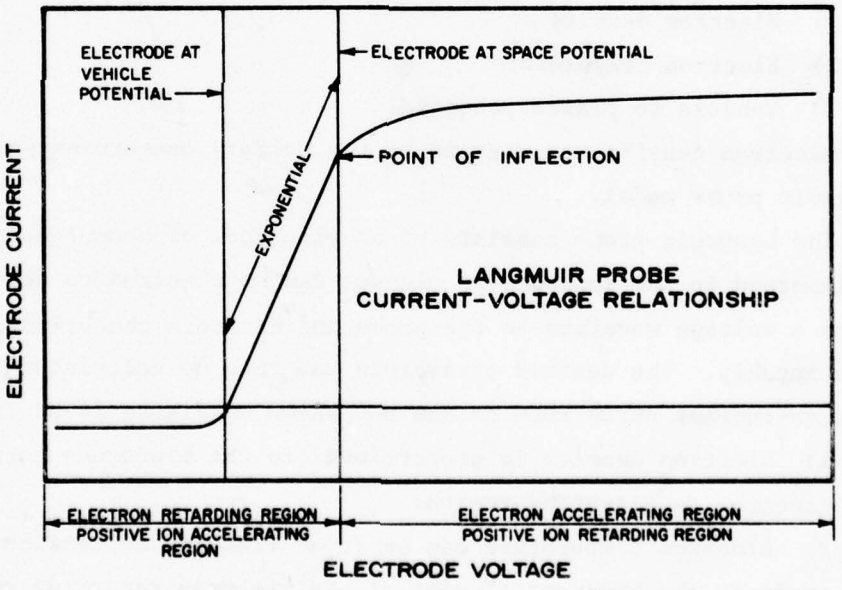


Figure 14. Langmuir probe characteristic voltage-current curve.

The probe consists of a guard electrode and a sensing electrode as shown in the block diagram of Figure 15. The electrode geometry is shown in Figure 16. Since the electrode currents are very small (10^{-9} to 5×10^{-5} amps), it is necessary to use a guard electrode to minimize displacement currents which flow as a result of the capacitance between the sensing electrode and the rocket. The guard electrode also minimizes field fringing effects on the end of the sensing electrode nearest the rocket and aids in defining electron density.

A voltage waveform (Figure 17) is applied by the function generator to the guard electrode and one input terminal of the logarithmic amplifier (see Figure 14). If the current in the sensing electrode from the ionospheric plasma is zero, the voltages at A, B, C, and D are forced to be equal to the function generator voltage. Since the voltages at C and D are equal, the output of the differential amplifier is zero. With a finite sensing electrode current, caused by electron attraction to the electrode, the voltages at C and D are not equal because the voltage at C is proportional to the log of the current into A and $V_A = V_B = V_D$. The differential stage amplifies the difference giving an output proportional to the sensing electrode current.

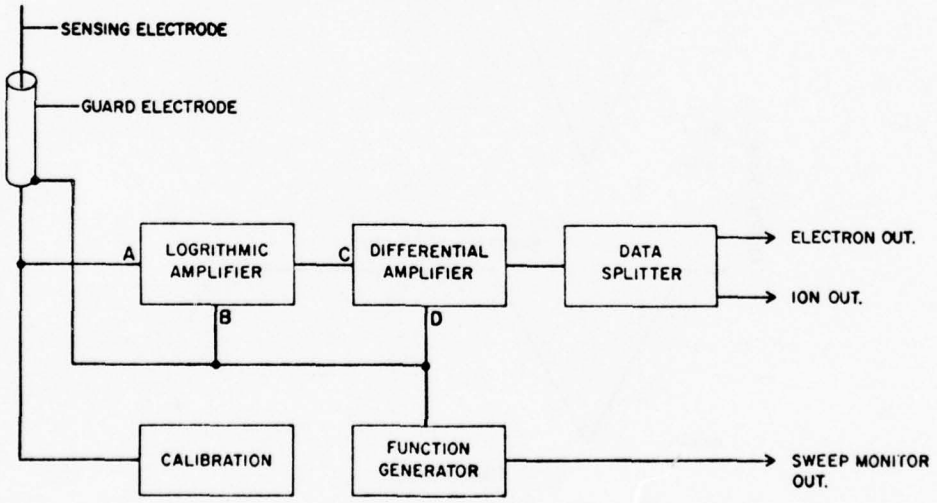


Figure 15. Langmuir probe block diagram.

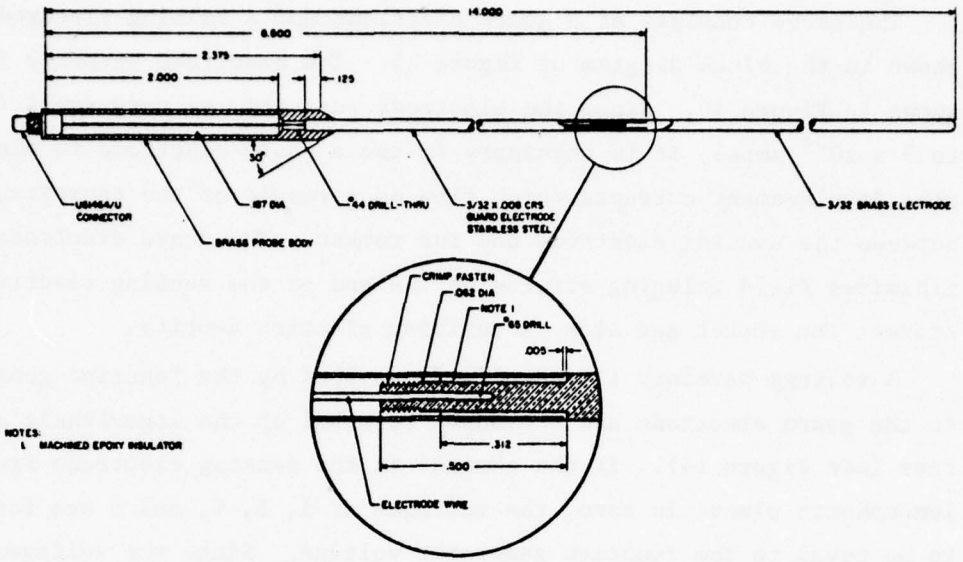


Figure 16. Langmuir probe electrode geometry.

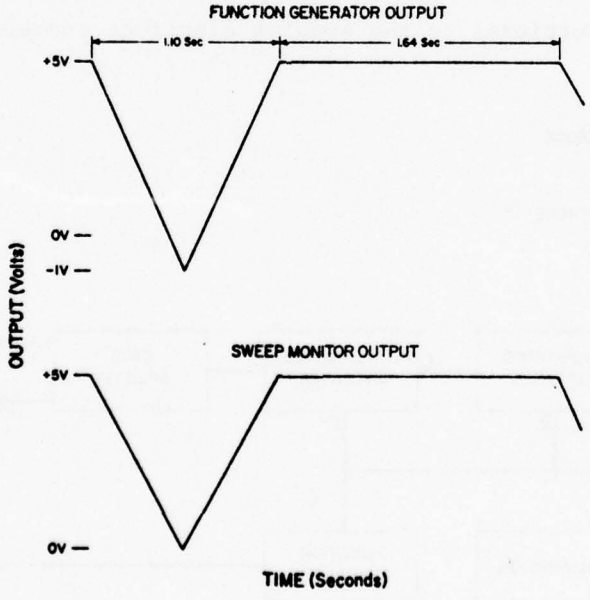


Figure 17. Langmuir probe function generator and sweep monitor waveforms.

The output from the differential amplifier is logarithmically compressed and may be either positive or negative. To make the signal compatible with the telemetry system, it is applied to the data splitter, which inverts one signal and provides two positive output signals. One output channel corresponds to positive ion current and the other to electron current. However, the output corresponding to ion current was not monitored on this flight, since other instruments measured ion density. The data splitter in these models has been designed to clip off instrument response for values of electrode current less than 10^{-10} amps.

The calibration circuit provides a means of verifying instrument operation both during and prior to flight. This is accomplished by momentarily connecting a 1 megohm resistor from the instrument input to ground each 20 seconds for 25 ms. The output pulse magnitude depends on the sweep voltage at the time.

Electromagnetic Emissions

Measurement of light emissions were made to supplement and add to the knowledge gained through the ionospheric measurements and to help answer the question, "What processes and reactions take place in the aurorally disturbed atmosphere?" Through understanding these reaction schemes, a more complete understanding of the energy transfer processes can be obtained. This in turn contributes to improved atmospheric modeling and predictive codes.

Light in the visible and ultraviolet regions was measured by six photometers. Two cooled radiometers, and one infrared spectrometer measured near-infrared emissions. The selected visible and ultraviolet emissions which were measured range between 3914 A and 5577 A and the infrared emissions ranged from 1.6 μm to 5.4 μm.

Radiometers

The Black Brant 18.219-1 payload included two cooled, dual-channel radiometers [*Jensen et al.*, 1972] for measuring selected infrared emissions in an aurora. One radiometer (NR-3B-6B) was mounted to the top deck plate of the payload looking forward along the payload axis. The

other radiometer (NR-3B-7B) was mounted beneath the vertical radiometer with a look angle of 80° from the payload axis.

The dual channel radiometer has two independent measurement channels mounted in a single dewar and using a common, motor driven chopper. Figure 18 is a cutaway view of the instrument showing the major components. The instrument is an integral unit with a .5 liter liquid nitrogen vessel in the center, a cold optical compartment on the fore end and an electronics compartment on the aft end. Tubes extending through the liquid nitrogen vessel permit connection of the electrical conductors and a motor drive shaft from the electronics compartment to the optical compartment. The baffles, lenses, filters, detectors, source follower, pre-amplifiers, and a motor driven chopper are located in the cold optics compartment. A cold cover is placed over the end of the optics compartment to maintain vacuum integrity and is removed at the appropriate altitude for measurements, exposing the optics to the atmospheric emissions. The electronics compartment contains the chopper motor, reference generator, and signal conditioning electronics.

The basic radiometric system is characterized by low background conditions achieved by cooling the entire optical compartment (detector, filter, lens and baffle) to near liquid nitrogen temperatures. This low background condition combined with a cooled preamplifier achieves detector detectivity (D*) equal to or greater than 5×10^{12} cm $Hz^{1/2}$ $watt^{-1}$ at 4.3 μm. The detectable signal range for each instrument as shown in Table 10 below.

TABLE 10

DETECTABLE SIGNAL LEVELS FOR COOLED RADIOMETERS

Instrument	Channel	Wavelength	Minimum Input (kR)	Maximum Input (MR)
NR-3B-6B	1	5.3 μm	25	30
(vertical)	2	4.3 μm	33	44
NR-3B-7B	1	4.3 μm	110	55
(80° from vertical)	2	2.8 μm	110	55

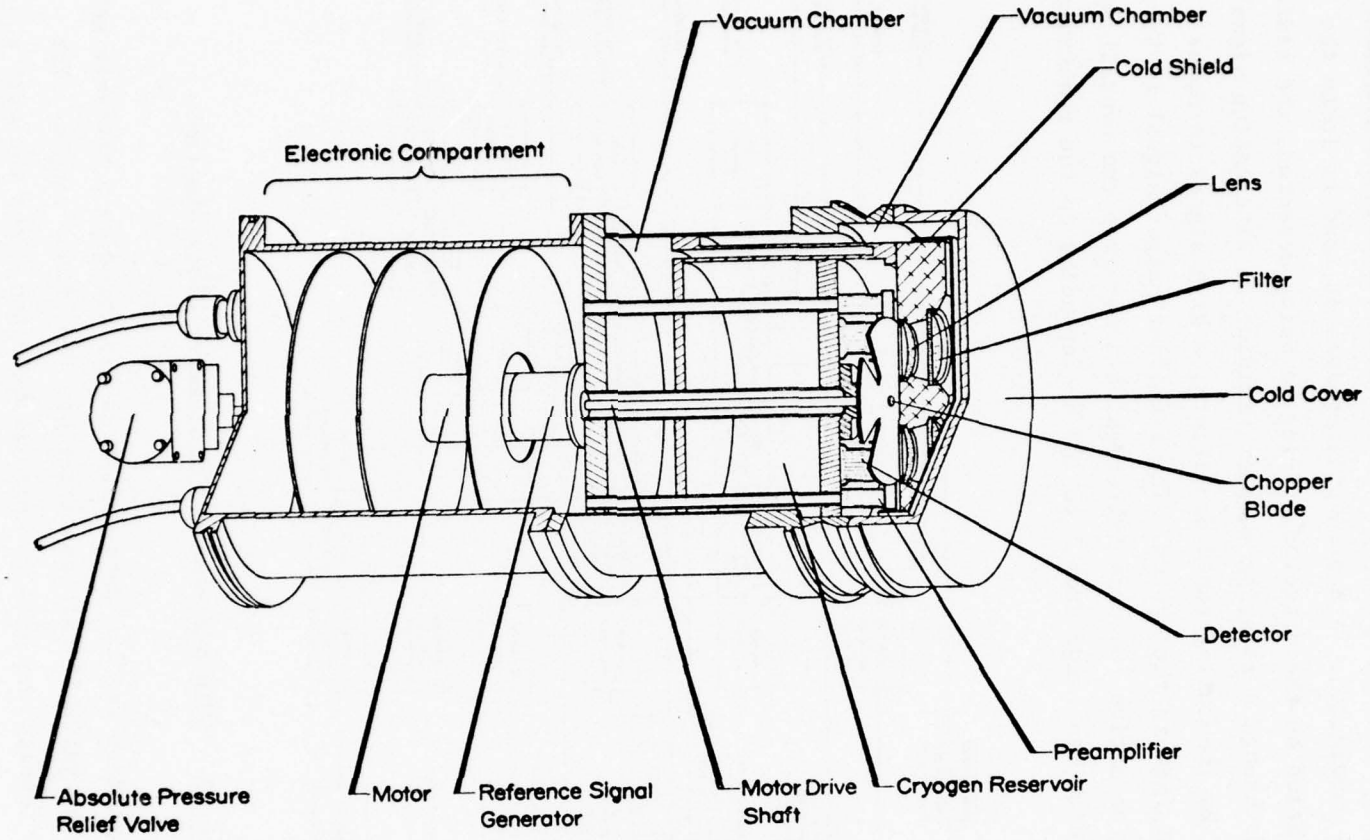


Figure 18. SWIR dual-channel radiometer cutaway view.

Figure 19 is a block diagram of the NR-3B system. As shown in the block diagram, incoming radiation is filtered to provide measurement of the desired wavelength. A coated silicon lens is used to focus the incident radiation on the detector. Prior to being detected, the radiation passes through a rotating chopper yielding an alternating signal of 533 Hz. By then using tuned amplifiers, a high signal to noise ratio is obtained in the system. The rectifier output signal is then filtered in an active low pass filter which determines the overall system bandwidth which can range from 1 to 100 Hz depending on the requirements.

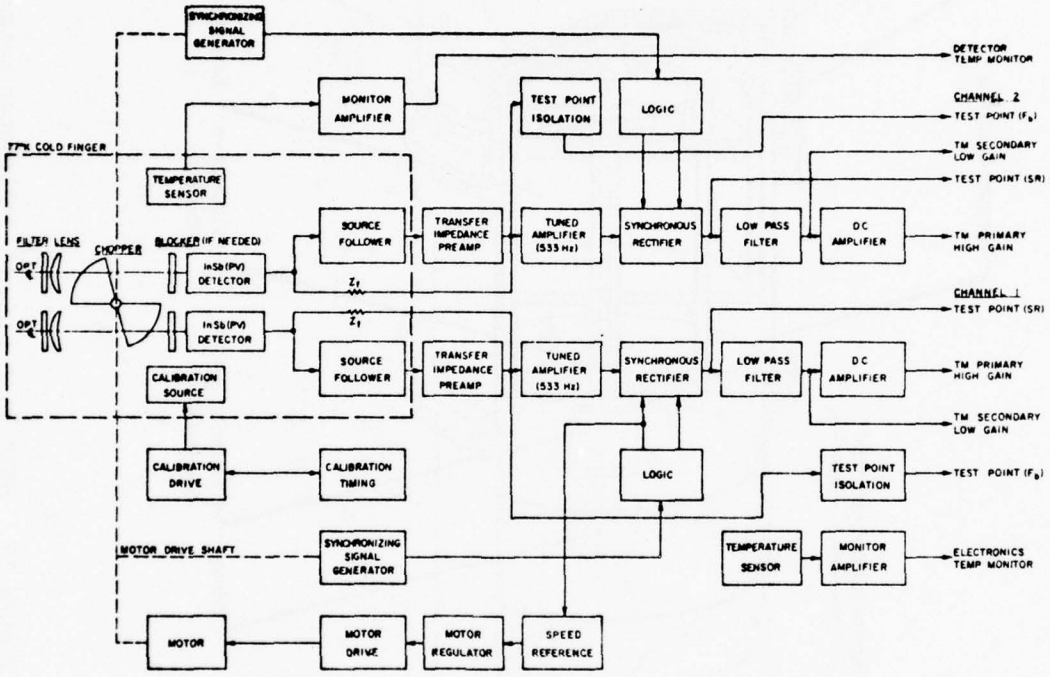


Figure 19. SWIR dual-channel radiometer block diagram.

The output from the low pass filter is amplified by a variable gain amplifier. The variable gain amplifier has two linear ranges. For small signal levels, the gain is approximately ten times the gain at large signal levels, thus extending the range of the instrument while providing good instrument sensitivity.

Two temperature monitor channels are provided to yield measurements of detector and optics temperatures. Internal, light emitting diodes periodically activate the detectors and provide an inflight measure of relative system responsivity.

Infrared Spectrometer

The nitrogen-cooled circular-variable-filter (CVF) infrared spectrometer [*Jensen et al.*, 1972] was mounted near the nose of the payload looking in a forward direction and measured atmospheric emissions from 1.80 to 5.91 μm. Atmospheric species of particular interest which emit in this range are hydroxyl (OH) between 1.8 and 2.1 μm, NO^+ centered at 2.15 μm, CO_2 at 4.3 μm and NO at 5.3 μm.

The CVF spectrometer is physically constructed much like the cooled radiometers. The radiometer cutaway view (Figure 17) is the same for the CVF spectrometer except that the chopper blade is replaced by the CVF, the filter is replaced by a window and there is only one measurement channel. Additionally, since the same cooling technique is employed, the spectrometer achieves the same degree of detectivity (5×10^{12} cm $Hz^{1/2}$ $watt^{-1}$ at 4.3 μm) as the radiometer. The minimum detectable signal level is 125 kR/μm at 4.3 μm and the maximum is 20.9 MR/μm at 4.3 μm. Both the minimum and maximum levels increase with decreasing wavelength as illustrated in the inverse spectral responsivity curve of Figure A-58.

Figure 20 is a block diagram of the instrument. The instrument achieves a spectral scan by rotating a circular-variable-filter over the field stop so that the instrument scans from approximately 1.6 μm to 5.4 μm during each revolution of the filter at a rate of 2 scans per second.

The optical system consists of a $f/1.0$ silicon coated lens imaging a point source at infinity on the indium antimonide detector which serves as the system field stop. The CVF rotates over the field stop which performs the function of a spectrometer slit. The resolution is a function of slit width and filter incident angle and varies between 3 and 5 percent depending upon the wavelength.

The electronic system includes two prime signal channels that

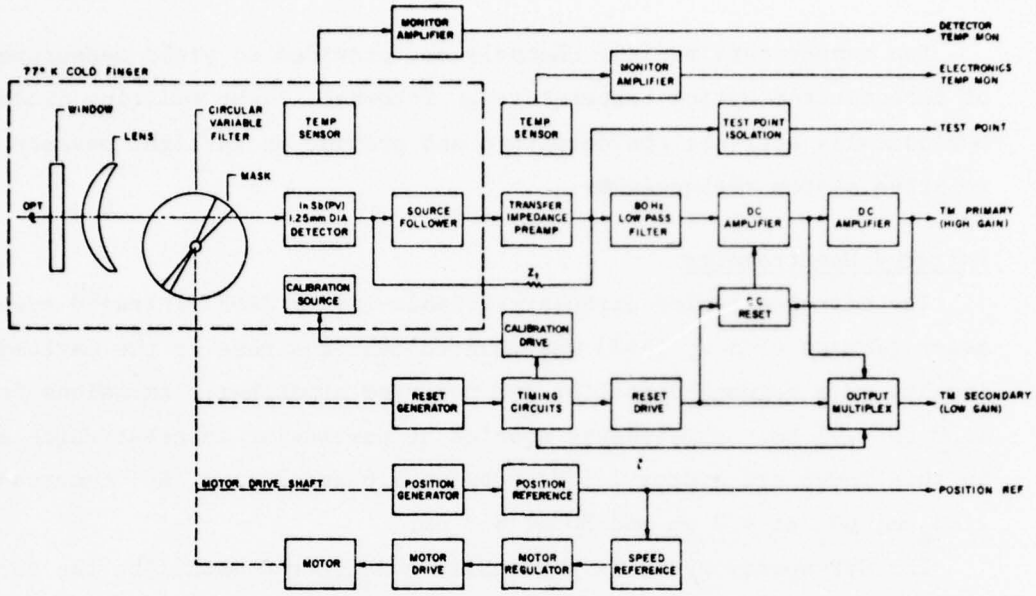


Figure 20. CVF spectrometer block diagram.

differ in gain by a factor of 10 to provide a dynamic range of about 1000. Two spectral position references are provided: One consists of a pulse that occurs at the beginning of the scan on the low gain channel, the other is a continuous train of square wave pulses providing 20 transition reference points throughout the scan. The latter position reference requires an additional wide band TM channel. Several temperature monitor channels are provided to yield detector and optics temperatures. An internal, light emitting diode periodically activates the detector and provides an inflight measure of relative system responsivity.

The electronic system includes a direct-coupled transfer impedance preamplifier operated at nitrogen temperatures, and a dc reset signal conditioning system.

The dc reset system requires that an opaque mask be installed on the filter, which when rotated over the detector, provides a zero reference by blocking all radiations coming through the optical system. When the mask is in position over the detector, the reset generator provides a logic signal which controls a feedback network which forces

the channel output signal to zero. The feedback network contains an integrator and storage circuit which holds the correction until the next cycle. Thus, during the subsequent scan, the system is dc coupled through the signal conditioning amplifier from detector to TM. The use of the dc reset signal conditioning allows high values of dc gain while overcoming the problems of drift introduced by temperature changes in the system.

Photometers

Six photometers were flown aboard the Black Brant 18.219-1 payload to measure various visible and ultraviolet emissions. The emissions measured were those of $N(^2D)$ at 5200 A, $N(^2P)$ at 3466 A, 0 at 5577 A, and N_2^+ at 3914 A. These four emissions were measured with photometers that viewed forward at an angle of 80° with the payload major axis. The horizontal viewing photometers were optically aligned to look in the same direction as the NR-3B-7B radiometer to within 1/2 degree. The sixth photometer viewed directly forward (via 45° mirror) and measured 3914 A emissions.

Figure 21 is a block diagram of the photometer. The photometer consists of a removable optical section, a miniature RCA phototube detector with its associated high voltage power supply, and a variable gain amplifier with its associated low voltage power supply. The photometer also contains a light emitting diode which is turned on for 0.1 seconds every 30 seconds to check the operation of the instrument.

The optical wavelength to be measured and the field of view are determined by the interference filter, the lens, and the aperture which make up the optical section. The photometers described here all have a field of view of approximately 5° full angle. The peak wavelength, optical bandwidth, filter transmission, detectable signal range, and photomultiplier tube type for each photometer are listed in Table 11.

The variable gain amplifier has a different gain for each of two input ranges. The gain at small signal levels is ten times the gain at large signals, thus extending the range of the instrument.

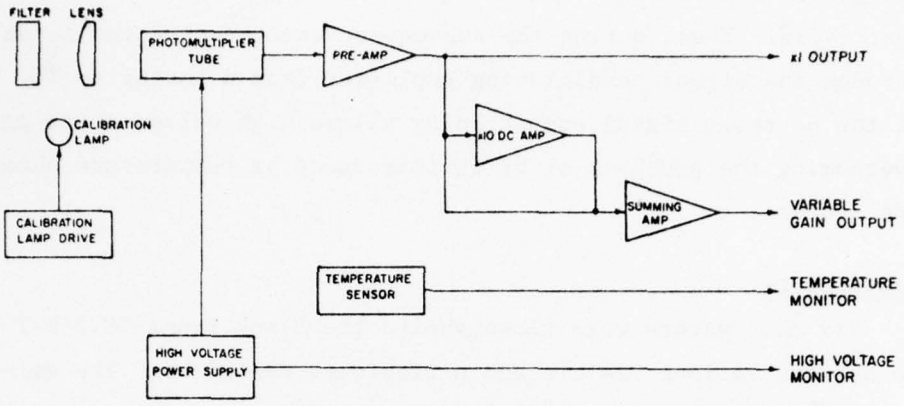


Figure 21. Photometer block diagram.

TABLE 11

Black Brant 18.219-1 photometer specifications

Characteristic	Photometer Number					
	PM-1-7	PM-1-24	PM-1-25	PM-1-26	PM-1-28	PM-1-30
Photometer wavelength (A)	5200	5200	3466	3914	5577	3914
Filter center wavelength (A)	5201	5203	3462	3919	5576	3917
Filter $\Delta\lambda$ (A)	26.5	10.0	21.0	18.4	17.5	19.1
Peak filter transmission (%)	75.8	48.3	10.0	13.9	53.3	14.1
Full angle field of view (°)	5.00	5.20	5.01	5.05	5.00	5.20
Detectable signal range (kR)	0.06-8.6	0.02-5.8	0.08-22.8	2.8-635	1.7-479	0.08-83
DC offset (volts)	0.18	0.01	0.00	-0.05	0.15	0.05
Monitor values during calibration						
H.V. Mon. (volts)	1.84	2.16	1.95	1.28	1.61	1.73
Temp. Mon. (volts)	1.96	2.25	1.92	1.95	1.99	2.77
Cal. Pulse (volts)	0.80	2.40	2.50	1.10	2.10	2.40
PM tube type (RCA)	4516	4516	4516	4516	8644	4516

GROUND SUPPORT SYSTEMS

Multiple ground-based supporting measurements were conducted both prior to and during the flight of Black Brant 18.219-1 to monitor auroral activity and energy deposition. These measurements were used as indicators to allow selection of optimum launch time and to define conditions prior to launch and during the flight. Table 12 provides a summary of instrument, experimenter and site, and measurements taken at each.

All ground stations experienced excellent observation conditions throughout the evening of the launch providing an excellent time history of the event.

TABLE 12

SCIENTIFIC GROUND SUPPORT, BLACK BRANT 18.219-1.

Instrument	Experimenter (Site)	Measurement
	AFCRL/Utah State University (Poker Flat Optics Site)	
Field-Widened Interferometer		Visible Atmospheric Spectra, 0.5 - 1 μm
Liquid Nitrogen Cooled Field-Widened Interferometer		IR Atmospheric Spectra, 1 - 3 μm
Spatial Scanning Photometers		Emission Intensity and Position (Along Rocket Flight Path) 3914 A (N_2^+) 5577 A (O) 6300 A (O)
IR Radiometers 1 Double Channel (Liquid Nitrogen Cooled) 1 Single Channel (Thermoelectrically Cooled) 2 Double Channel (Thermoelectrically Cooled)		OH and $O_2(^1\Delta_g)$ Emissions
Fixed Photometers		Emission Intensity (Time History of Rocket at 100 km Entry Point) 5577 A (O) 3914 A (N_2^+)
Tilting Filter Photometer		Emission Intensity 4278 A (N_2^+) 6300 A (O) 5577 A (O) 5893 A (NO) 8690 A (OH)
Wide-Angle Auroral Television (U of A)		Auroral Forms
Wide-Angle Camera		Auroral Forms
Riometer		30-MHz Auroral Absorption
All Sky Camera (Photometrics)		Auroral Morphology
Remote Readout, U. of Alaska Data		Meridian Scanning Photometer Data - FYU, EDO - 5577 A Magnetometer - FYU, PF H-Component

TABLE 12 (cont.)

Instrument	Experimenter (Site)	Measurement
	University of Alaska (Ft. Yukin)	
Meridian Scanning Photometers		Emission Intensity, Spatial Distribution Along Magnetic Meridian 5577 A (O) 6300 A (O) 4278 A (N_2^+) 4861 A (H_β)
Magnetometers (3-Axis)		Magnetic Field Fluctuations
Riometer		30-MHz Auroral Absorption
	University of Alaska (Poker Flat)	
Magnetometer (3-Axis)		Magnetic Field Fluctuations
	(Ester Dome)	
Meridian Scanning Photometers		Emission Intensity, Spatial Distribution Along Magnetic Meridian 5577 A (O) 6800 A (O) 4278 A (O) 4861 A (H_β)
All Sky Camera		Auroral Morphology
	(College)	
Ionosonde		Electron Density
	SRI (Chatanika)	
Incoherent Scatter Radar		Electron Density, Temperature, Ion Temperature, Winds
	SRI (Homer)	
Clutter Radar		Auroral Mapping
	Lockheed (Chatanika)	
Photometers		Energy Input Definition
	Photometrics (Ester Dome)	
Tilting Filter Photometer		OH Rotational Temperature

Preceding Page Blank - Not Filmed

FLIGHT RESULTS

Black Brant 18.219-1 was successfully flown at 0738:30.3 UT, February 25, 1974, from Poker Flat Research Range. The general auroral condition accompanying the launch was that of a bright arc that moved out of the north until it intersected the anticipated rocket trajectory (100 km point of penetration). The vehicle was launched when this condition occurred. On ascent the rocket passed approximately 40 km south of the main arc due to arc movement and the fact that the rocket flight path was actually considerably south of that predicted. All primary vehicle functions were accomplished successfully. The payload achieved an apogee of 195 km allowing the payload to successfully accomplish its measurements mission.

The payload recovery system operated normally resulting in a successful payload recovery. All instruments were recovered in good shape for refurbishment and future use.

In general the total payload was successful. However, some anomalies occurred which were recorded herein.

1. The cover on the Mass Spectrometer was not removed. This resulted in a complete loss of data for that instrument.
2. The data from the radiometers indicated that a projectile passed the payload and traveled in front for a long period of time. Careful examination of this data indicates that it was probably the rocket motor itself. This can be explained due to the payload separating and assuming a higher drag angle of attack. This body in the field of view makes the data reduction on the radiometers more difficult.
3. The 5.34 μm channel on the horizontal radiometer malfunctioned before launch and was disabled to prevent it from influencing the other channel.
4. The particle counter data appeared strange while being reduced. An examination of the instrument showed a defect in its design causing crosstalk between channels.

Preceding Page Blank - NOT FILMed

REFERENCES

Burt, D. A. and C. S. Davis, Rocket instrumentation for Icecap 73A auroral measurements program -- Black Brant 18.205-1, *USU Scientific Report No. 3, Hayes Report No. 3, AFCRL-TR-74-0195*, 147 pp., Contract F19628-72-C-0255, Space Science Laboratory, Utah State University, Logan, 1974.

Burt, D. A., J. C. Kemp, L. C. Howlett, E. F. Pound, G. K. LeBaron, and G. D. Allred, ICECAP 72 - A rocket measurements program for the investigation of auroral infrared emissions -- Black Brant 17.110-3. *SSL Scientific Report No. 5, HAES Report No. 12, AFCRL-TR-75-0001*, 160 pp., Contract F19628-72-C-0255, Space Science Laboratory, Utah State University, Logan, September 1974.

Jensen, L. L., J. C. Kemp, and R. J. Bell, Small rocket instrumentation for measurements of infrared emissions -- Astrobee D 30.205-3 and Astrobee D 30.205-4, *SSL Scientific Report No. 3, AFCRL 72-0691*, 89 pp., Contract F19628-70-C-0302, Space Science Laboratory, Utah State University, Logan, November 1972.

Narcisi, R. S., Composition studies of the lower ionosphere, in *Physics of the Upper Atmosphere*, edited by Franco-Varniani, pp. 12-59, Editrice Compositori, Bologna, Italy, 1971.

Narcisi, R. S. and A. D. Bailey, Mass spectrometry in the D-region ionosphere - apparatus, techniques and first measurements *AFCRL 65-81*, 60 pp., Air Force Cambridge Research Laboratories, Office of Aerospace Research, Bedford, Massachusetts, February 1965.

Neal, P. C., Design and calibration of a rocket-borne electron spectrometer, *SSL Scientific Report No. 1, HAES Report No. 8, AFCRL-TR-74-0629*, 78 pp., Contract F19628-74-C-0130, Space Science Laboratory, Utah State University, Logan, December 1974.

Pound, E. F. and K. D. Baker, A superheterodyne plasma frequency probe for ionospheric research, *Contract GCA PO 12161*, Space Science Laboratory, Utah State University, Logan, July 1971.

Visidyne, Inc., Post-flight Evaluation Report of Electron Electrostatic Analyzer Serial No. 201, *VI-190*, 16 pp., Burlington, Massachusetts, July 1973.

APPENDIX A

INSTRUMENT TECHNICAL DATA

Black Brant 18.219-1

(A-2 BLANK PAGE)

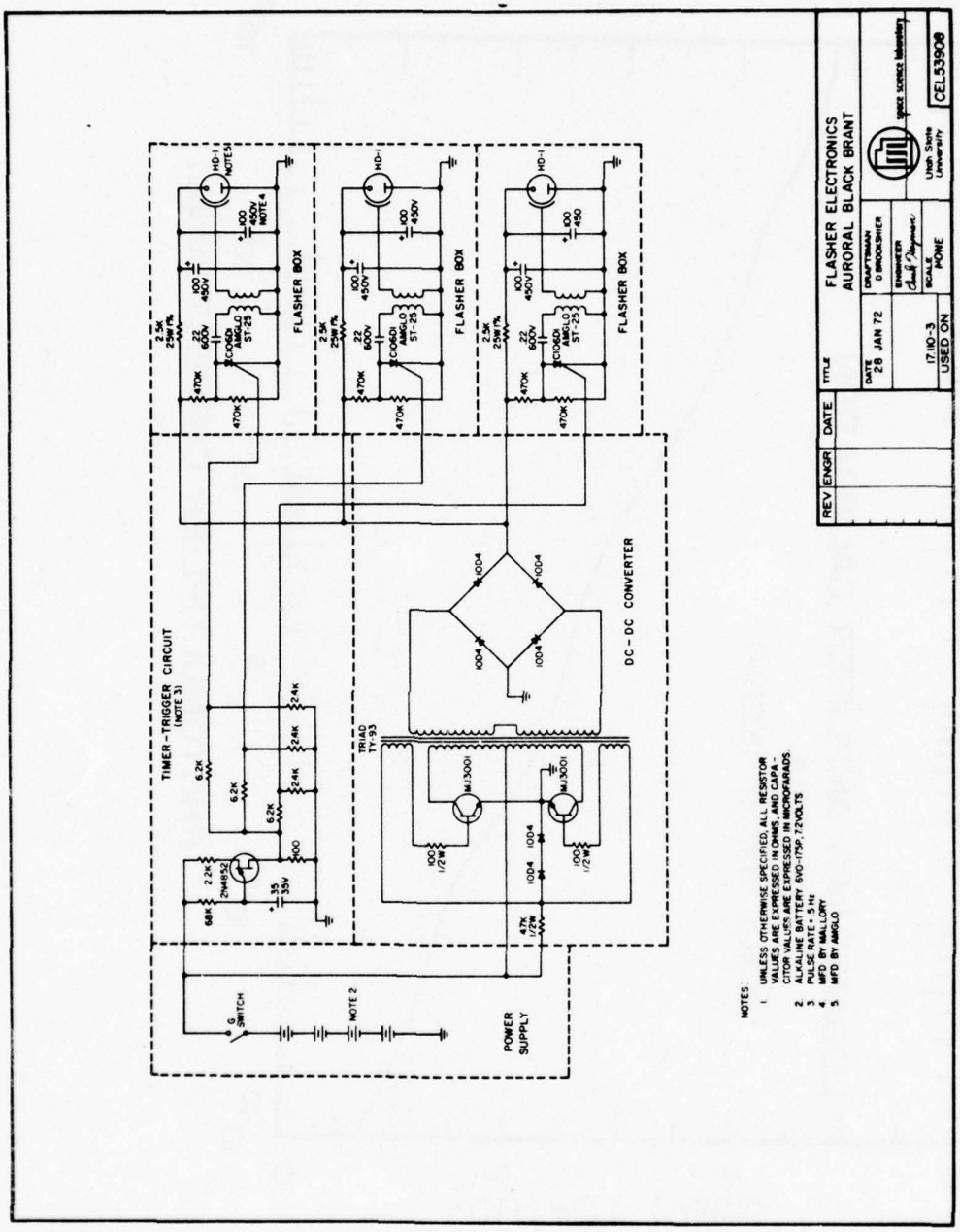


Figure A-1. Flasher electronics schematic diagram.

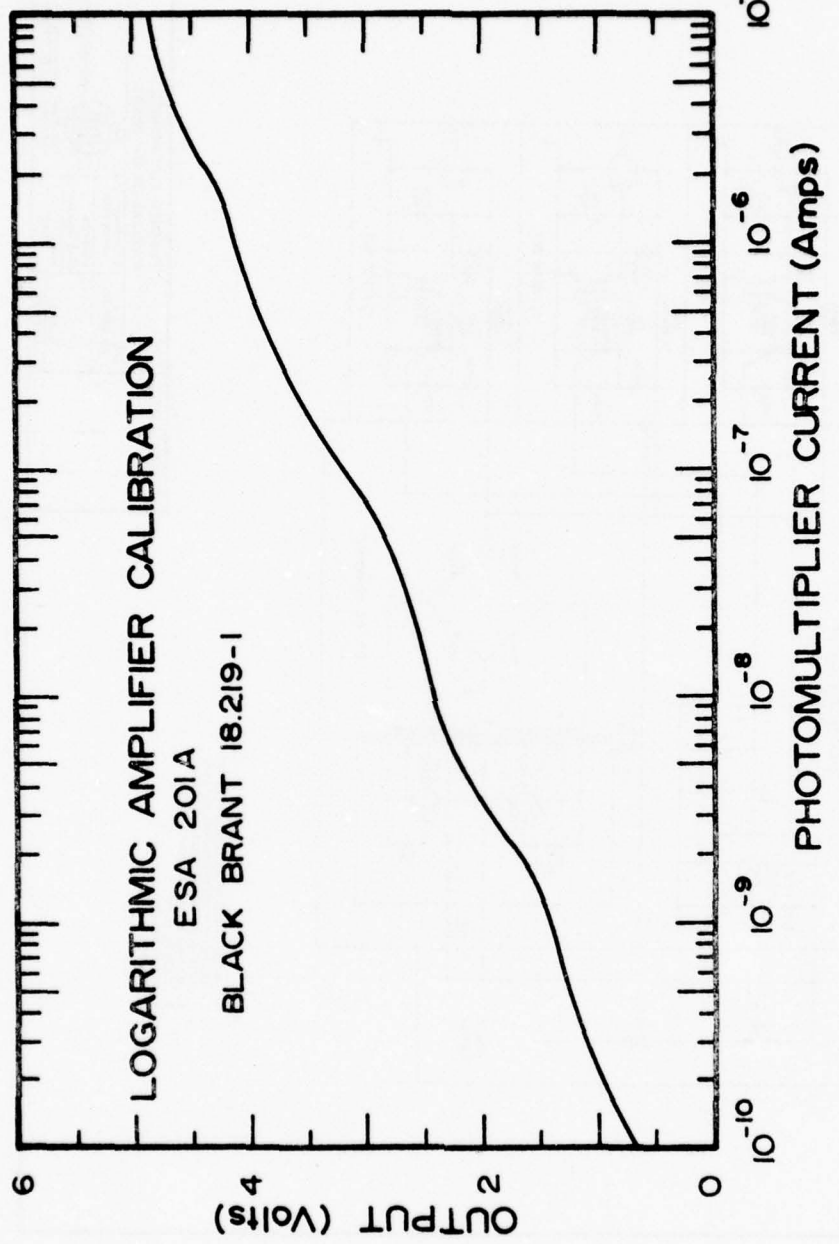


Figure A-2. ESA logarithmic amplifier calibration.

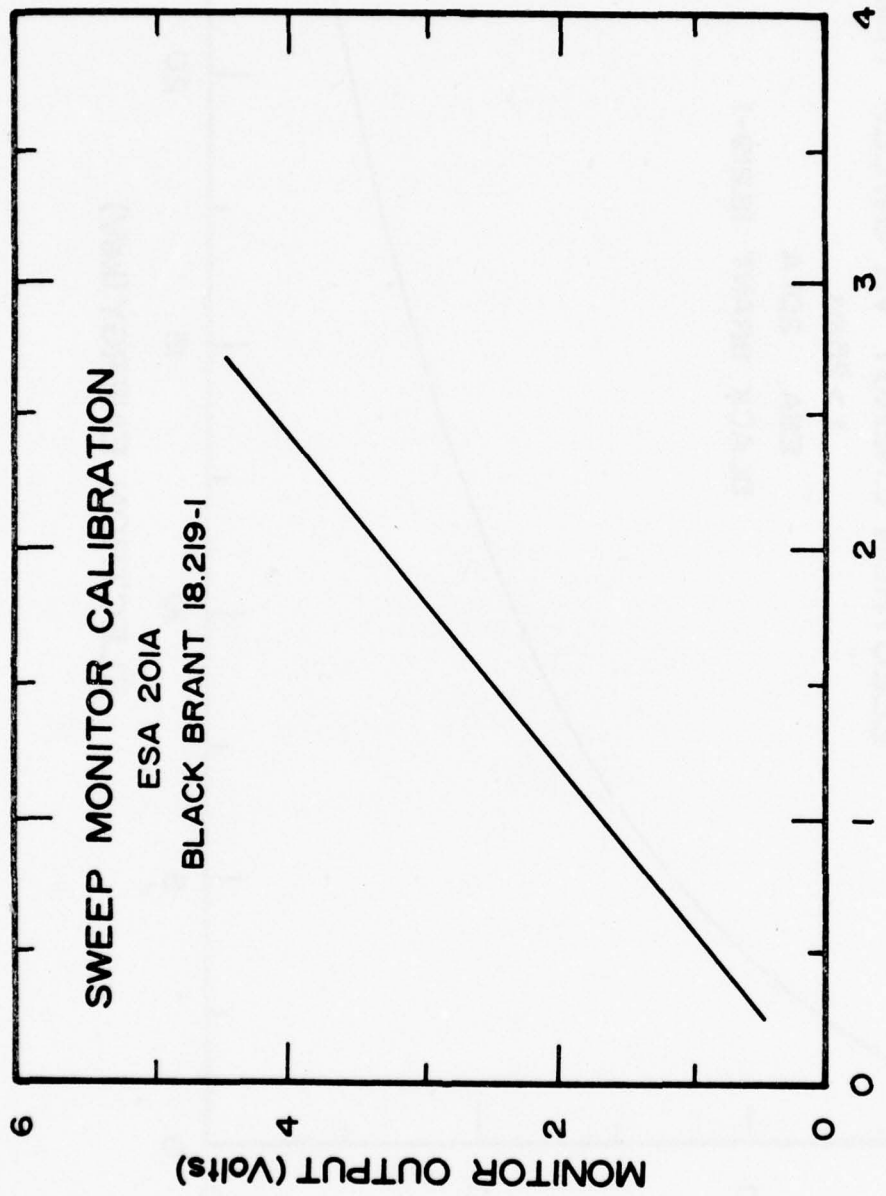


Figure A-3. ESA high voltage sweep monitor calibration.

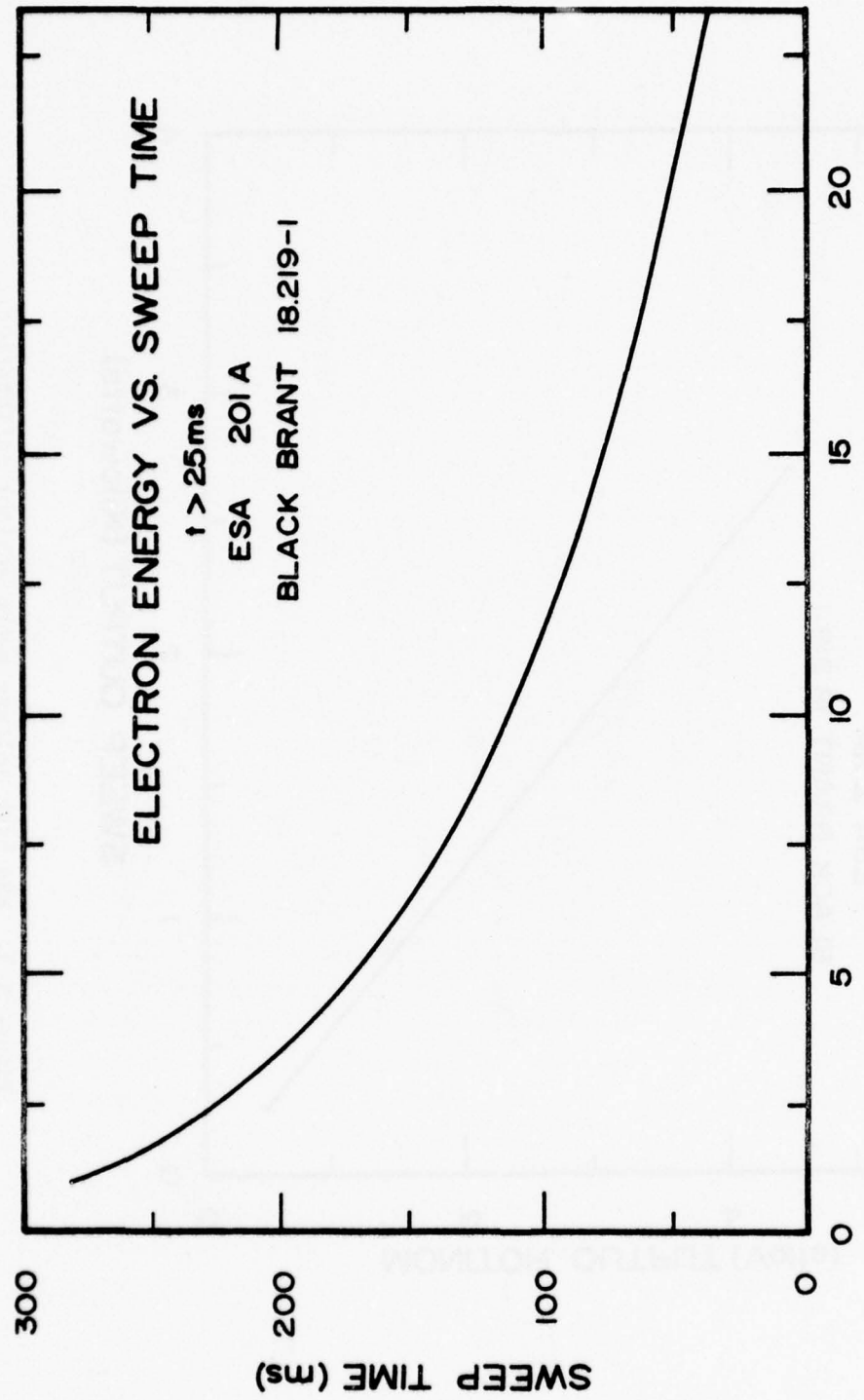


Figure A-4. ESA electron energy vs. sweep time (t > 25 ms).

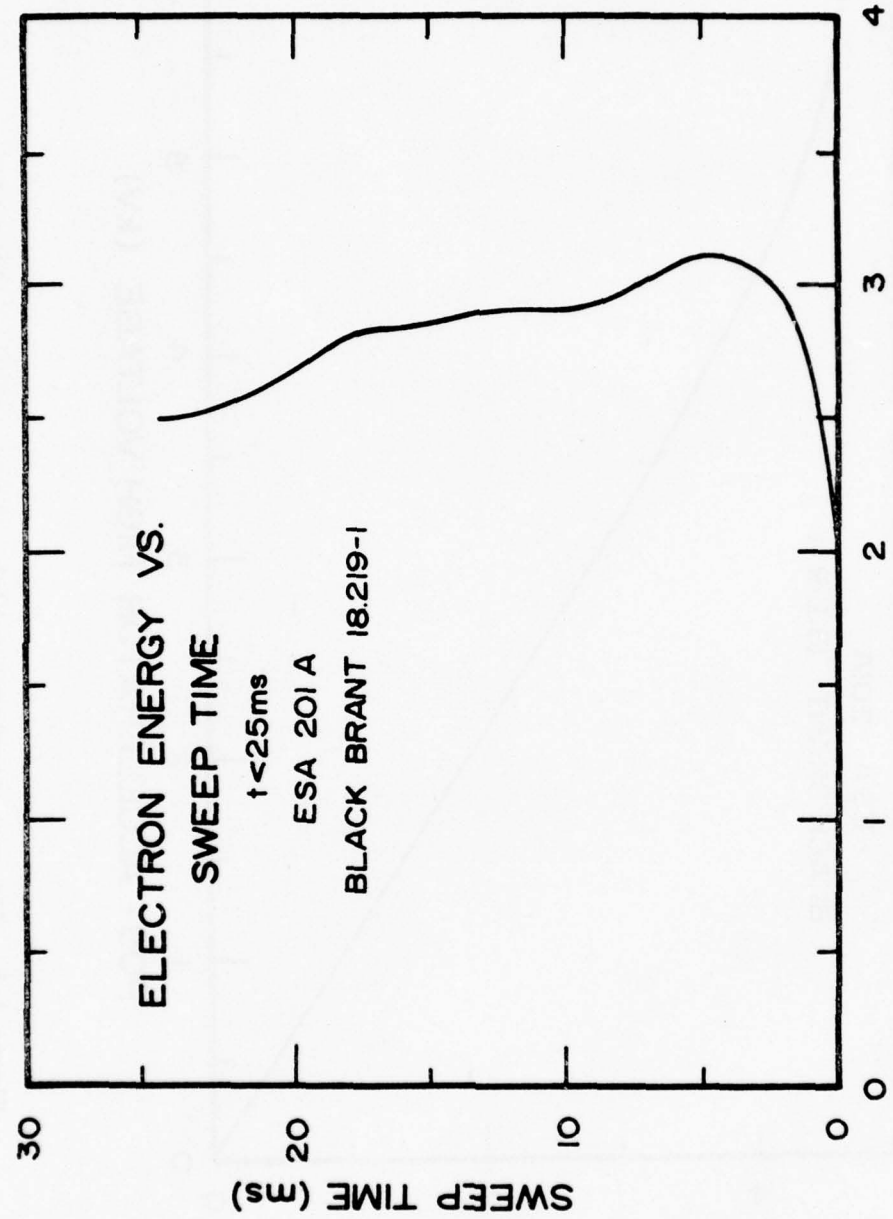


Figure A-5. ESA electron energy vs. sweep time (t < 25 ms).

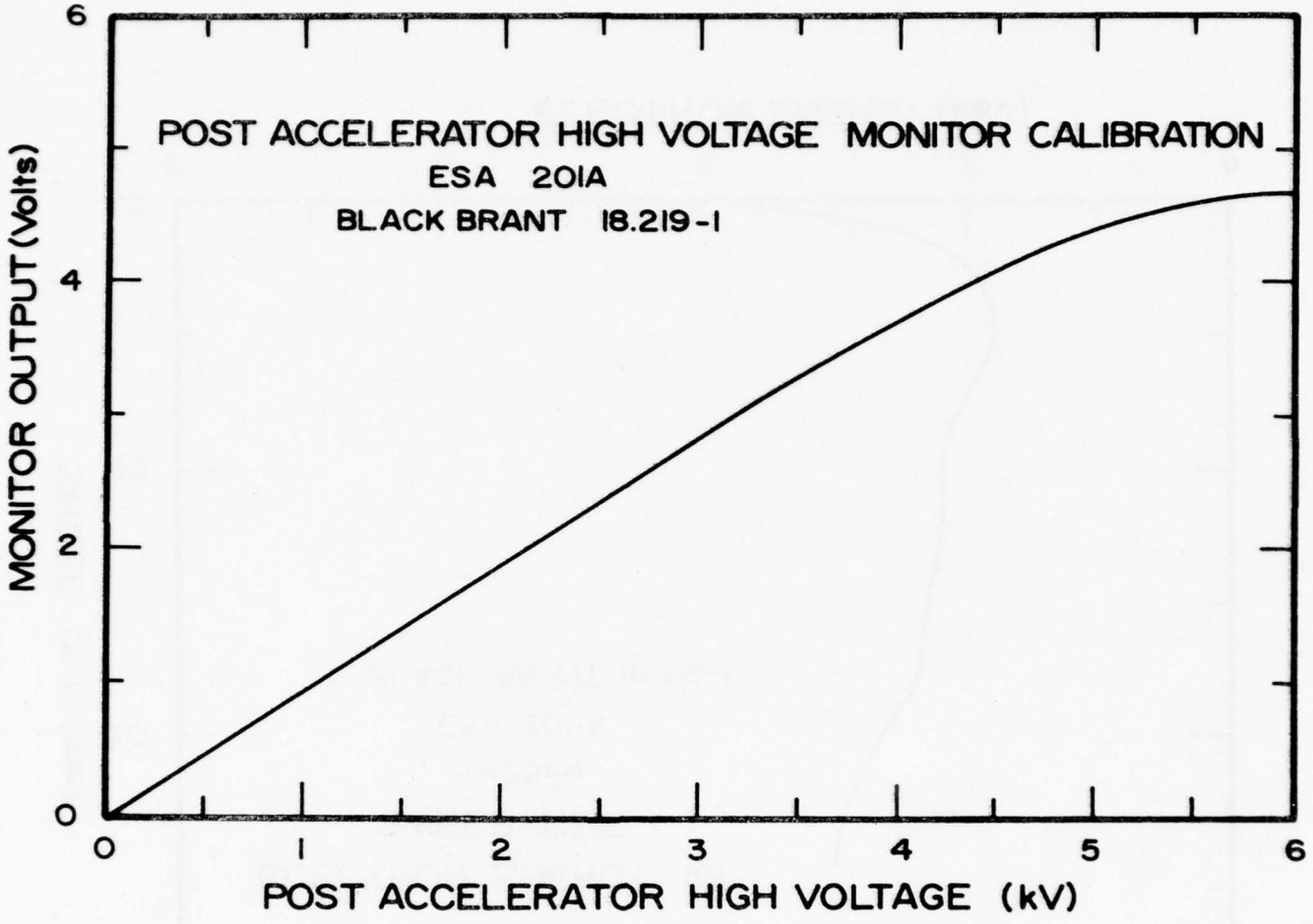


Figure A-6. ESA post accelerator high voltage monitor calibration.

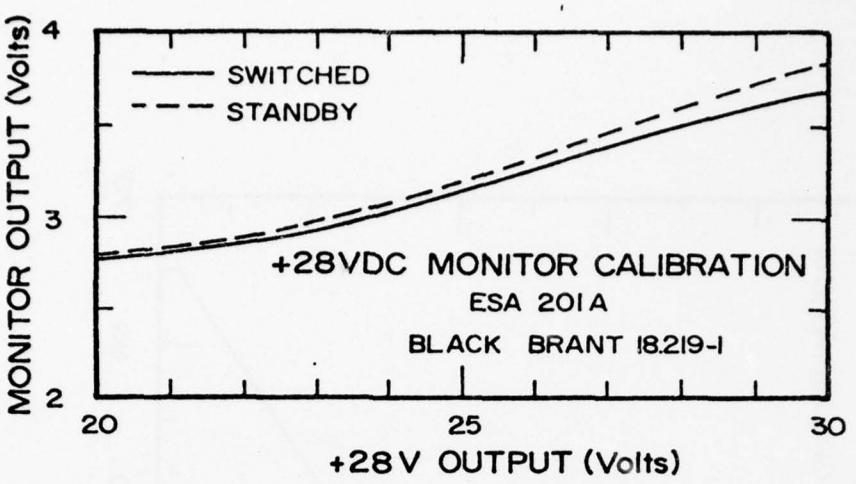


Figure A-7. ESA +28 VDC monitor calibration.

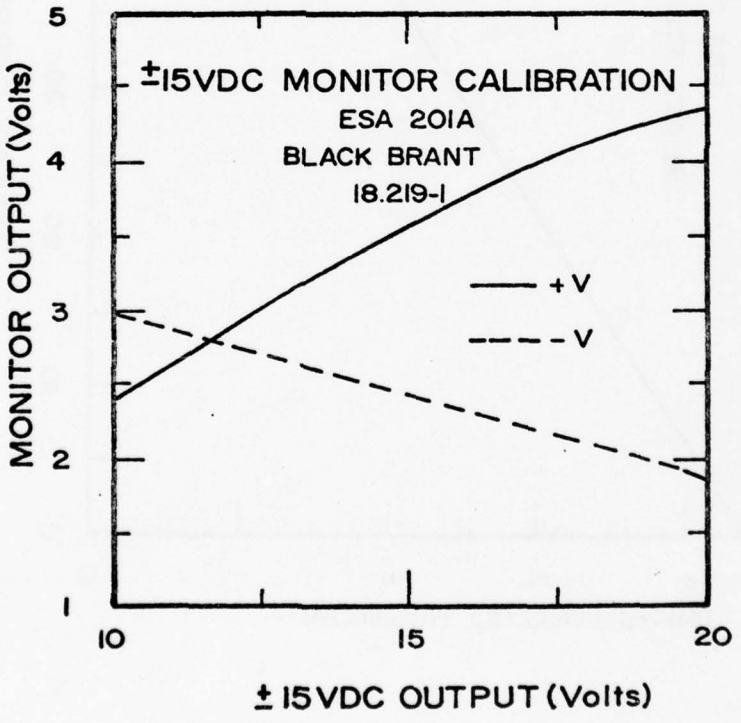


Figure A-8. ESA ± 15 VDC monitor calibration.

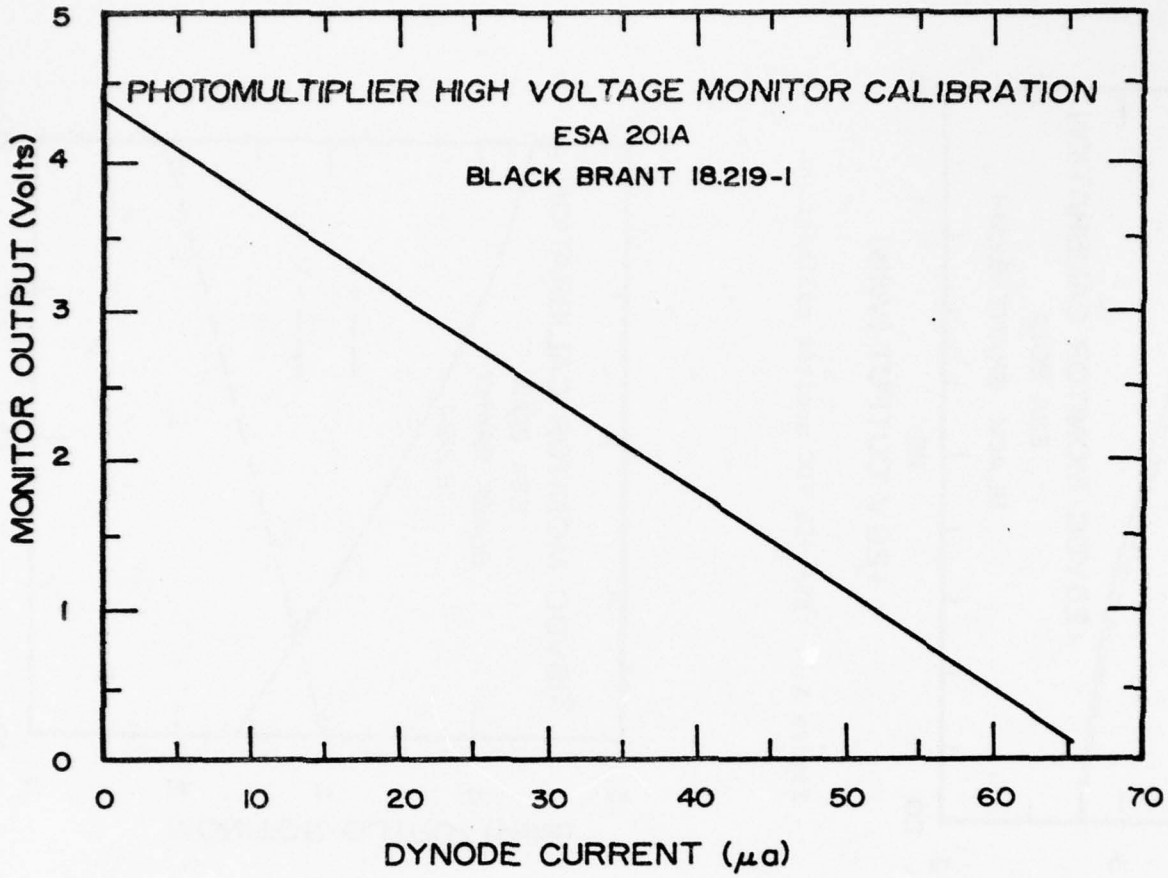


Figure A-9. ESA photomultiplier high voltage monitor calibration.

TABLE A-1

LOG AMPLIFIER CALIBRATION

Output (V)	Input (μa)
4.82	10
4.68	5
4.33	2
4.11	1
3.92	.5
3.57	.2
3.19	.1
2.82	.05
2.55	.02
2.40	.01
2.19	.005
1.65	.002
1.42	.001
1.25	.0005
.99	.0002
.64	.0001

TABLE A-2

SWEEP MONITOR CALIBRATION

V_{mon} (V)	V_{sweep} (kV)
.44	.25
.60	.36
.76	.44
.95	.56
1.20	.71
1.50	.89
1.95	1.12
2.45	1.45
3.0	1.75
3.65	2.21
4.40	2.72

TABLE A-3

ELECTRON ENERGY vs. SWEEP TIME

Time (ms)	Energy (keV)	Time (ms)	Energy (keV)
0	1.6	80	14.5
2.5	3.0	90	13.0
5.0	3.1	100	11.5
10.0	2.9	120	9.2
12.5	2.9	140	7.3
15.0	2.85	160	5.8
17.5	2.83	180	4.6
25	2.50	200	3.6
30	25	220	2.7
40	22.5	240	2.0
50	20.5	260	1.5
60	18	280	1.0
70	16.5		

TABLE A-4

POST ACCELERATOR HIGH VOLTAGE CALIBRATION

V_{PA} (kilovolts)	V_{mon} (volts)
0	0
1.0	.95
2.0	1.84
3.0	2.86
4.0	3.72
5.0	4.39
6.0	4.68

TABLE A-5

PHOTOMULTIPLIER HIGH VOLTAGE CALIBRATION

Dynode Current (microamps)	V_{mon} (volts)
65	.11
60	.453
50	1.13
40	1.81
30	2.49
20	3.18
10	3.83

TABLE A-6

+28VDC MONITOR CALIBRATION

+28VDC (volts)	Switched V_{mon} (volts)	Standby V_{mon} (volts)
0	2.53	2.55
20	2.78	2.80
24	3.02	3.05
26	3.26	3.32
28	3.48	3.56
30	3.67	3.82

TABLE A-7

±15VDC MONITOR CALIBRATION

+15VDC (volts)	$+15VDC_{mon}$ (volts)	-15VDC (volts)	$-15VDC_{mon}$ (volts)
0	0	0	3.47
5	1.20	-5	3.00
10	2.40	-10	2.78
12	2.88	-12	2.55
14	3.35	-14	2.44
15	3.56	-15	2.32
16	3.77	-16	2.09
18	4.11	-18	2.09
20	4.35	-20	1.86

TABLE A-8

COMMUTATOR SEGMENT ASSIGNMENTS (PC 72B-2A)

Segment No.	Assignment	Segment No.	Assignment
1	28 keV electrons	9	17 keV electrons
2	90 keV electrons	10	42 keV electrons
3	17 keV elect	11	9 keV electrons
4	42 keV electrons	12	0 volts
5	9 keV electrons	13	+5 volts
6	4.5 keV electrons	14	+5 volts
7	28 keV electrons	15	+5 volts
8	90 keV electrons	16	0 volts

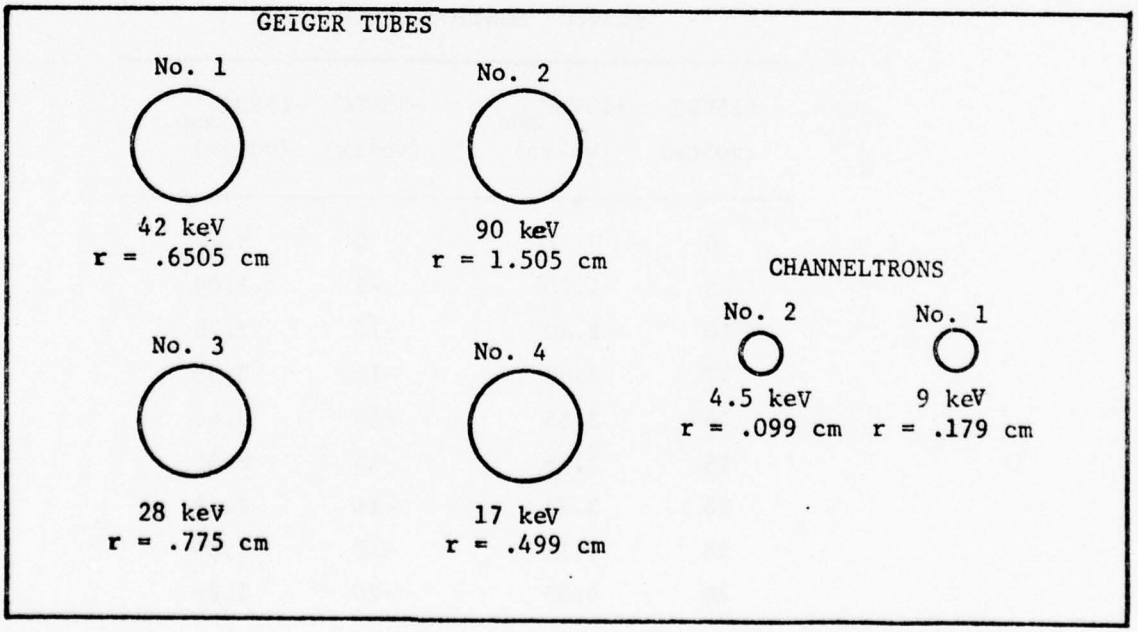


Figure A-10. Particle counter window locations.

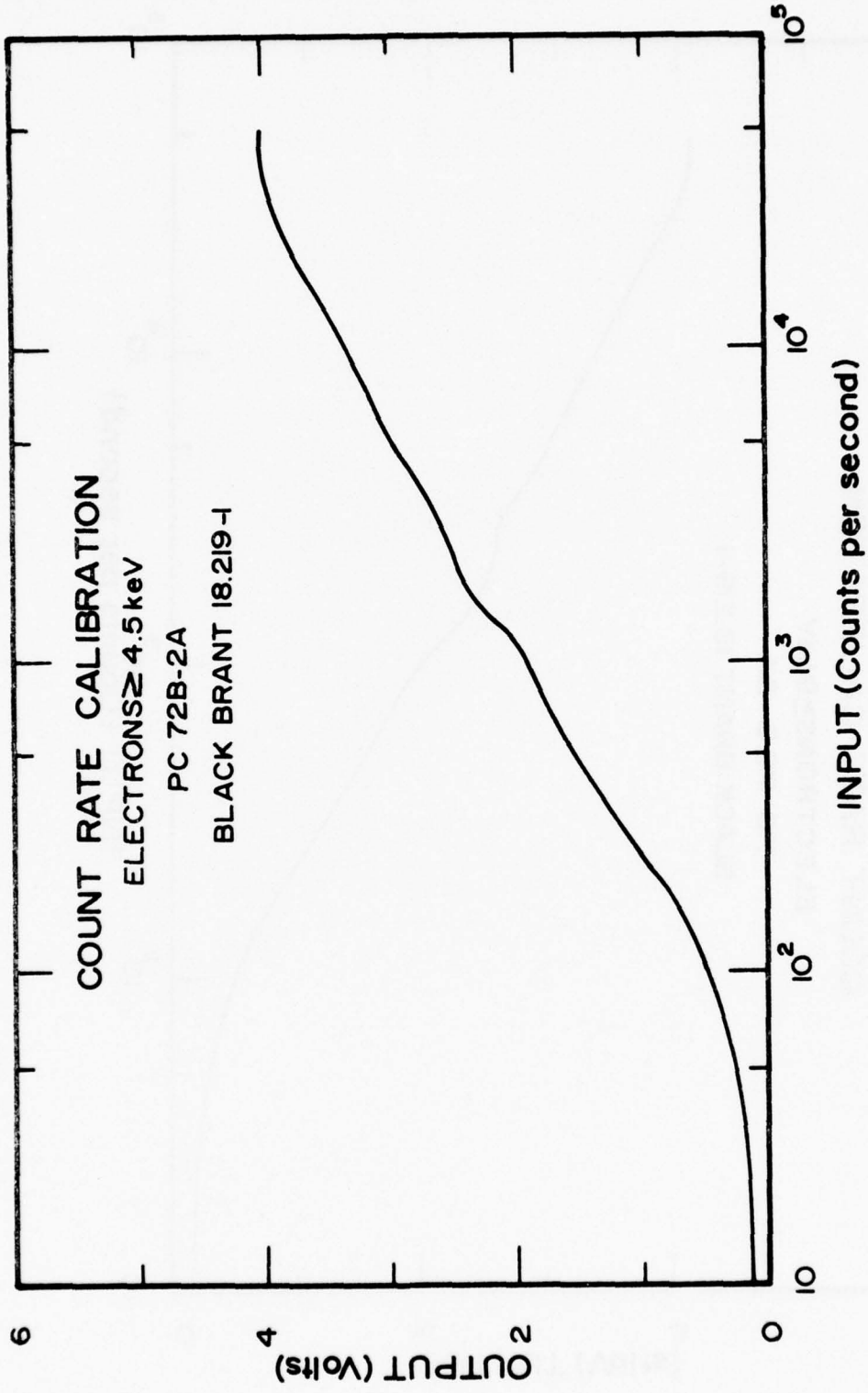


Figure A-11. Particle counter count rate calibration.

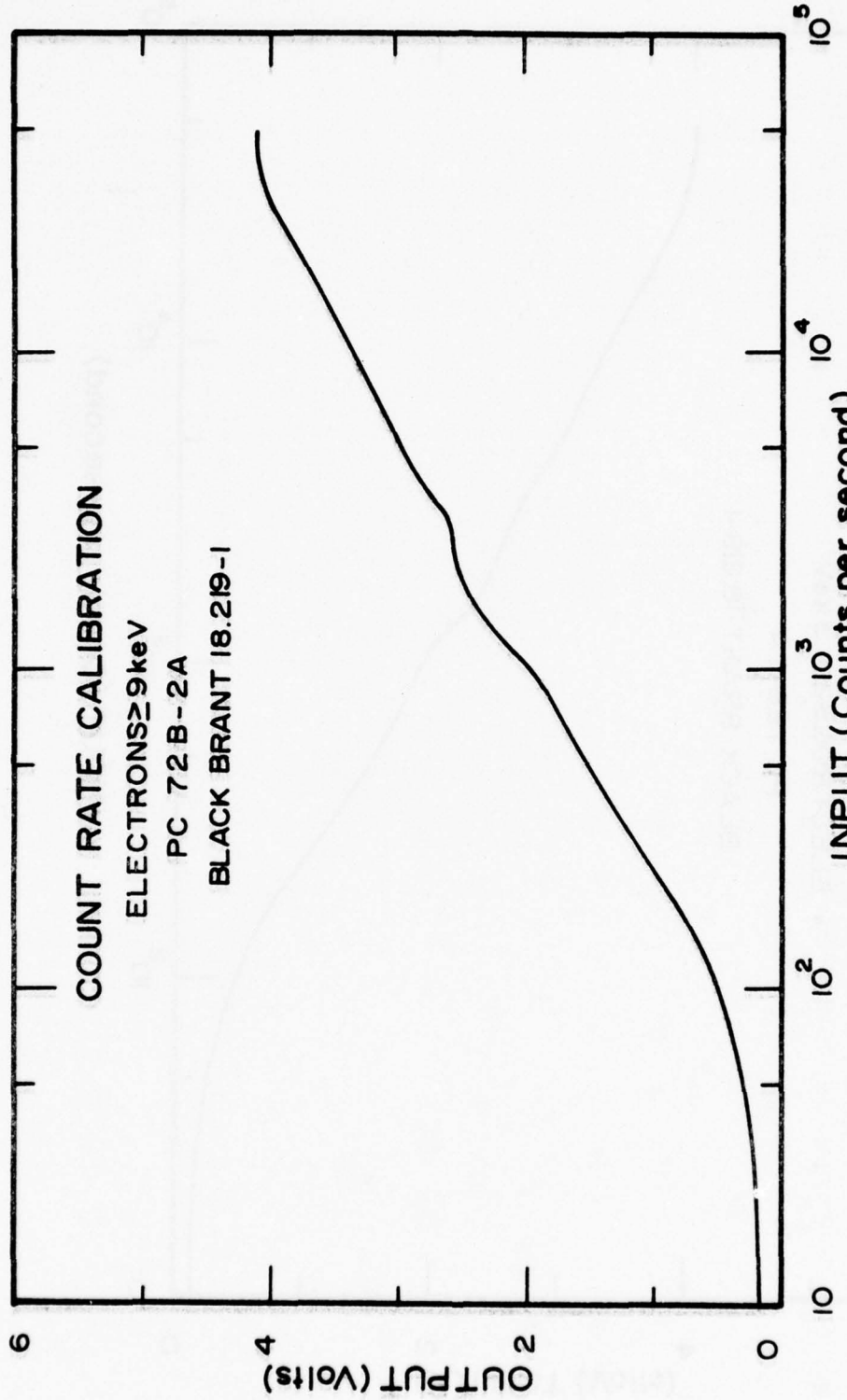


Figure A-12. Particle counter count rate calibration.

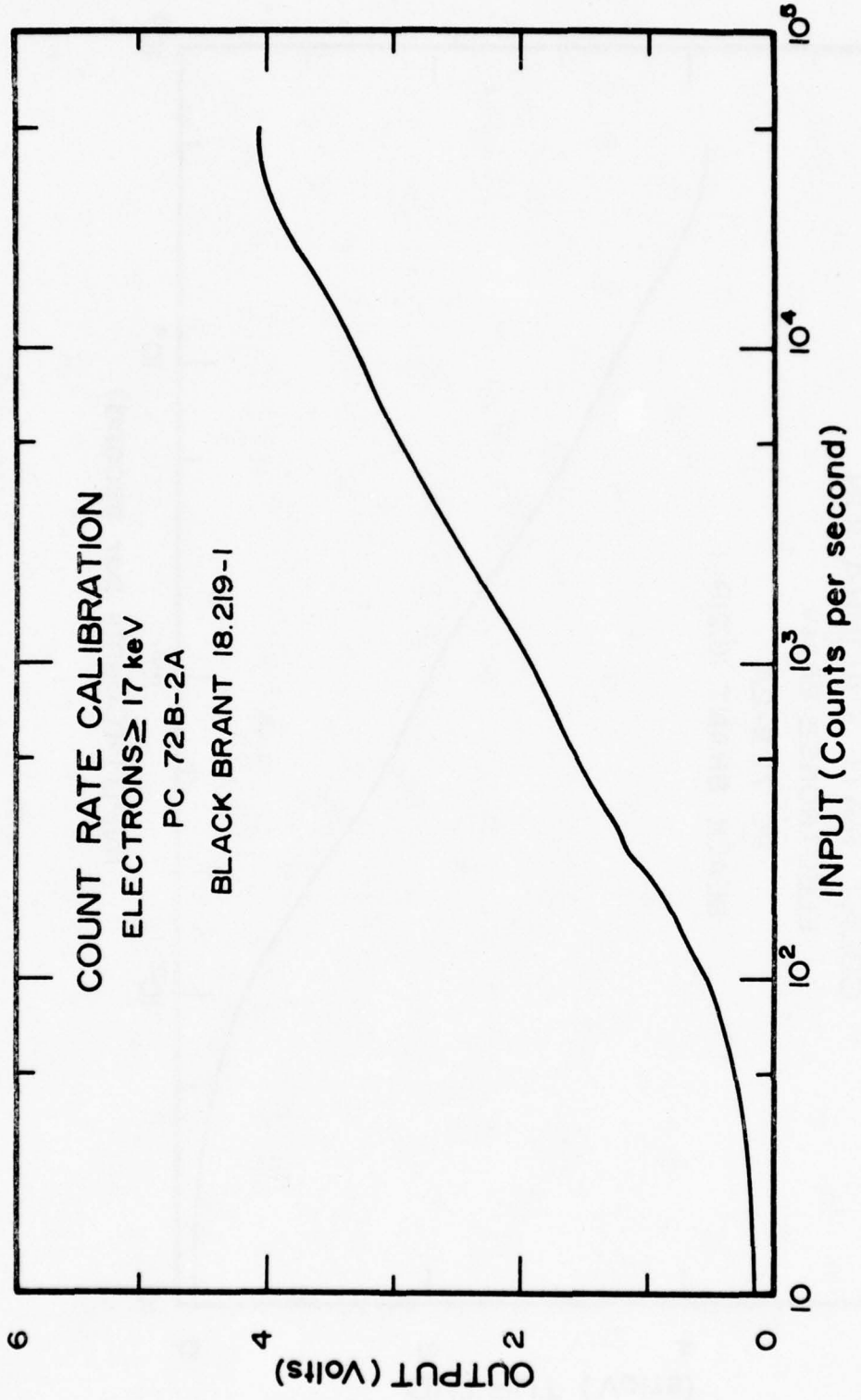


Figure A-13. Particle counter count rate calibration.

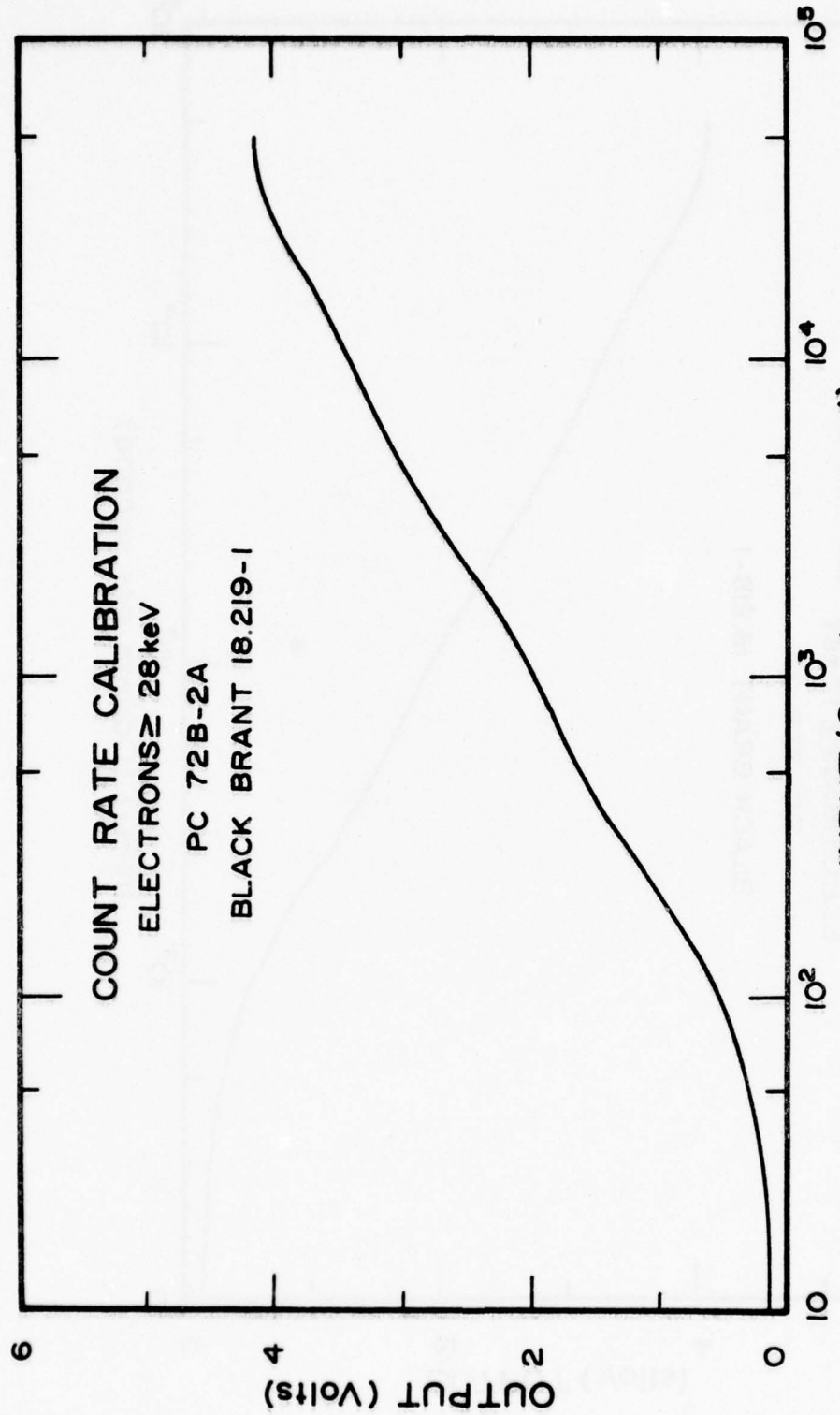


Figure A-14. Particle counter count rate calibration.

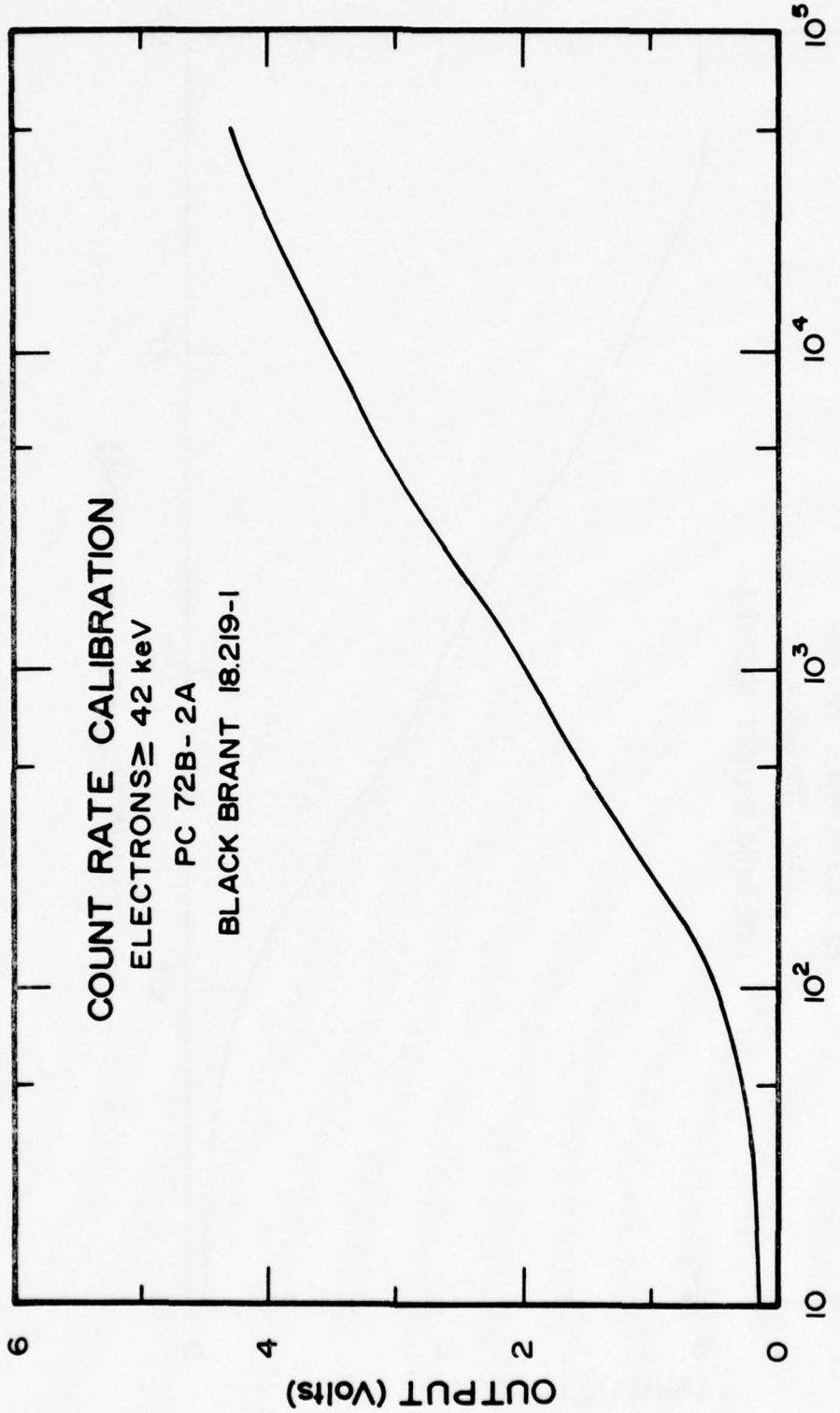


Figure A-15. Particle counter count rate calibration.

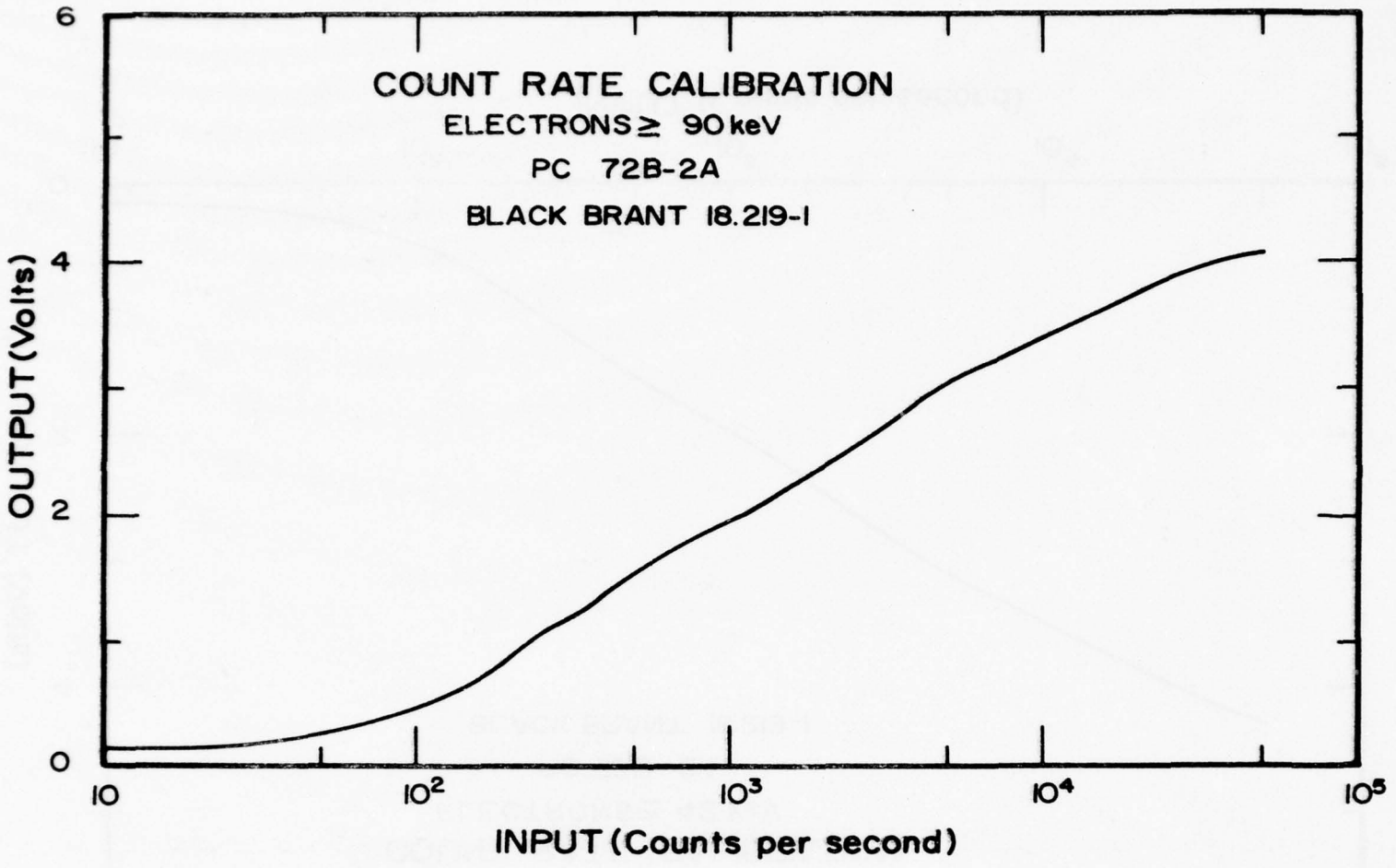


Figure A-16. Particle counter count rate calibration.

TABLE A-9

PC 72B-2A COUNT RATE CALIBRATION POINTS

Input (Counts/second)	Output (volts) 4.5 keV	9 keV	17 keV	28 keV	42 keV	90 keV
0	.04	.07	.07	.04	.03	.05
50	.27	.31	.31	.29	.25	.26
75	.36	.37	.42	.41	.35	.36
100	.50	.52	.55	.55	.48	.47
150	.68	.72	.79	.80	.70	.68
200	.89	.91	.98	1.00	.90	.87
250	1.07	1.08	1.18	1.17	1.07	1.04
300	1.19	1.21	1.27	1.30	1.20	1.17
400	1.41	1.41	1.45	1.48	1.41	1.38
500	1.53	1.54	1.59	1.62	1.57	1.54
700	1.72	1.72	1.75	1.78	1.76	1.73
1000	1.92	1.93	1.95	1.98	1.97	1.94
1300	2.10	2.23	2.10	2.13	2.13	2.09
1600	2.36	2.39	2.24	2.27	2.27	2.24
2000	2.47	2.50	2.40	2.43	2.44	2.40
2500	2.54	2.57	2.55	2.59	2.60	2.56
3000	2.66	2.62	2.67	2.72	2.74	2.69
4000	2.85	2.84	2.85	2.91	2.94	2.89
5000	2.98	2.97	2.97	3.05	3.08	3.02
7000	3.15	3.16	3.14	3.22	3.26	3.19
9000	3.29	3.29	3.26	3.35	3.39	3.33
10000	3.34	3.34	3.33	3.41	3.45	3.39
12000	3.43	3.44	3.42	3.51	3.56	3.48
14000	3.54	3.55	3.51	3.60	3.65	3.57
16000	3.61	3.62	3.59	3.68	3.73	3.65
18000	3.69	3.70	3.66	3.75	3.77	3.68
20000	3.75	3.76	3.72	3.81	3.83	3.74
25000	3.88	3.89	3.86	3.94	3.96	3.86
30000	3.97	3.99	3.96	4.02	4.06	3.94
50000	4.00	4.08	4.16	4.17	4.24	4.08

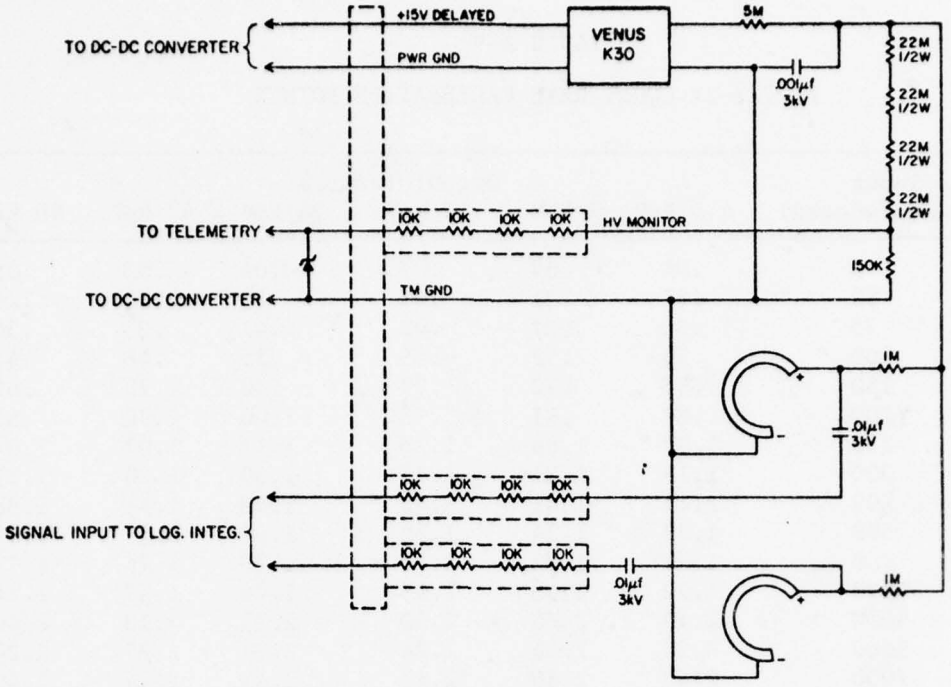


Figure A-17. Particle counter channeltron board schematic diagram.

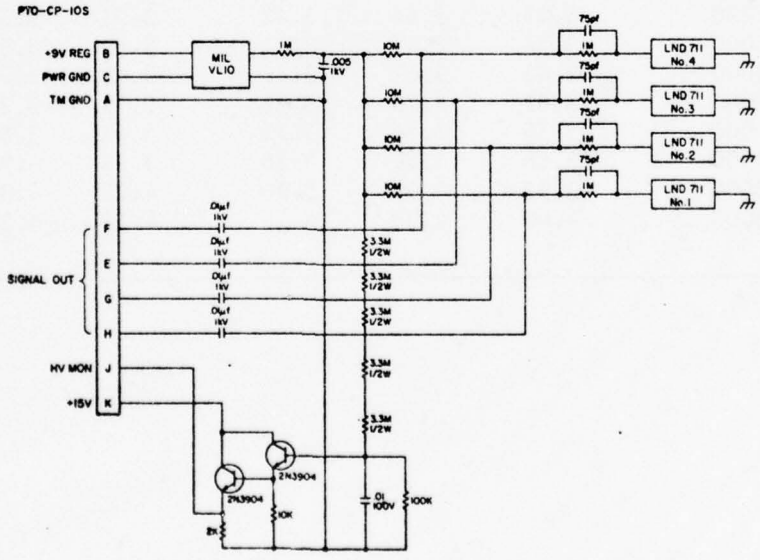


Figure A-18. Particle counter geiger tube board schematic diagram.

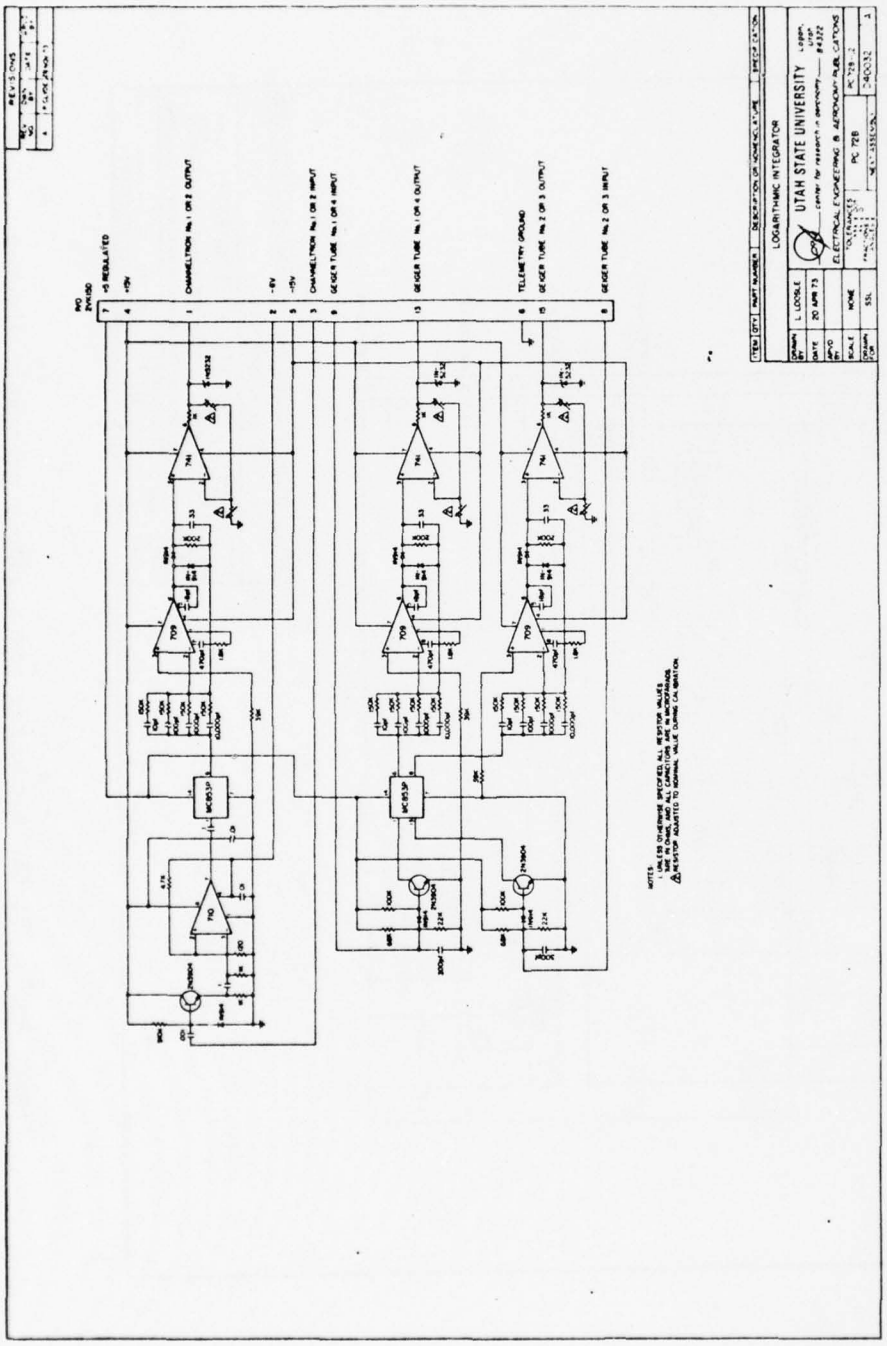


Figure A-19. Particle counter logarithmic integrator board schematic diagram.

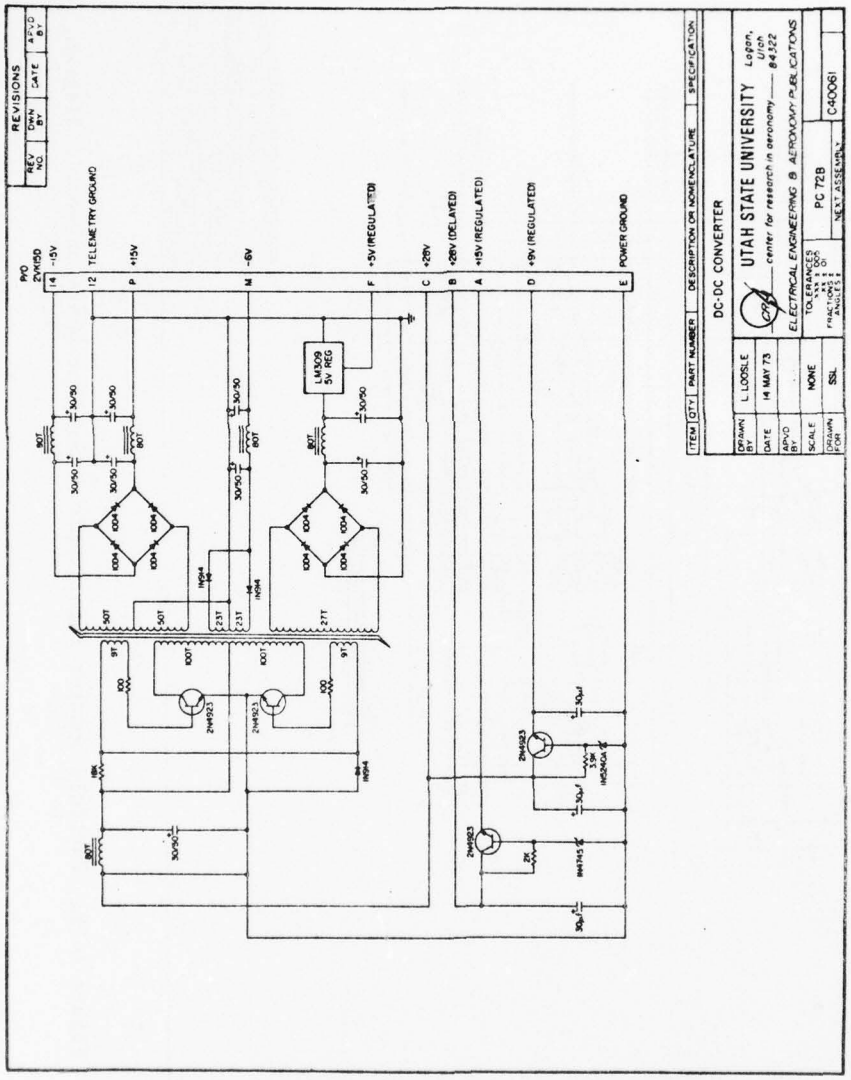


Figure A-20. Particle counter power supply schematic diagram.

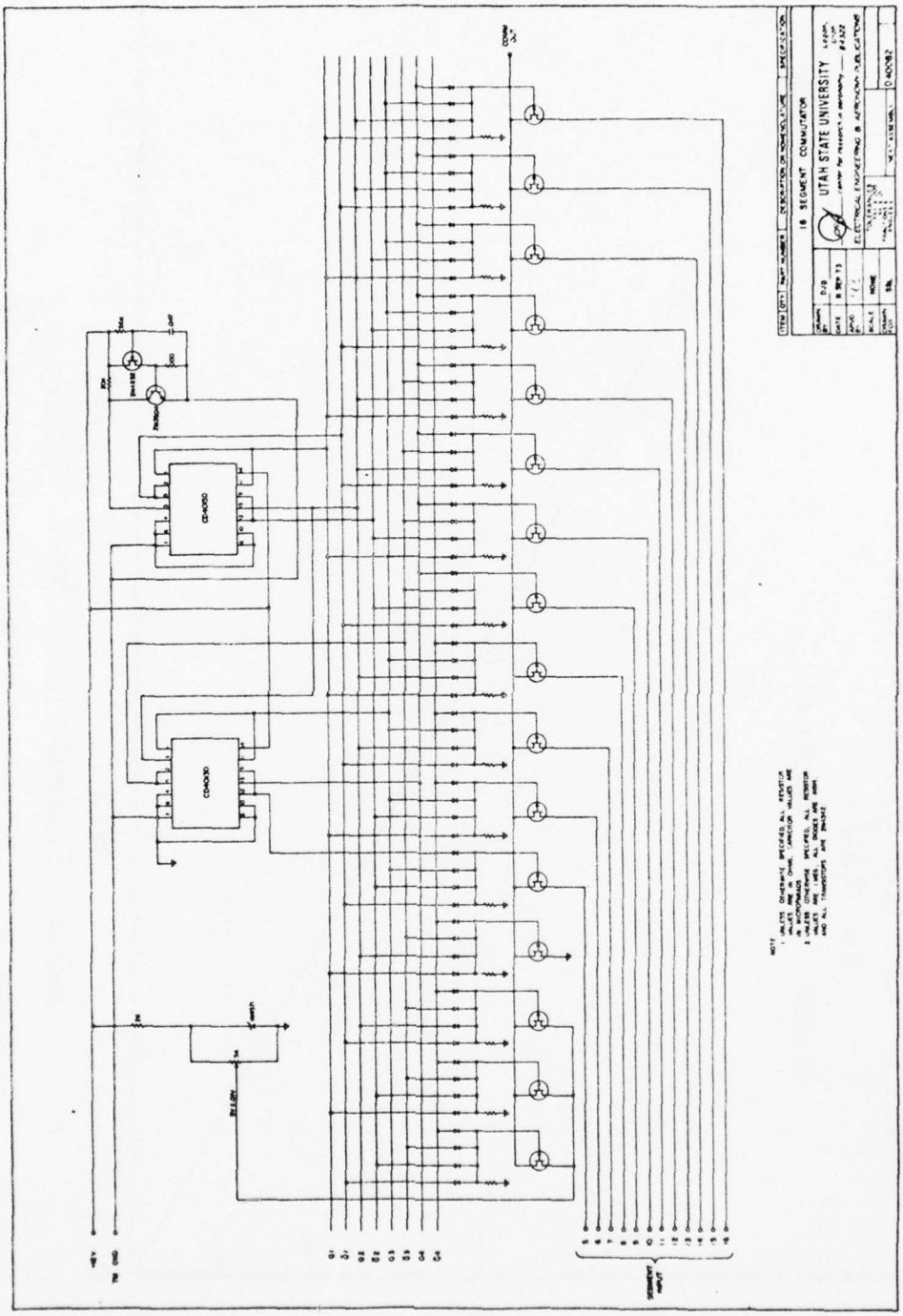


Figure A-21. Particle counter 16 segment commutator schematic diagram.

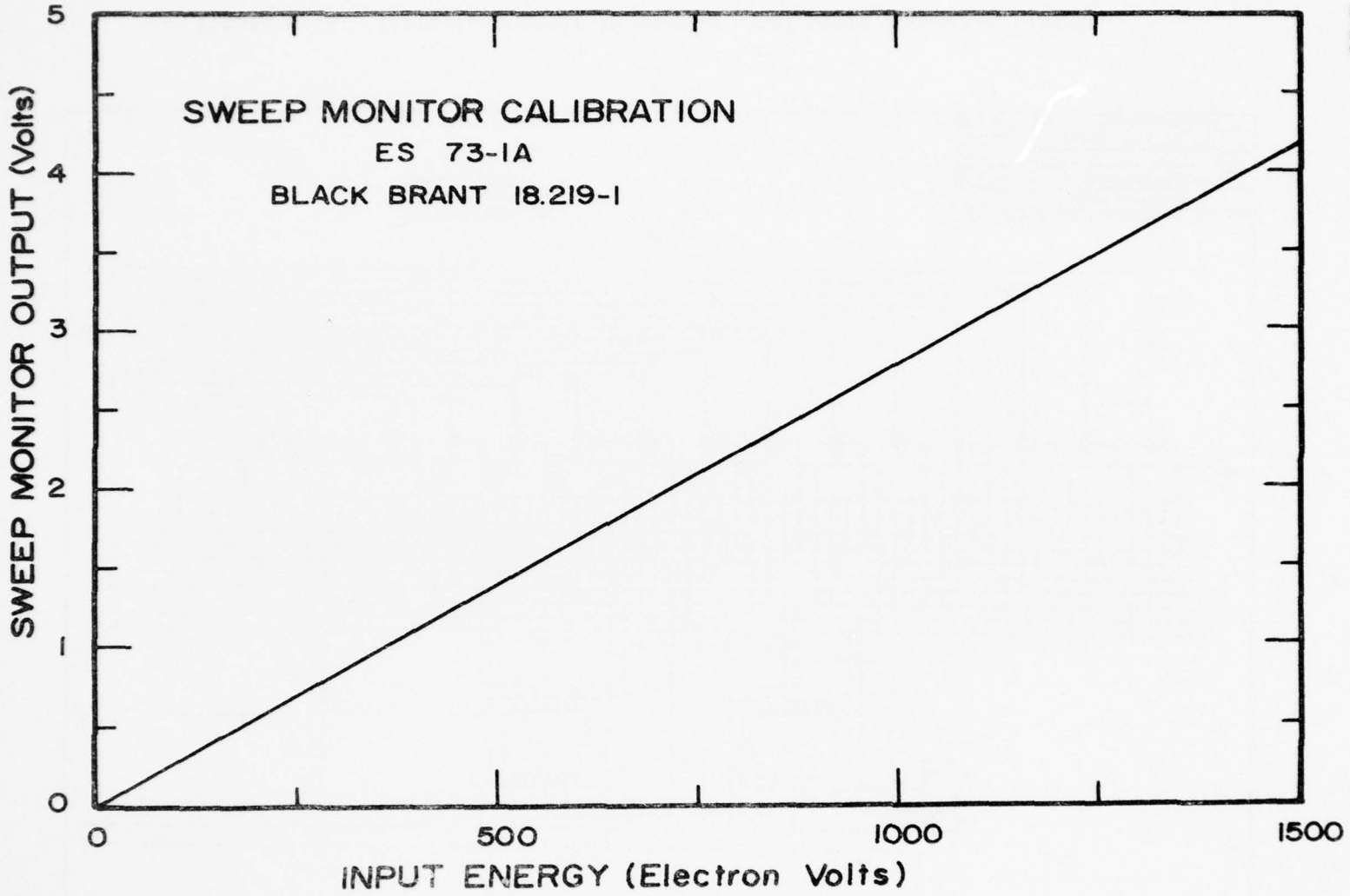


Figure A-22. Electron spectrometer energy calibration.

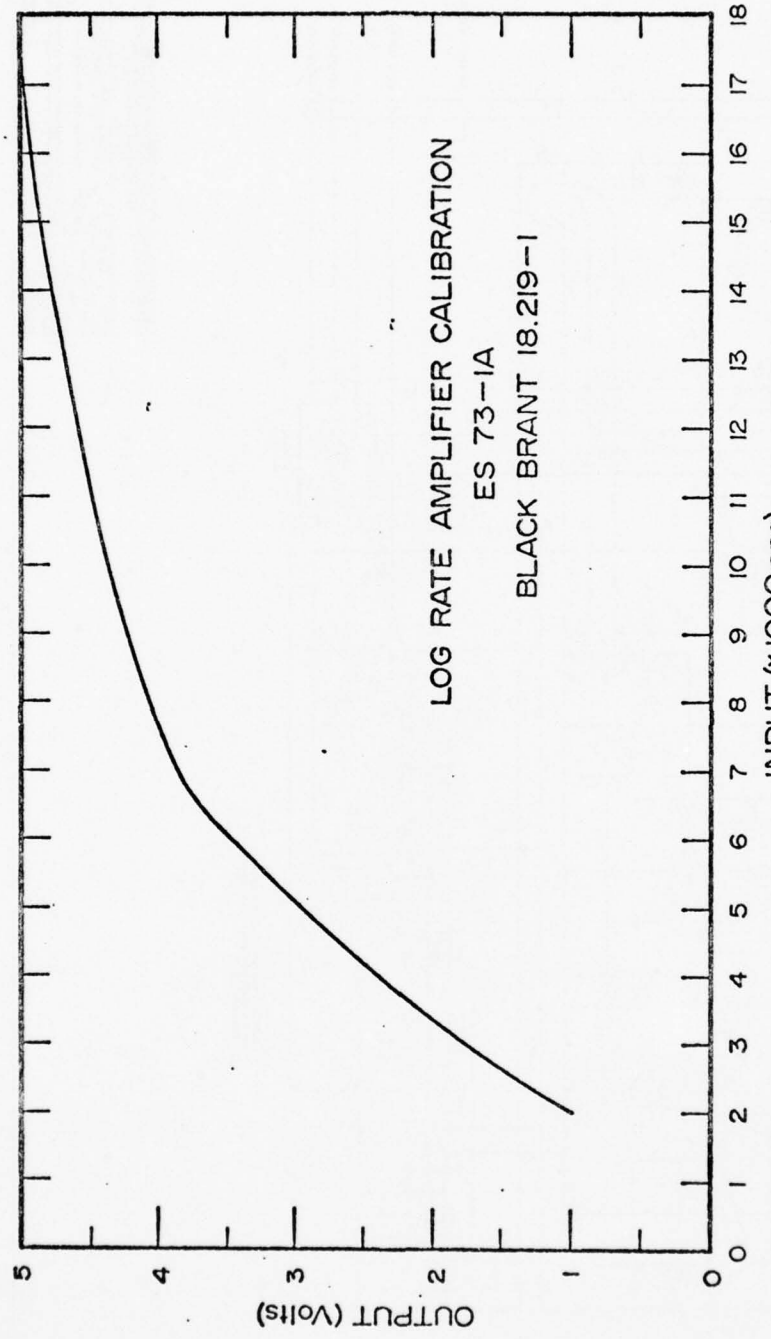


Figure A-23. Electron spectrometer log rate calibration.

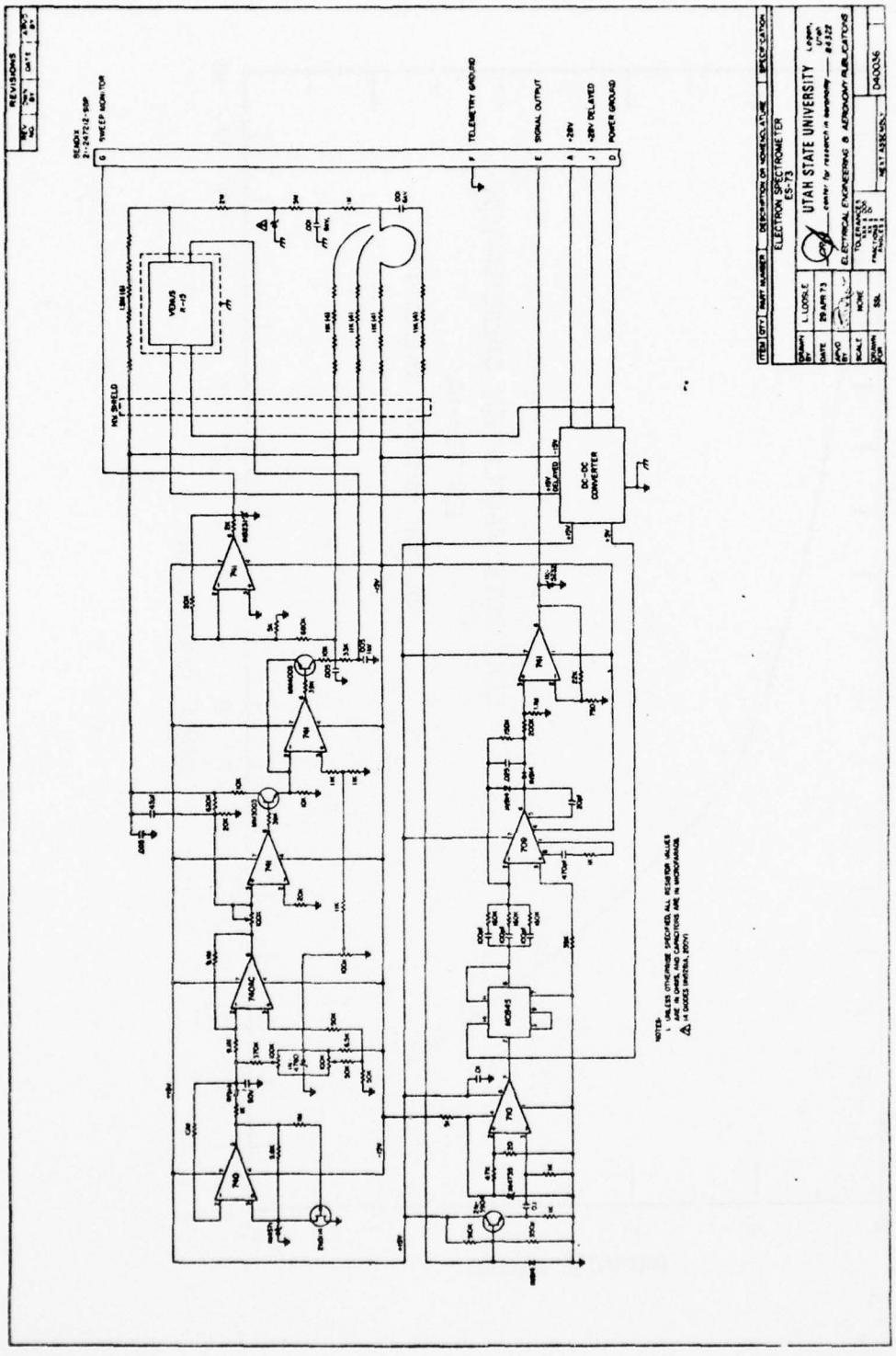


Figure A-24. Electron spectrometer schematic diagram.

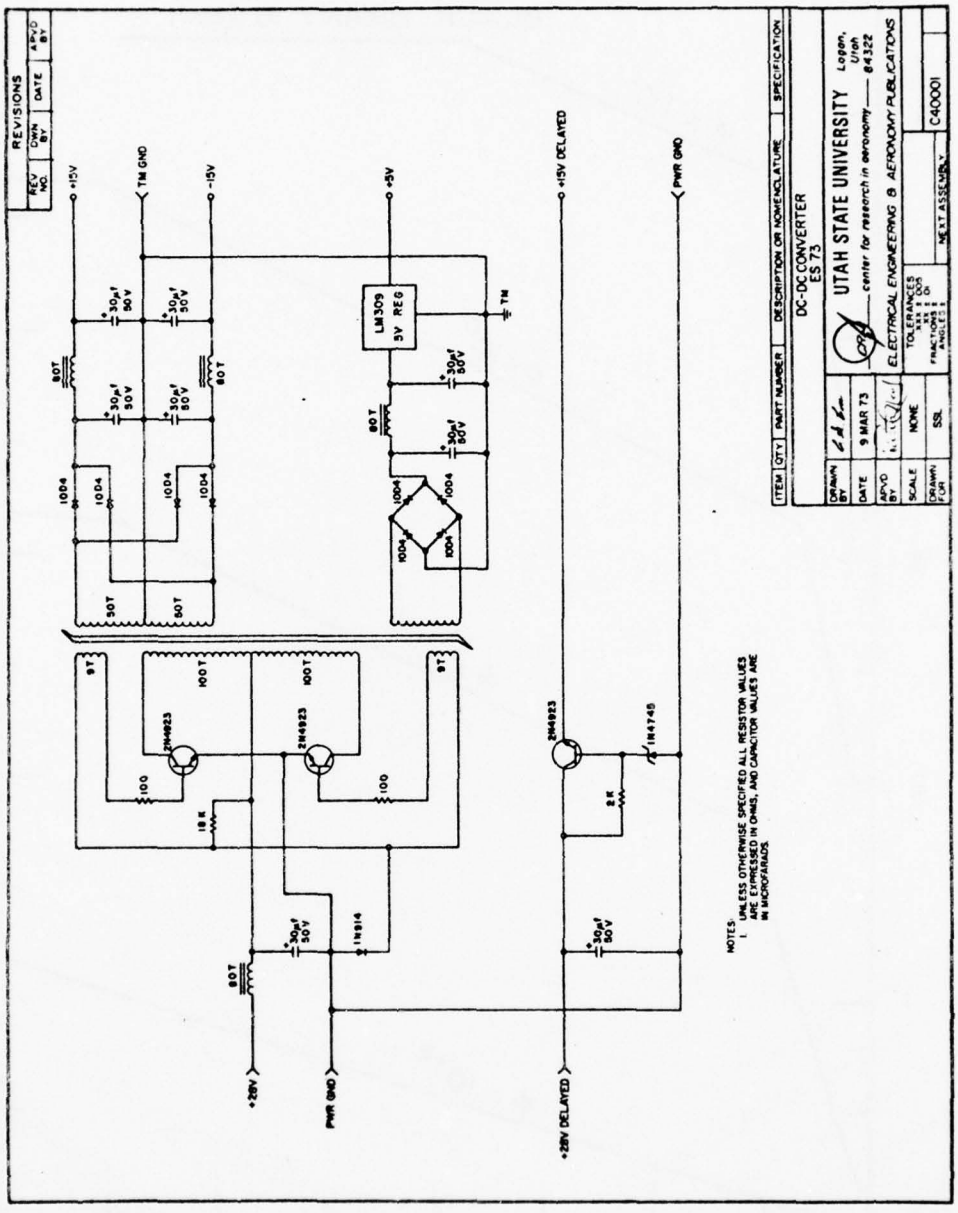


Figure A-25. Electron spectrometer DC-DC converter.

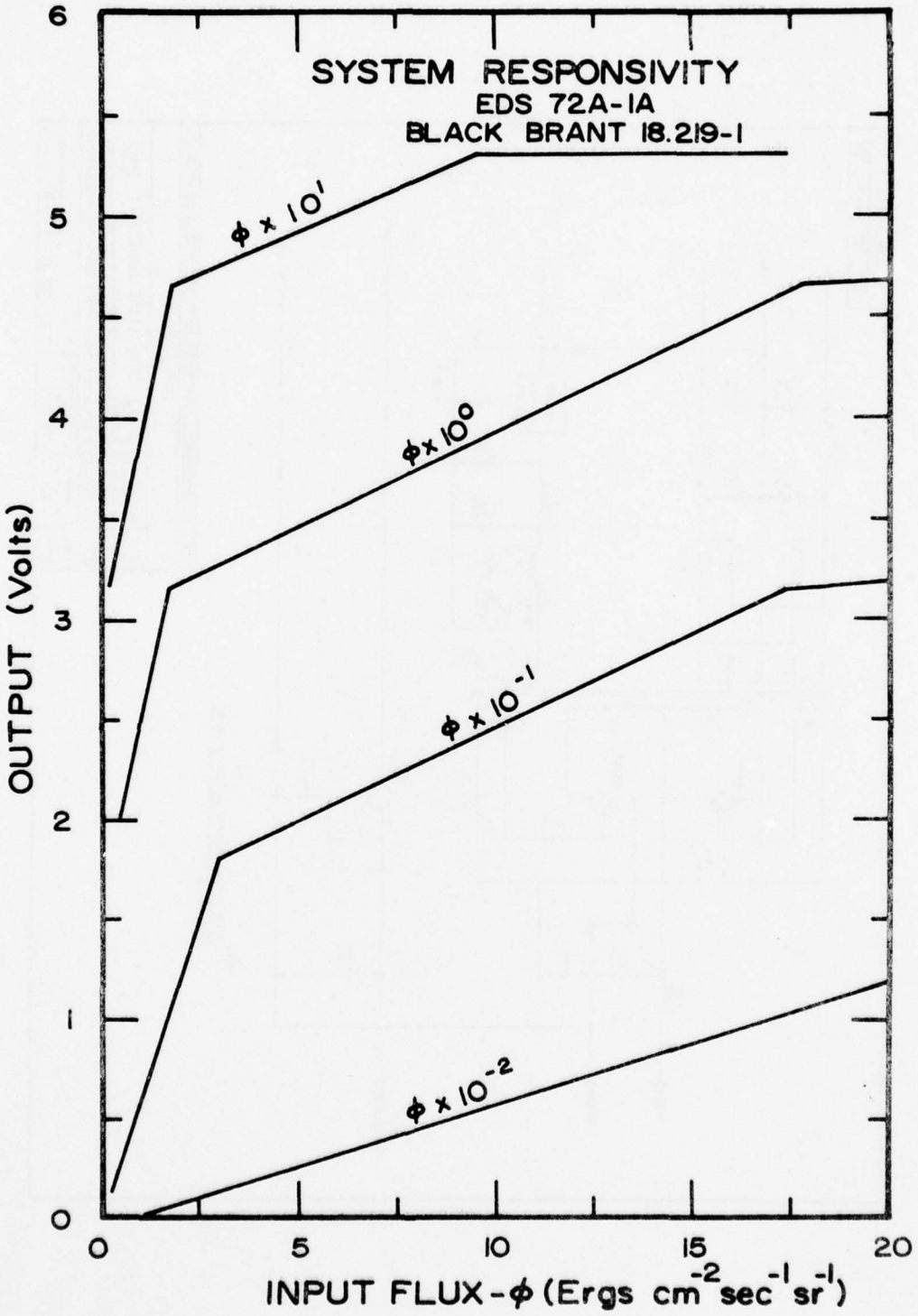


Figure A-26. Energy deposition scintillator responsivity.

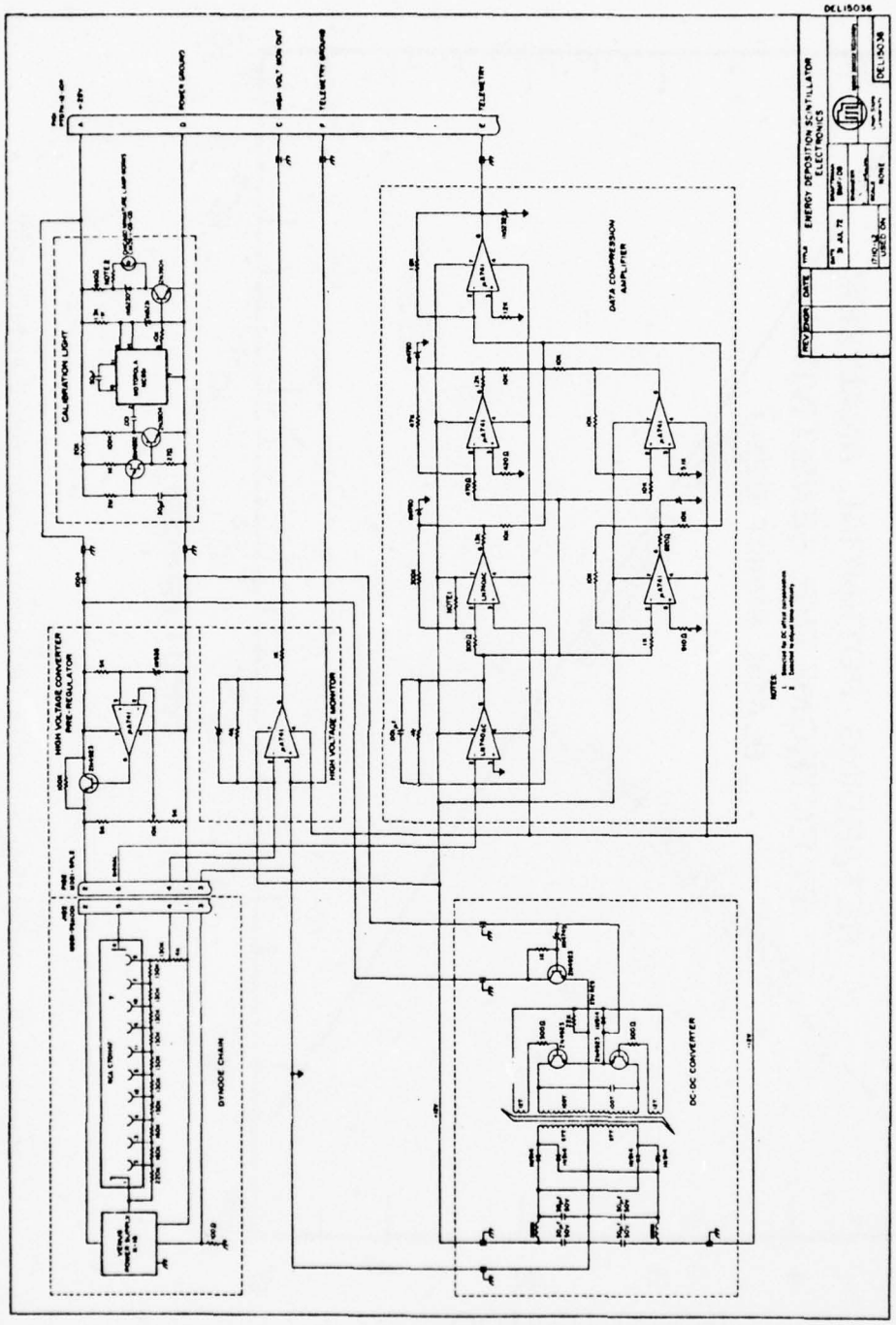


Figure A-27. Energy deposition scintillator schematic diagram.

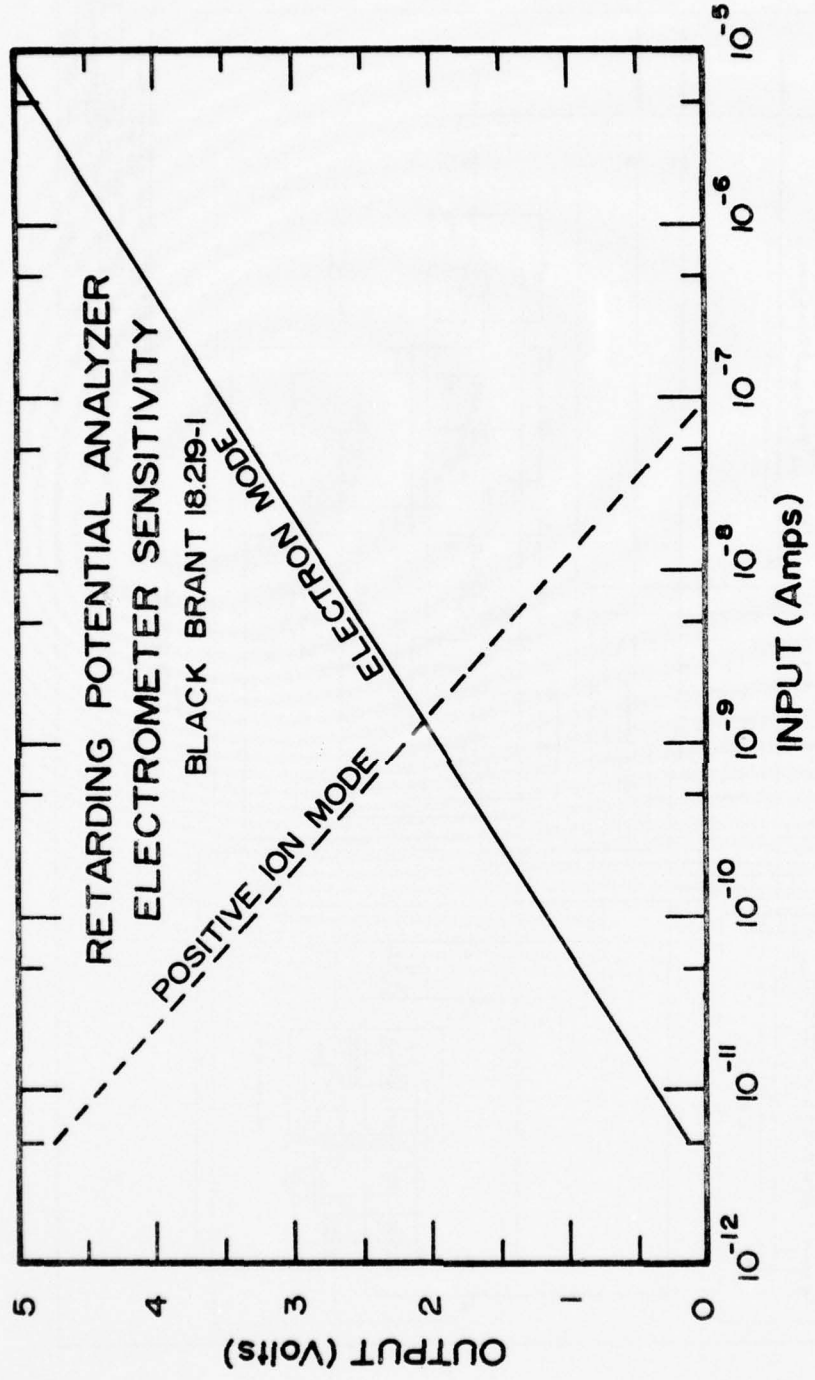


Figure A-28. Retarding potential analyzer electrometer sensitivity.

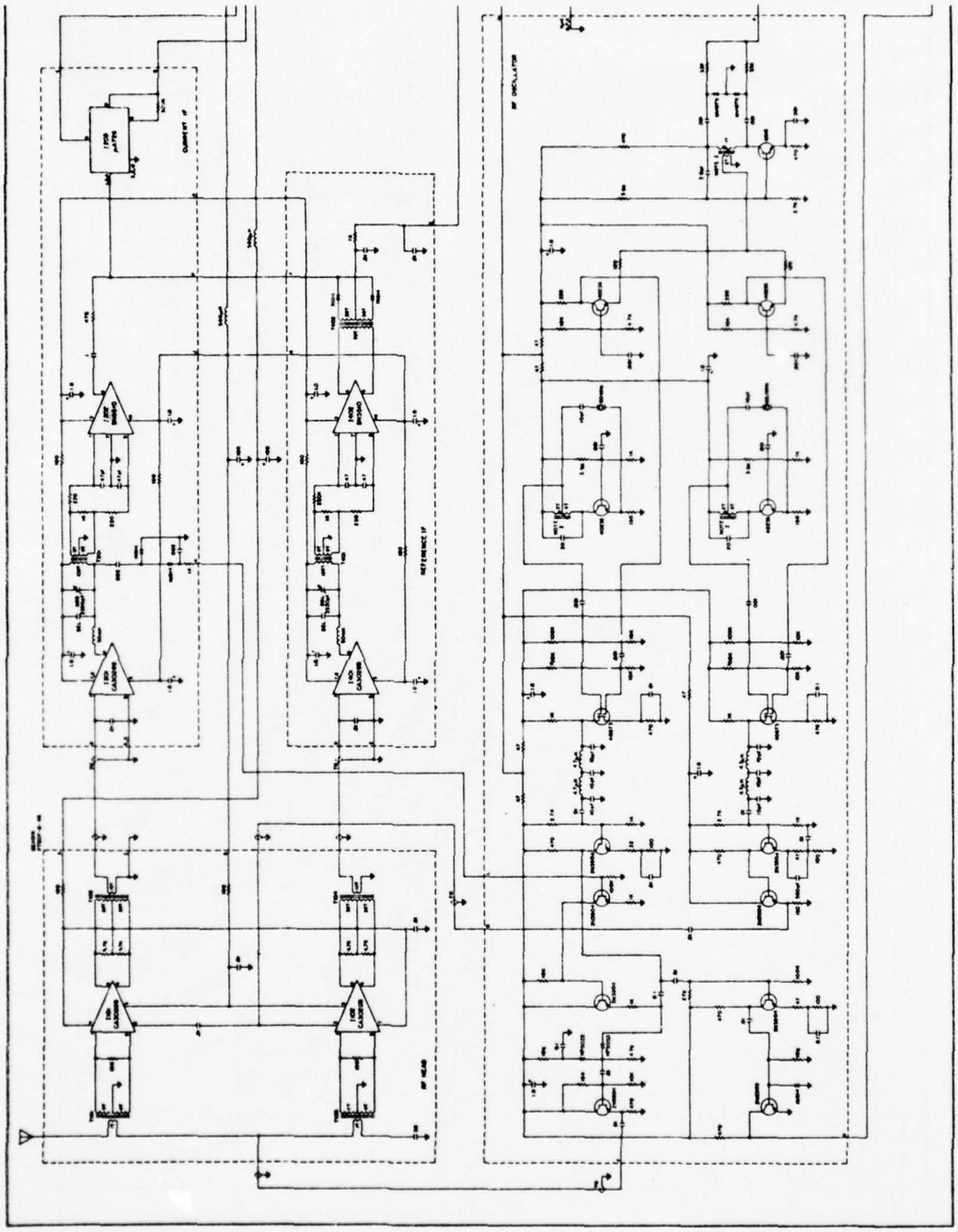


Figure A-29. Plasma frequency probe schematic diagram (page 1 of 2).

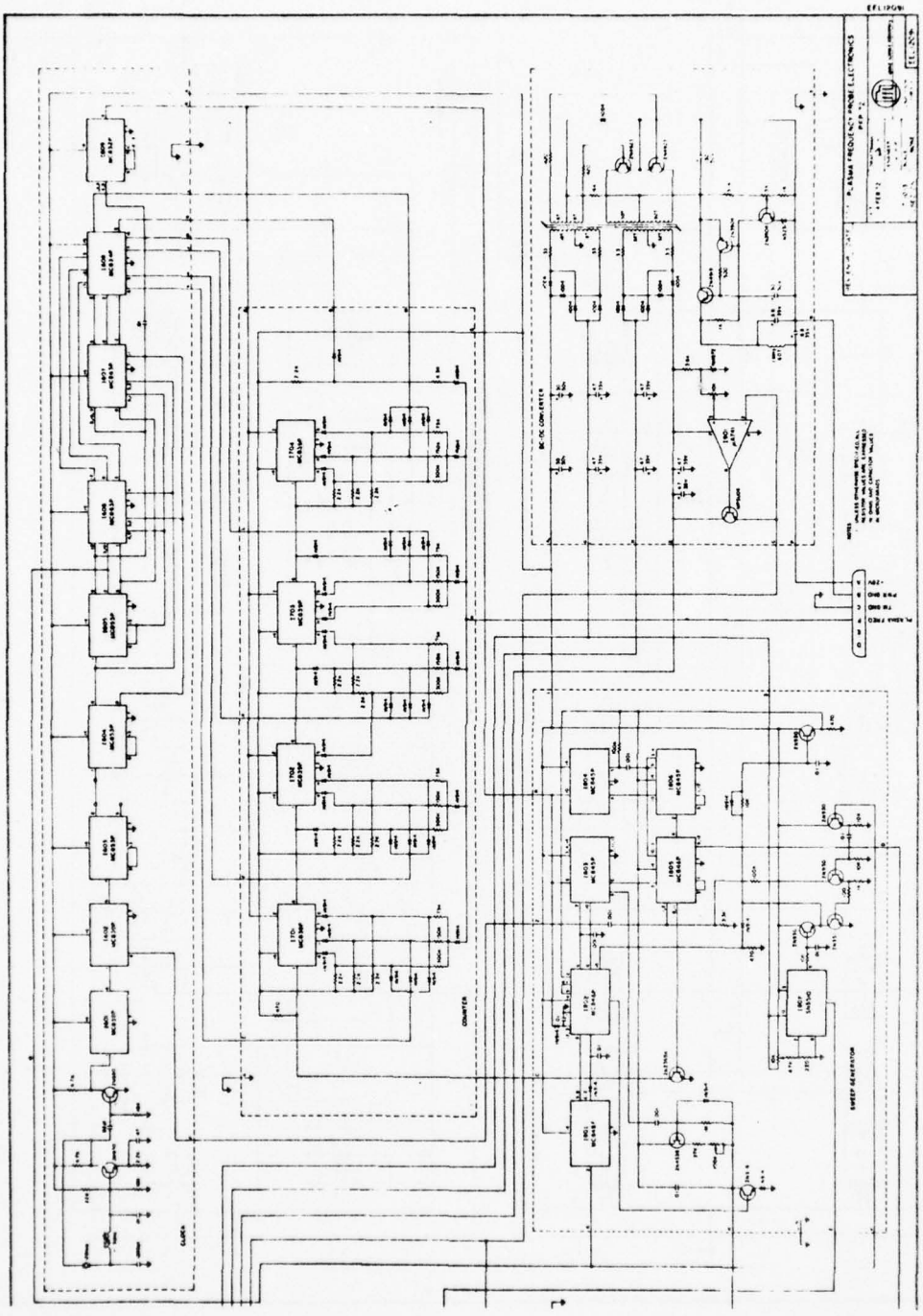


Figure A-29. Plasma frequency probe schematic diagram (page 2 of 2).

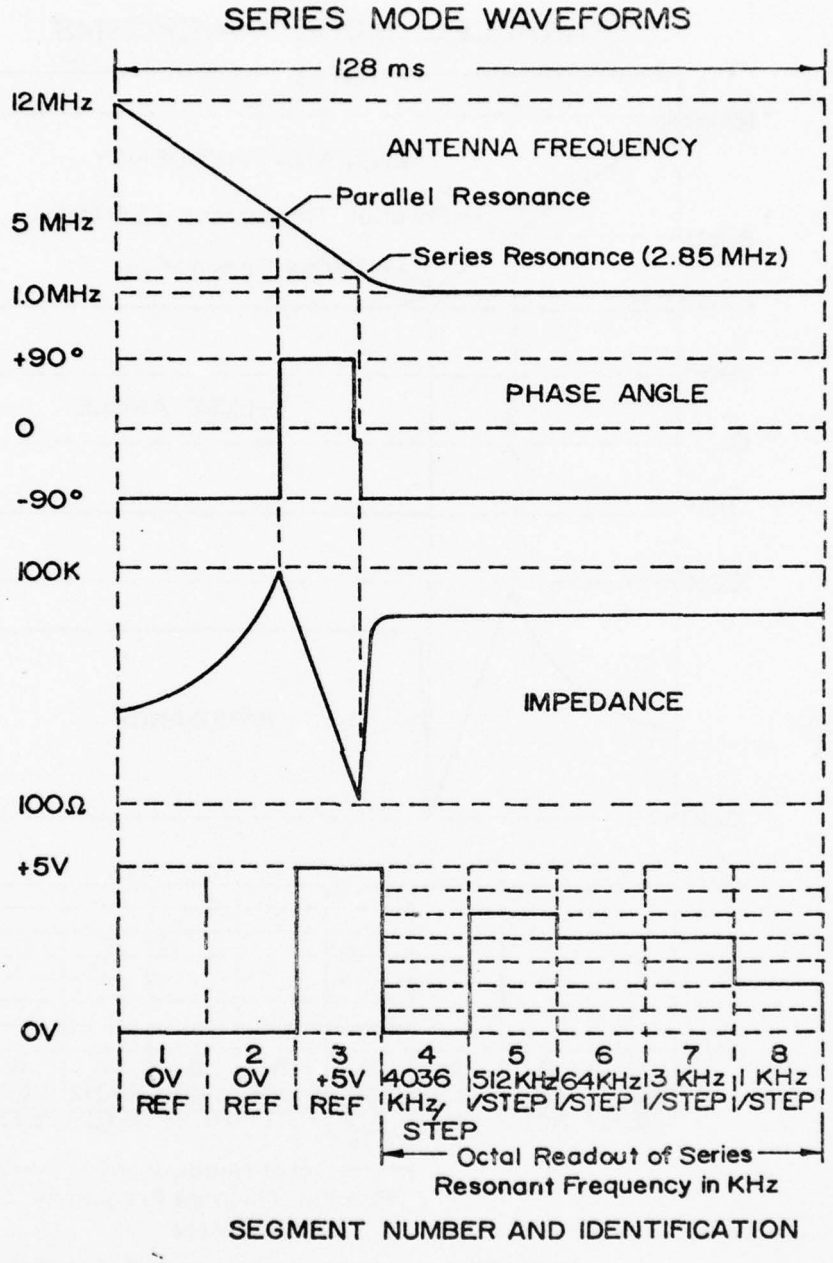


Figure A-30. Plasma frequency probe series mode output format.

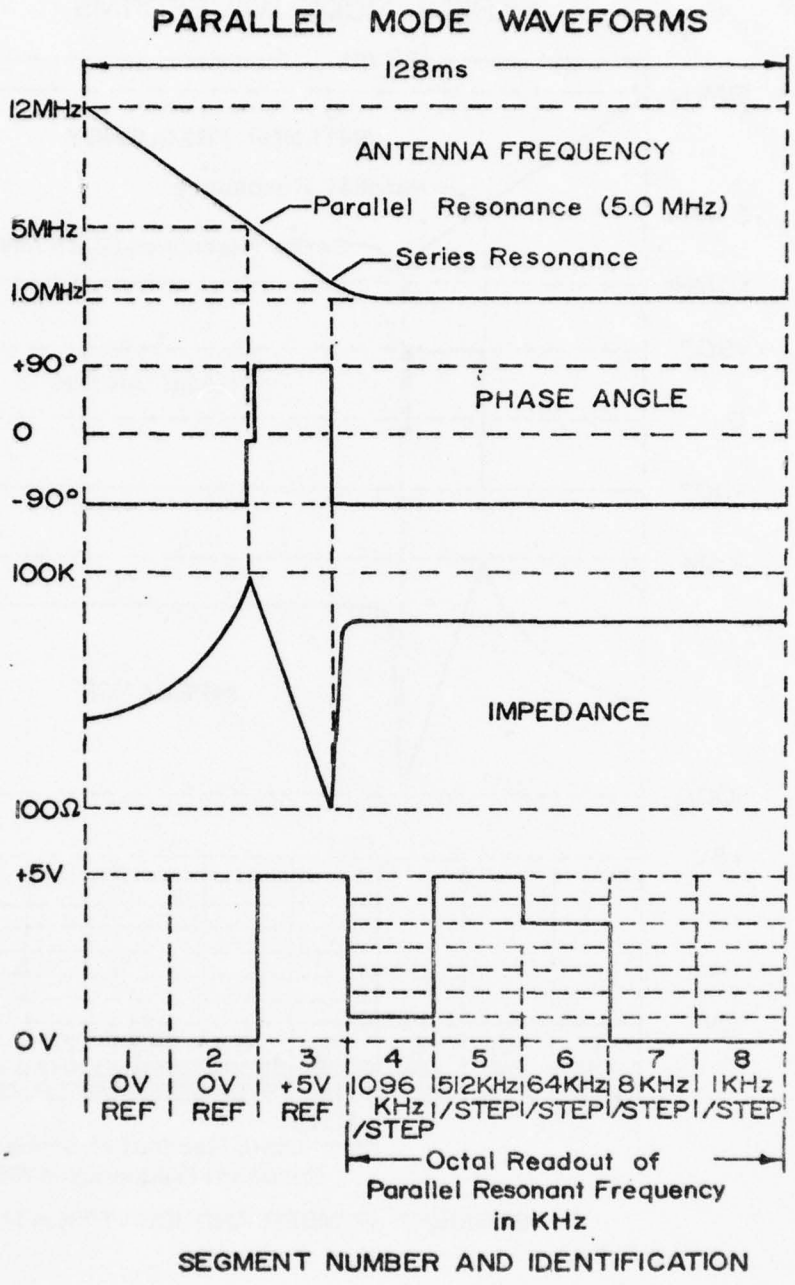


Figure A-31. Plasma frequency probe parallel mode output format.

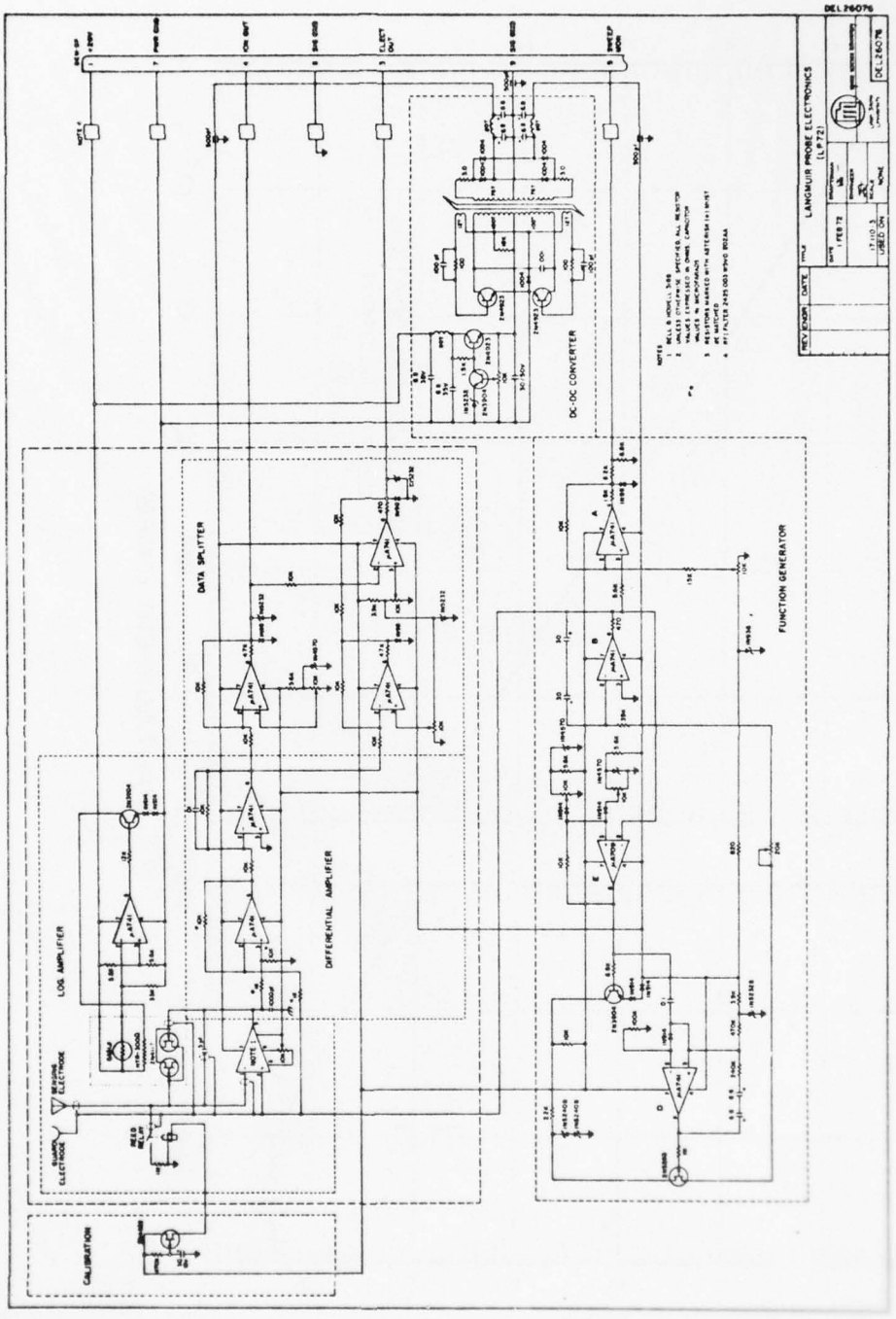


Figure A-32. Langmuir probe schematic diagram.

AD-A051 169 UTAH STATE UNIV LOGAN ELECTRO-DYNAMICS LAB F/G 4/1
BLACK BRANT 18.219-1 INSTRUMENTATION FOR ICECAP 74A,(U)
JUN 75 D A BURT F19628-73-C-0048
UNCLASSIFIED SCIENTIFIC-3 AFGL-TR-76-0058 NL

2 OF 2
AD
A051169



END
DATE
FILMED
4-78
DDC

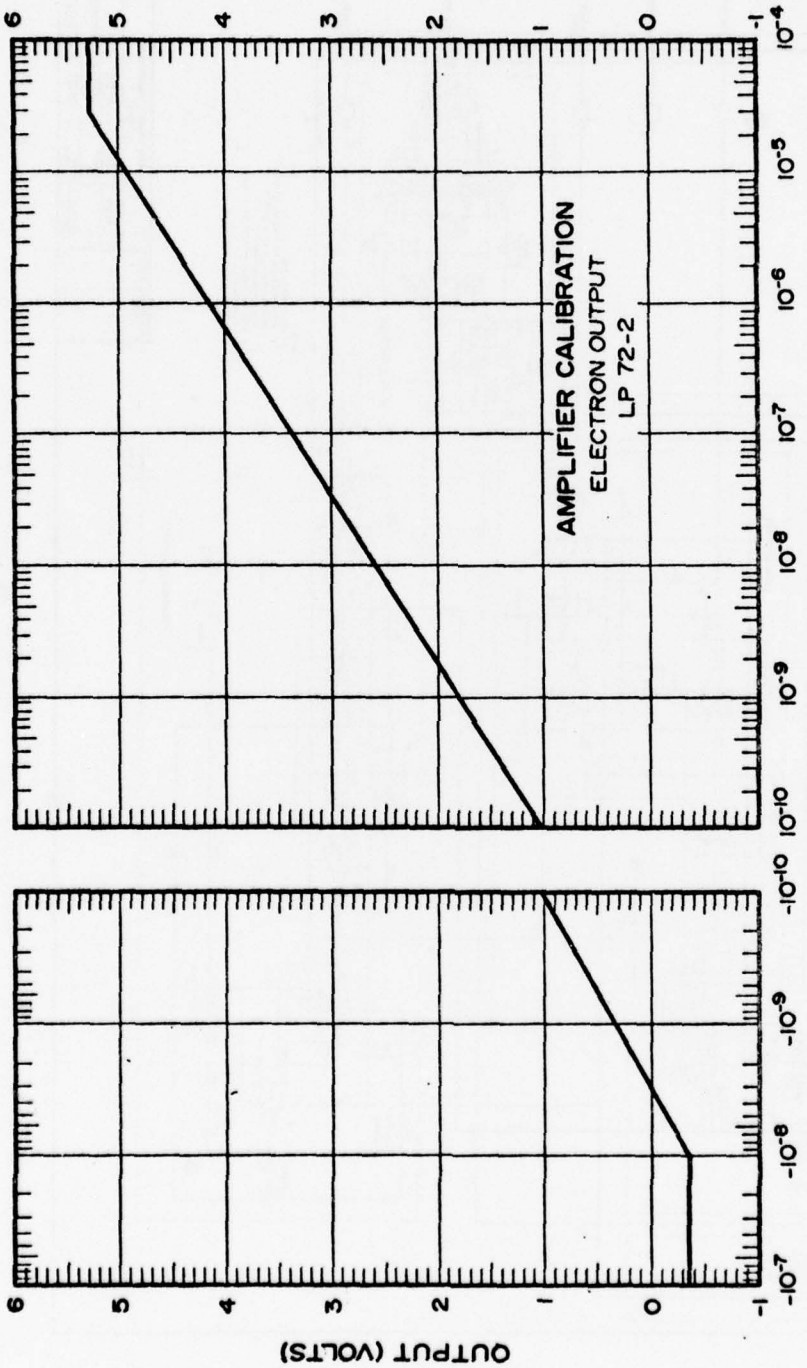


Figure A-33. Langmuir probe amplifier calibration - electron output.

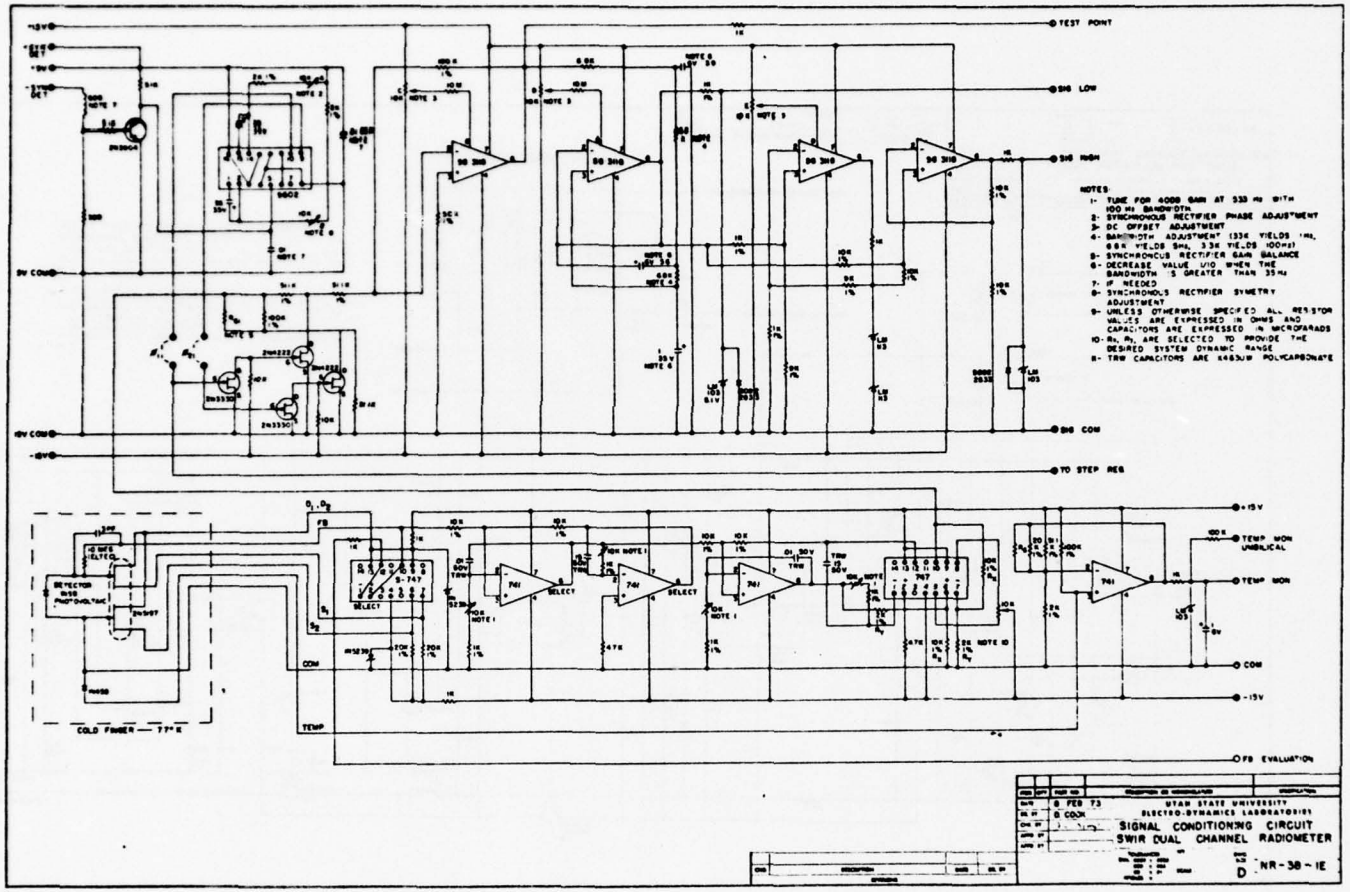


Figure A-34. SWIR dual-channel radiometer signal conditioning electronics schematic diagram.

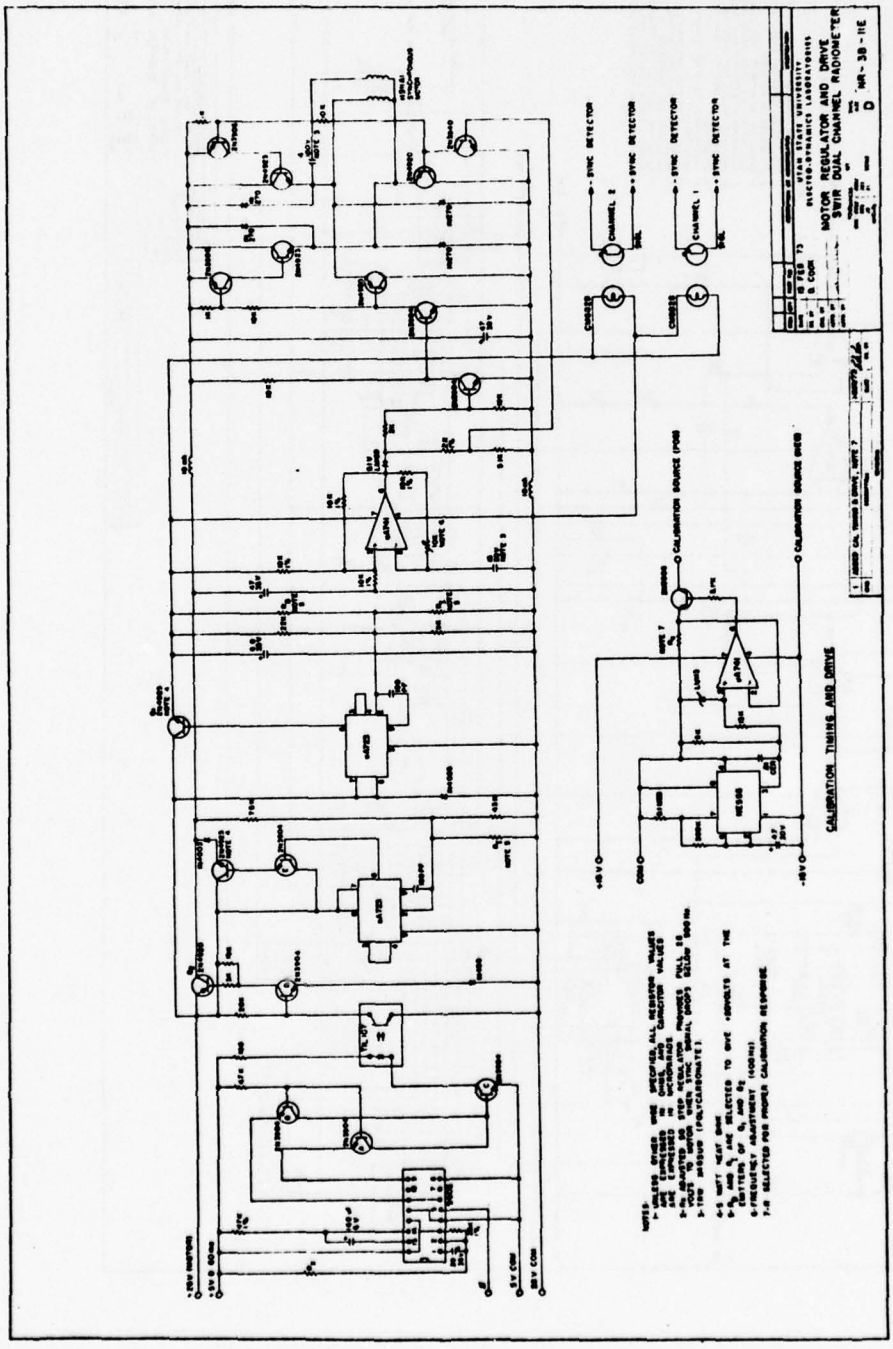


Figure A-35. SWIR dual-channel radiometer motor regulator and drive schematic diagram.

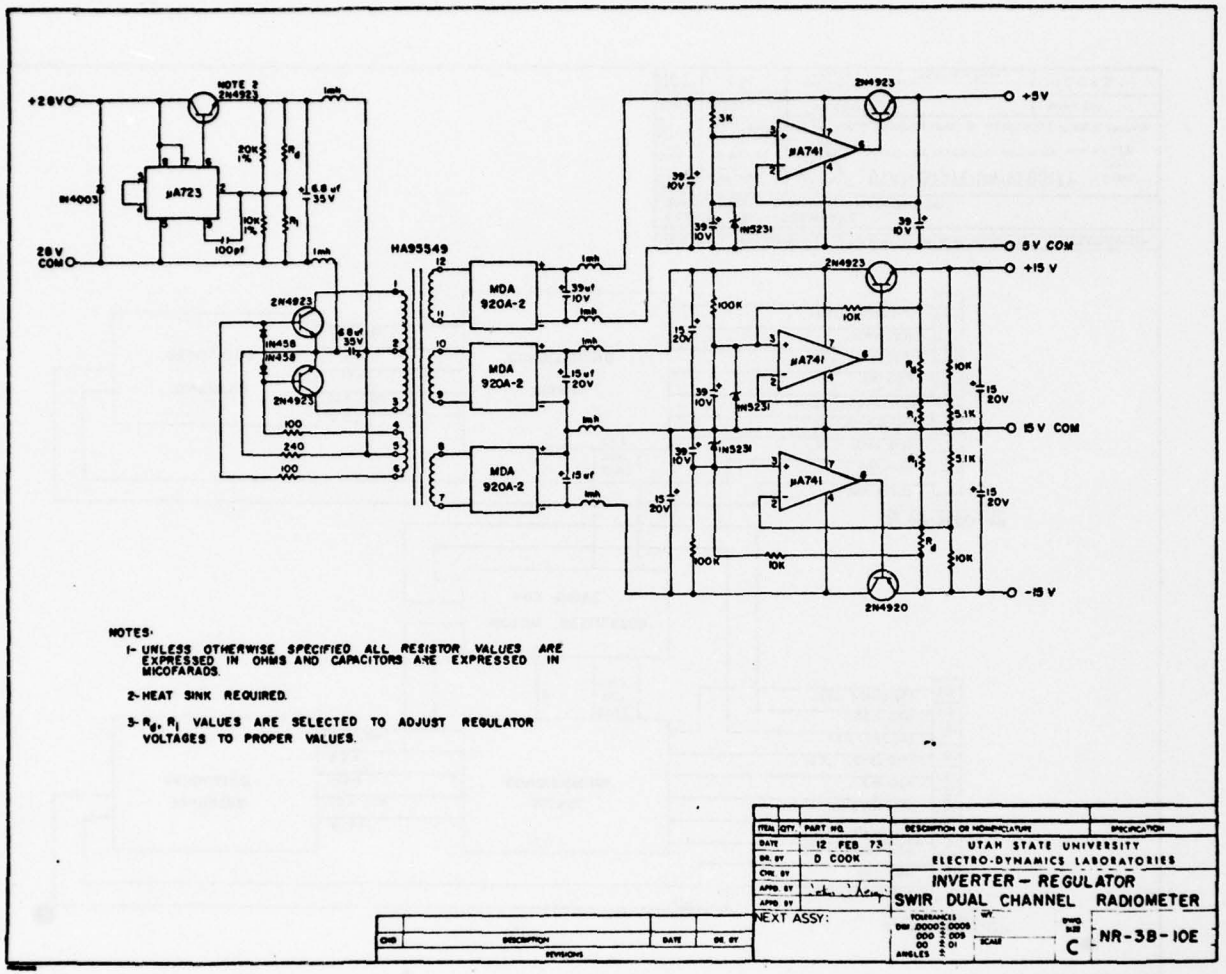


Figure A-36. SWIR dual-channel radiometer inverter-regulator schematic diagram.

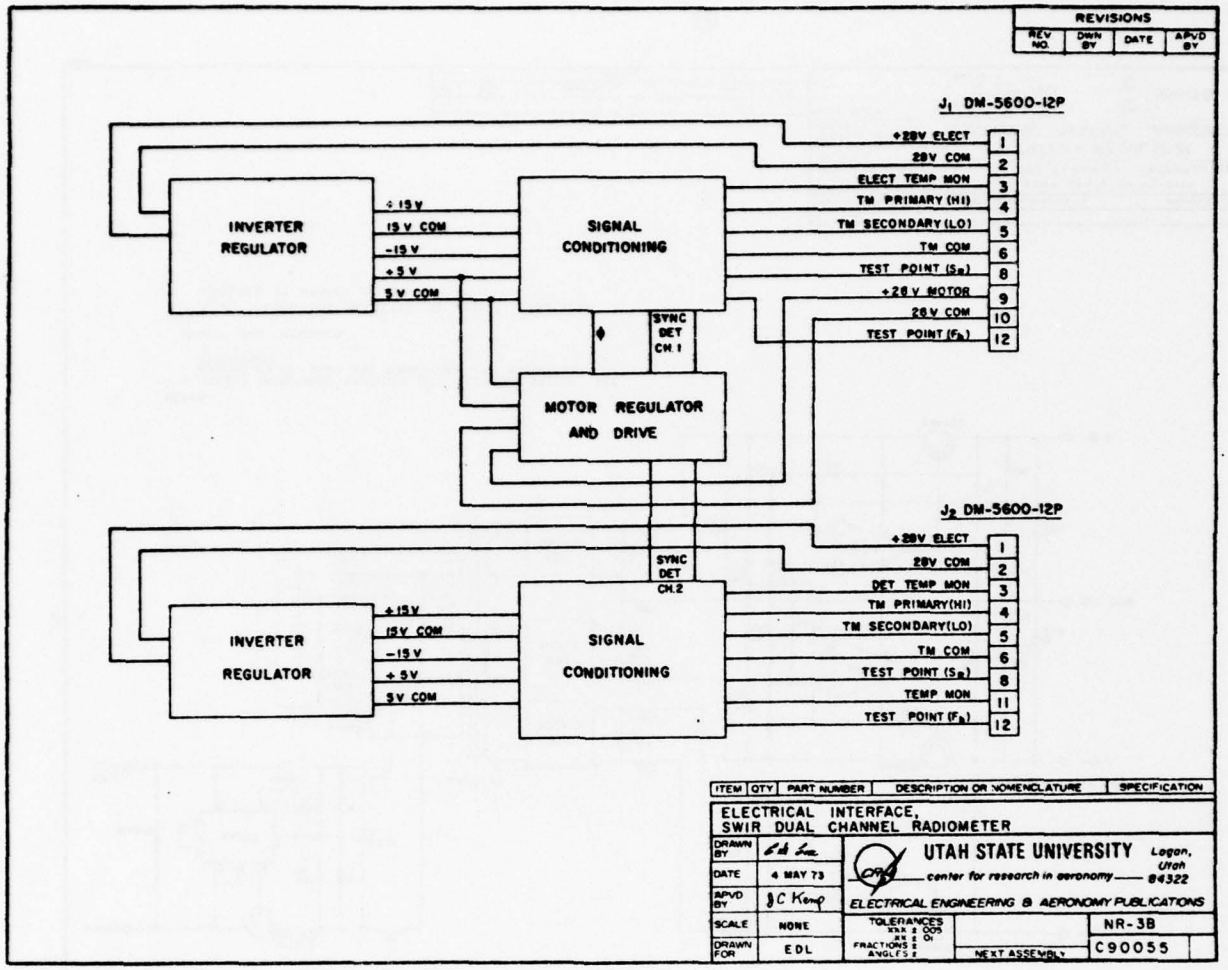


Figure A-37. SWIR dual-channel radiometer electrical interface.

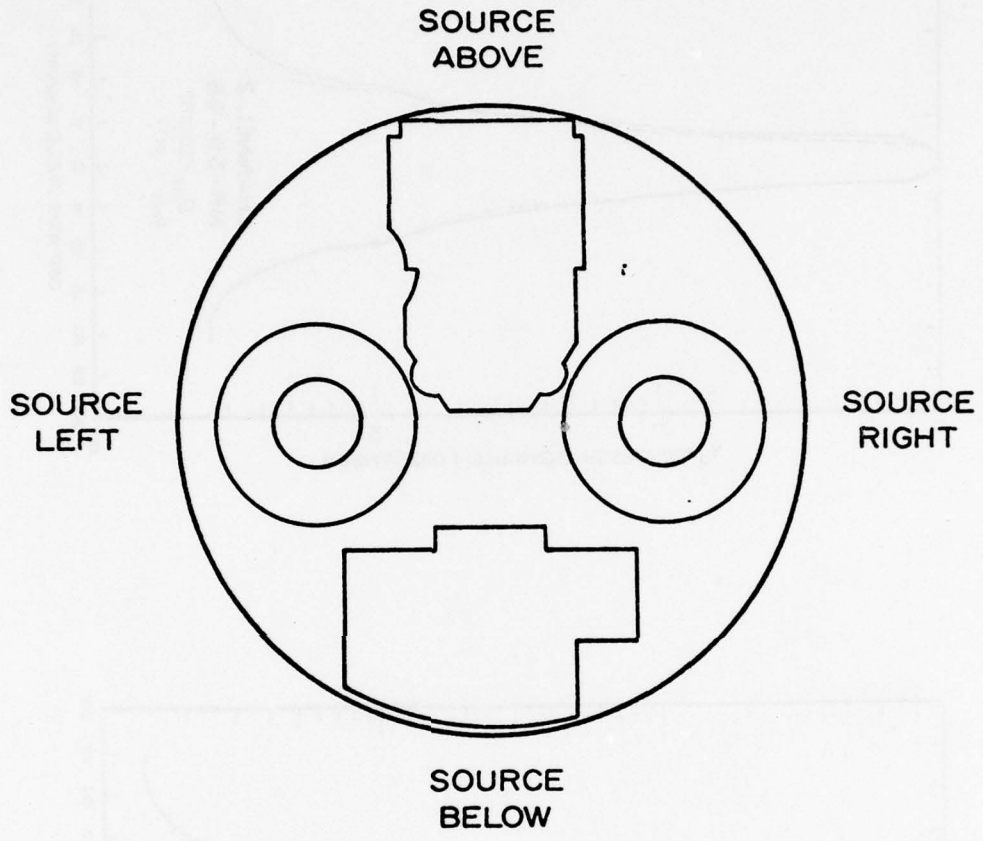


Figure A-38. Raddiometer and spectrometer orientation (looking at aft end of instrument) for field of view measurements shown in Figures A-39, A-43, A-50 and A-51.

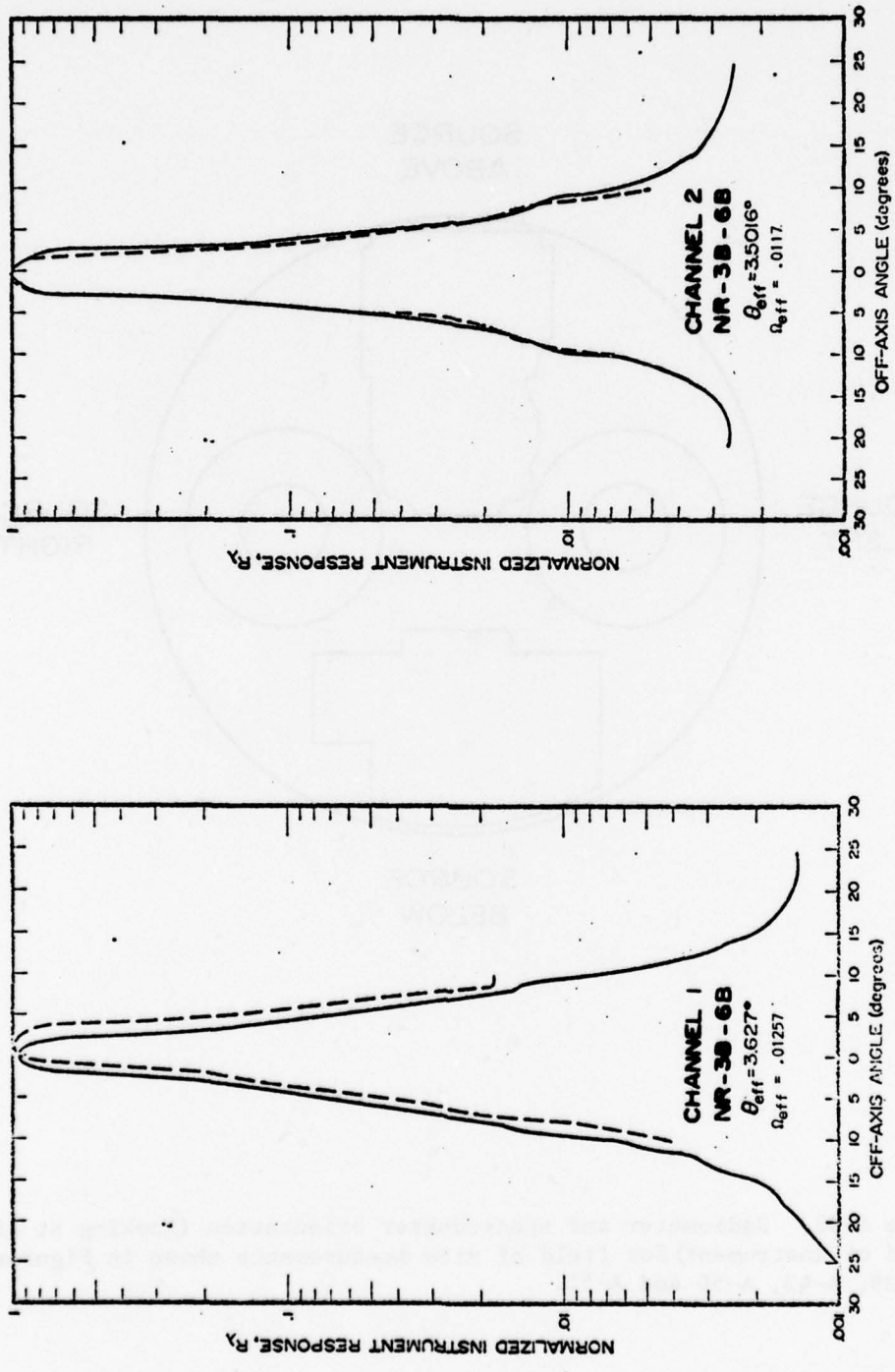


Figure A-39. SWIR dual-channel radiometer field of view - NR-3B-6B.

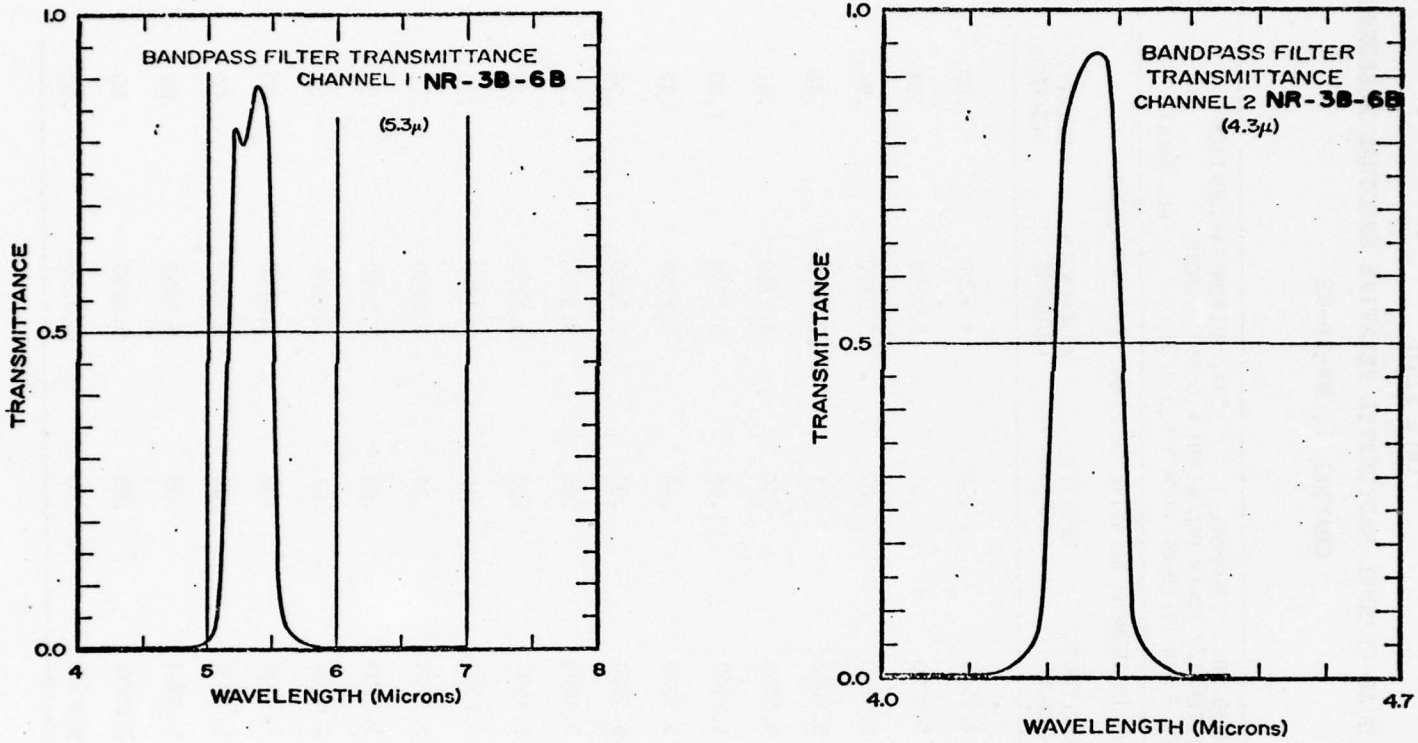


Figure A-40. SWIR dual-channel radiometer bandpass filter transmittance - NR-3B-6B.

TABLE A-10

SWIR DUAL-CHANNEL RADIOMETER RELATIVE SPECTRAL RESPONSE

CHANNEL 1, NR-3B-6B

NR-3B-6B CHANNEL 1 5.342 MICRON CALIBRATION
FILTER 1/2 POWER BANDWIDTH > 0.358 MICRONS
1/2 POWER FIELD OF VIEW > 5.0 DEGREES FULL ANGLE

THE INSTRUMENT RELATIVE SPECTRAL RESPONSE CURVE

WAVELENGTH (MICRONS)	RELATIVE RESPONSE	WAVELENGTH (MICRONS)	RELATIVE RESPONSE
4.9500	.00	4.9750	.00
5.0000	.01	5.0250	.01
5.0500	.02	5.0750	.04
5.1000	.11	5.1250	.20
5.2000	.50	5.1750	.81
5.2500	1.00	5.2250	1.00
5.3000	.99	5.2750	.97
5.3500	.97	5.3250	.98
5.4000	.85	5.3750	.75
5.4500	.53	5.4250	.53
5.5000	.45	5.4750	.33
5.5500	.21	5.5250	.11
5.6000	.05	5.5750	.03
5.6500	.01	5.6250	.01
5.7000	.00	5.6750	.00
5.7500	.00	5.7250	.00
5.8000	.00	5.7750	.00
5.8500	.00	5.8250	.00
5.9000	.00	5.8750	.00

TABLE A-11

SWIR DUAL-CHANNEL RADIOMETER RELATIVE SPECTRAL RESPONSE

CHANNEL 2, NR-3B-6B

NR-3B-6B CHANNEL 2 4.25 MICRON
EXTENDED SOURCE

THE INSTRUMENTS RELATIVE SPECTRAL RESPONSE CURVE

WAVELENGTH (MICRONS)	RELATIVE RESPONSE	WAVELENGTH (MICRONS)	RELATIVE RESPONSE
4.1650	.00	4.1700	.00
4.1750	.02	4.1800	.02
4.1850	.03	4.1900	.06
4.1950	.12	4.2000	.23
4.2050	.36	4.2100	.52
4.2150	.66	4.2200	.79
4.2250	.86	4.2300	.91
4.2350	.95	4.2400	.96
4.2450	.97	4.2500	.98
4.2550	.98	4.2600	.99
4.2650	.99	4.2700	1.00
4.2750	1.00	4.2800	1.00
4.2850	.97	4.2900	.90
4.2950	.80	4.3000	.67
4.3050	.51	4.3100	.31
4.3150	.21	4.3200	.11
4.3250	.06	4.3300	.04
4.3350	.03	4.3400	.02
4.3450	.01	4.3500	.01
4.3550	.01	4.3600	.01
4.3650	.01	4.3700	.00
4.3750	.00	4.3800	.00
4.3850	.00	.0000	.00

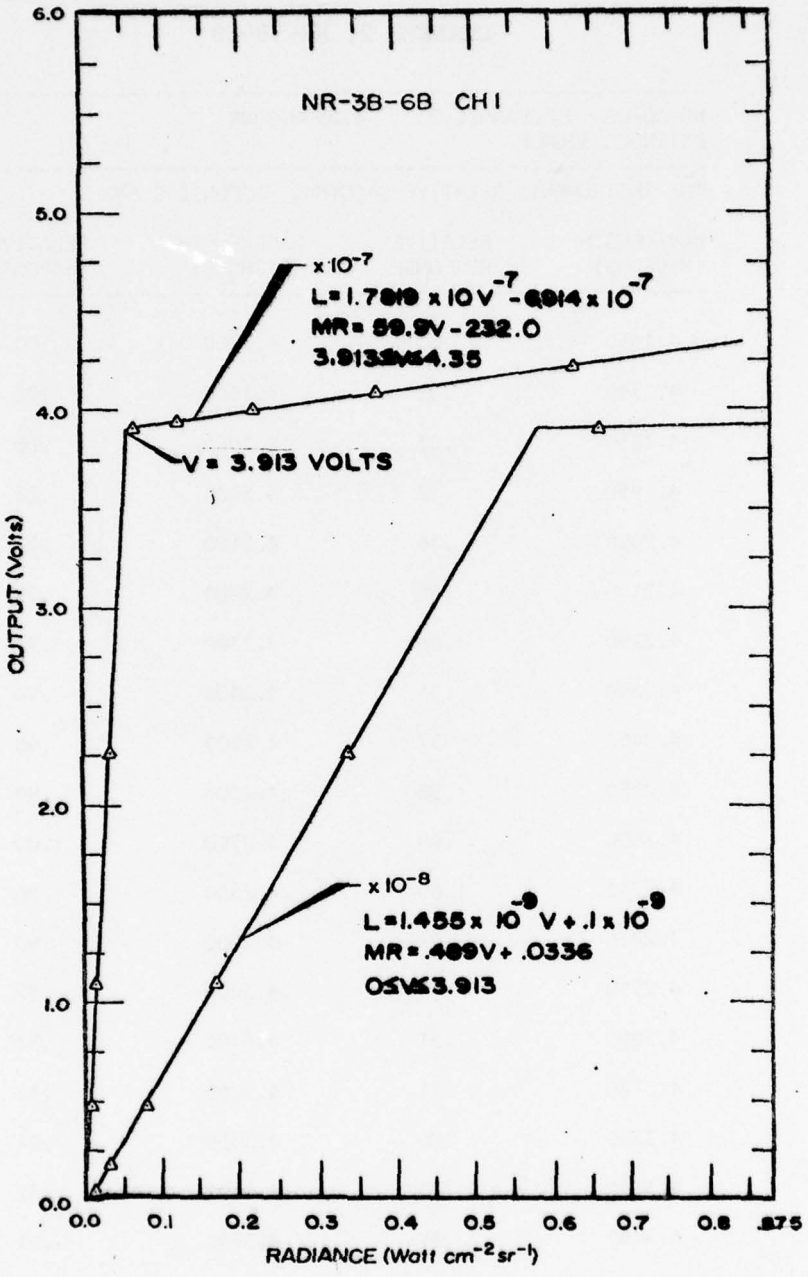


Figure A-41. SWIR dual-channel radiometer high gain responsivity - channel 1, NR-3B-6B.

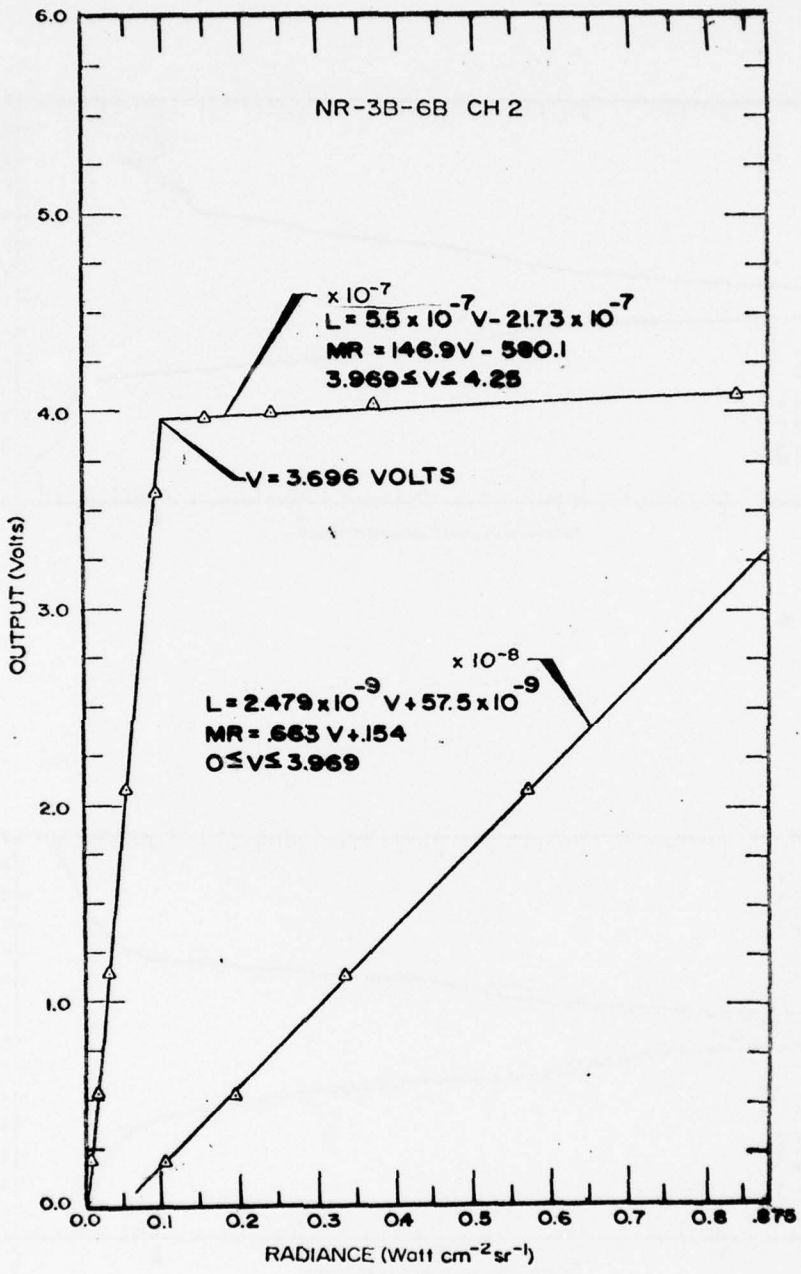


Figure A-42. SWIR dual-channel radiometer high gain responsivity - channel 2, NR-3B-6B.

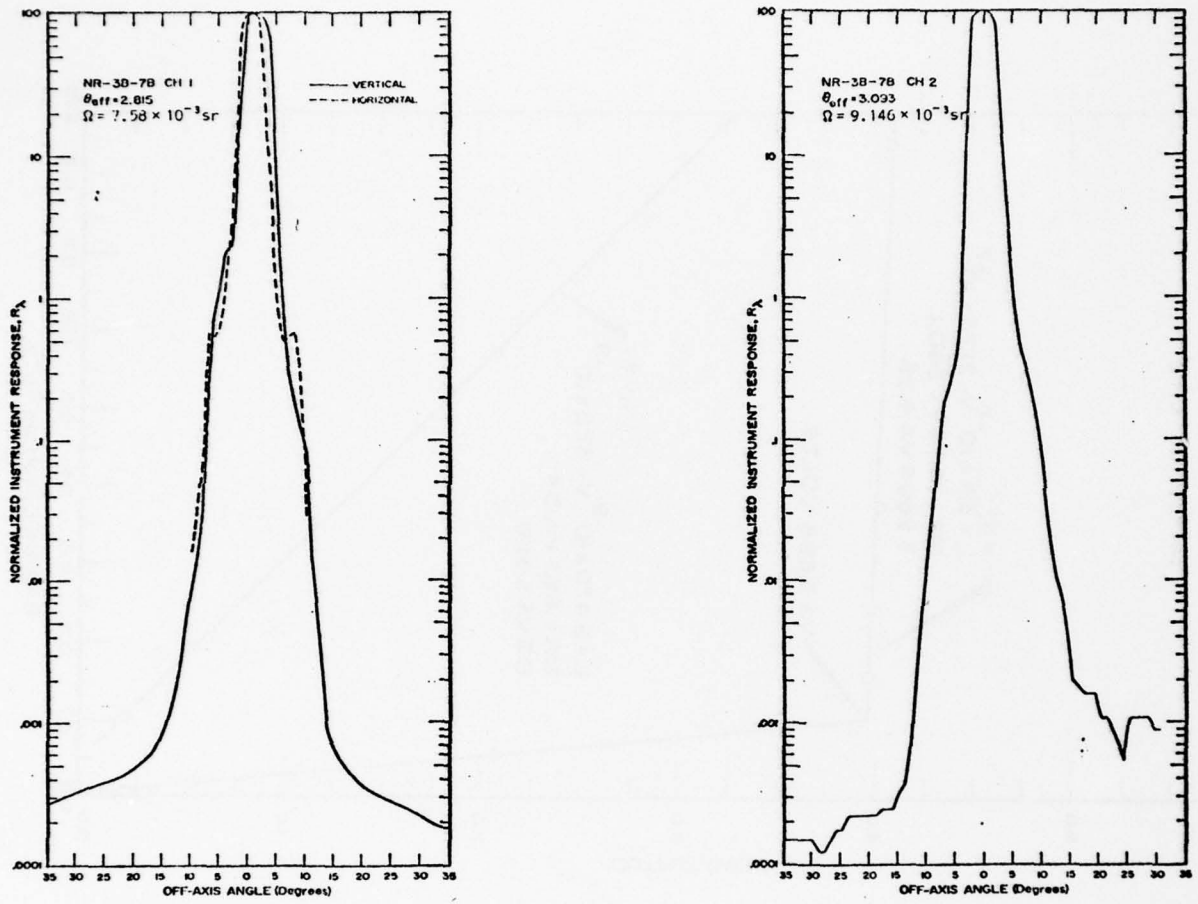
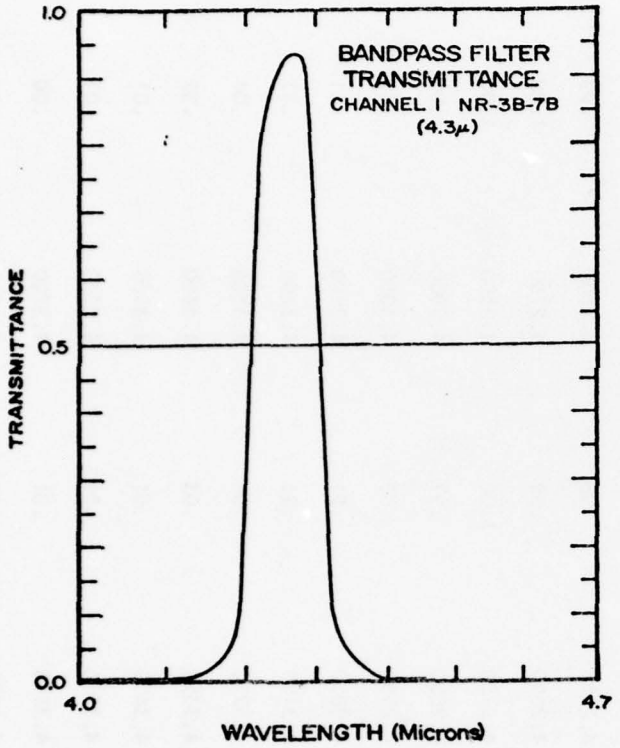


Figure A-43. SWIR dual-channel radiometer field of view, NR-3B-7B - response to a point source (see Figure A-38).



Special OH filter

Figure A-44. SWIR dual-channel radiometer bandpass filter transmittance - NR-3B-7B.

TABLE A-12

SWIR DUAL-CHANNEL RADIOMETER RELATIVE SPECTRAL RESPONSE

CHANNEL 1, NR-3B-7B

NR-3B-7B 4.25 MICRON
EXTENDED SOURCE

THE INSTRUMENTS RELATIVE SPECTRAL RESPONSE CURVE

WAVELENGTH (MICRONS)	RELATIVE RESPONSE	WAVELENGTH (MICRONS)	RELATIVE RESPONSE
4.1650	.00	4.1700	.00
4.1750	.02	4.1800	.02
4.1850	.03	4.1900	.06
4.1950	.12	4.2000	.23
4.2050	.36	4.2100	.52
4.2150	.66	4.2200	.79
4.2250	.86	4.2300	.91
4.2350	.95	4.2400	.96
4.2450	.97	4.2500	.98
4.2550	.98	4.2600	.99
4.2650	.99	4.2700	1.00
4.2750	1.00	4.2800	1.00
4.2850	.97	4.2900	.90
4.2950	.80	4.3000	.67
4.3050	.51	4.3100	.31
4.3150	.21	4.3200	.11
4.3250	.06	4.3300	.04
4.3350	.03	4.3400	.02
4.3450	.01	4.3500	.01
4.3550	.01	4.3600	.01
4.3650	.01	4.3700	.00
4.3750	.00	4.3800	.00
4.3850	.00	.0000	.00

TABLE A-13

SWIR DUAL-CHANNEL RADIOMETER RELATIVE SPECTRAL RESPONSE

CHANNEL 2, NR-3B-7B

NR-3B-7B 2.75 MICRON CALIBRATION
FILTER 1/2 POWER BANDWIDTH > 0.69 MICRONS
1/2 POWER FIELD OF VIEW > 5.0 DEGREES FULL ANGLE

THE INSTRUMENTS RELATIVE SPECTRAL RESPONSE CURVE

WAVELENGTH (MICRONS)	RELATIVE RESPONSE	WAVELENGTH (MICRONS)	RELATIVE RESPONSE
2.1500	.00	2.1750	.00
2.2000	.01	2.2250	.00
2.2500	.01	2.2750	.01
2.3000	.01	2.3250	.03
2.3500	.05	2.3750	.12
2.4000	.32	2.4250	.50
2.4500	.72	2.4750	.74
2.5000	.77	2.5250	.80
2.5500	.83	2.5750	.84
2.6000	.86	2.6250	.87
2.6500	.88	2.6750	.88
2.7000	.89	2.7250	.89
2.7500	.90	2.7750	.90
2.8000	.91	2.8250	.92
2.8500	.93	2.8750	.93
2.9000	.93	2.9250	.94
2.9500	.95	2.9750	.97
3.0000	1.00	3.0250	.99
3.0500	.97	3.0750	.79
3.1000	.60	3.1250	.30
3.1500	.17	3.1750	.10
3.2000	.06	3.2250	.04
3.2500	.03	3.2750	.03
3.3000	.01	3.3250	.01
3.3500	.02	3.3750	.01
3.4000	.01	3.4250	.01
3.4500	.01	3.4750	.00
3.5000	.00	.0000	.00

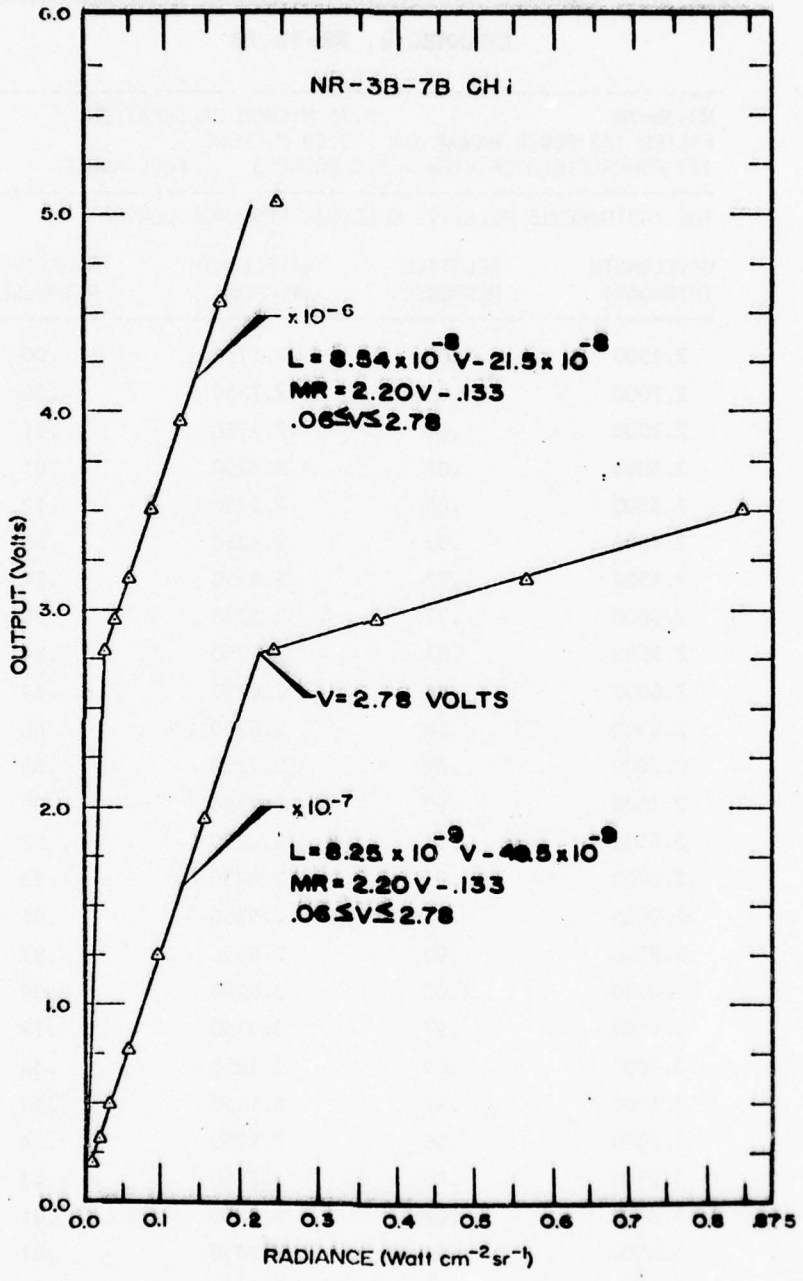


Figure A-45. SWIR dual-channel radiometer high gain responsivity - channel 1, NR-3B-7B.

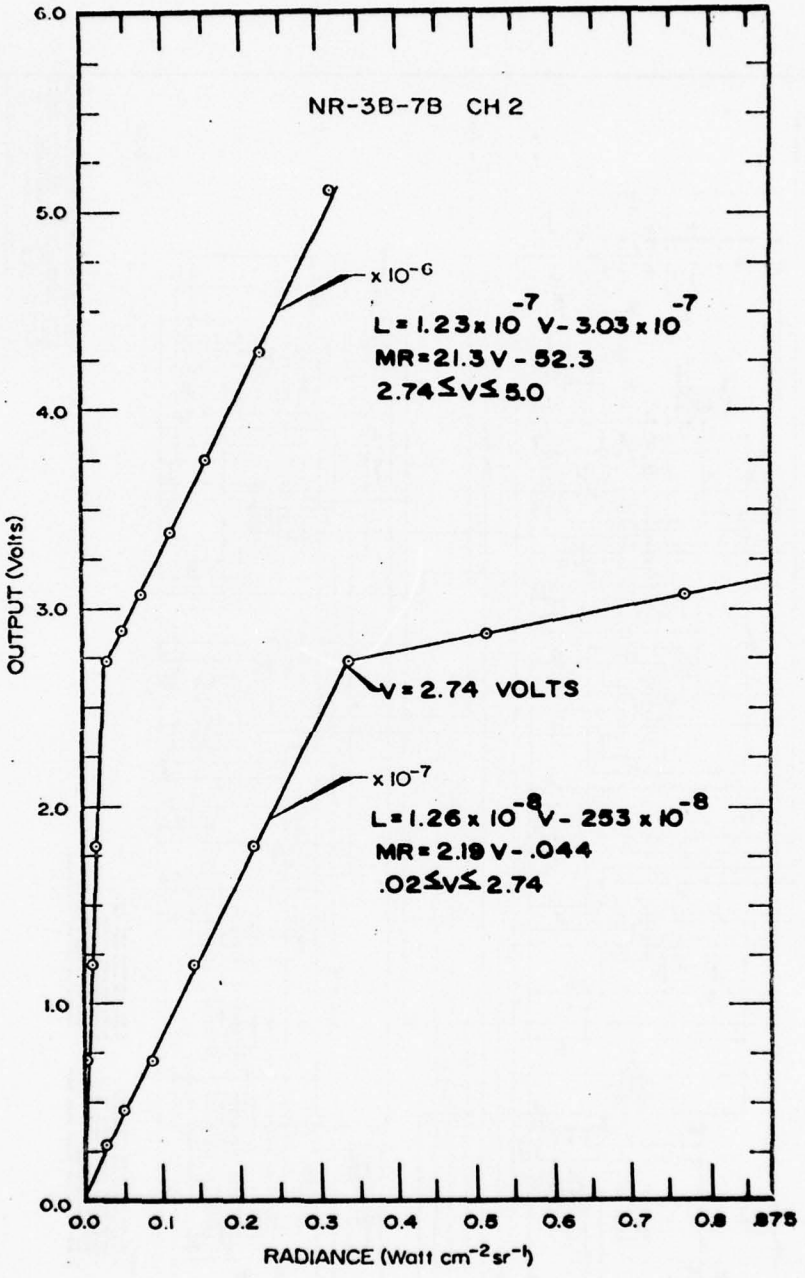


Figure A-46. SWIR dual-channel radiometer high gain responsivity - channel 2, NR-3B-7B.

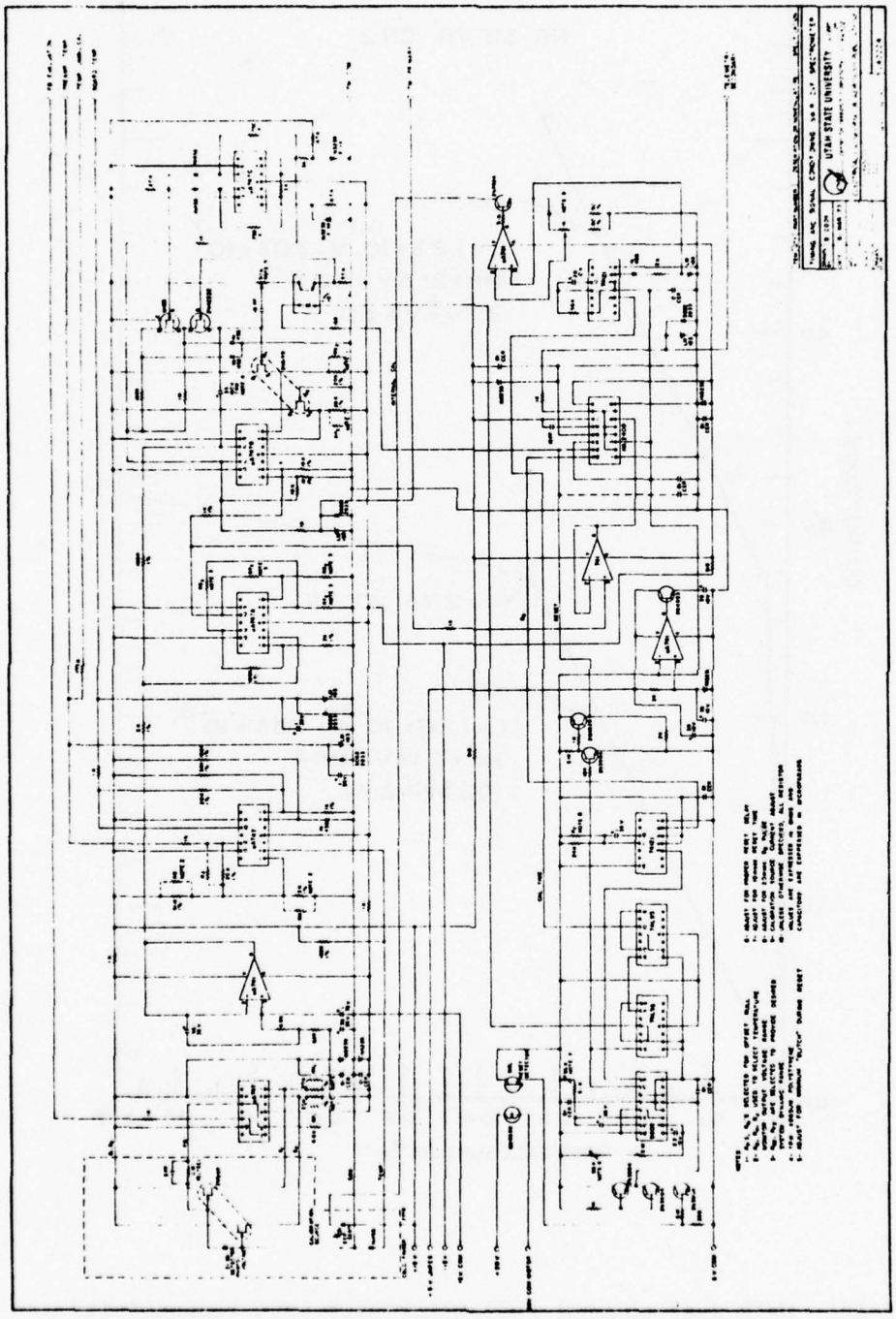


Figure A-47. CVF spectrometer timing and signal conditioning electronics schematic diagram.

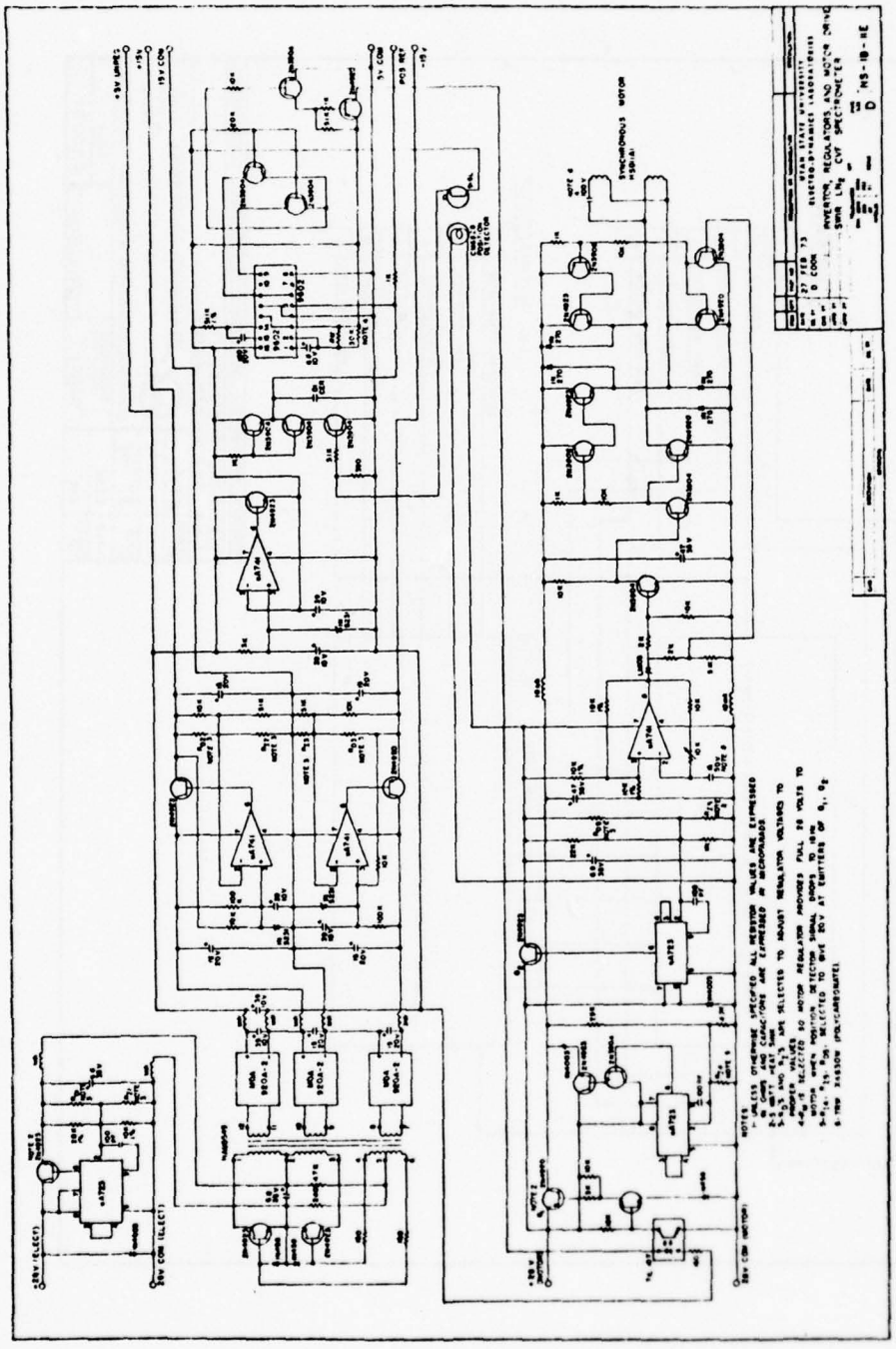


Figure A-48. CVF spectrometer inverter, regulators and motor drive schematic diagram.

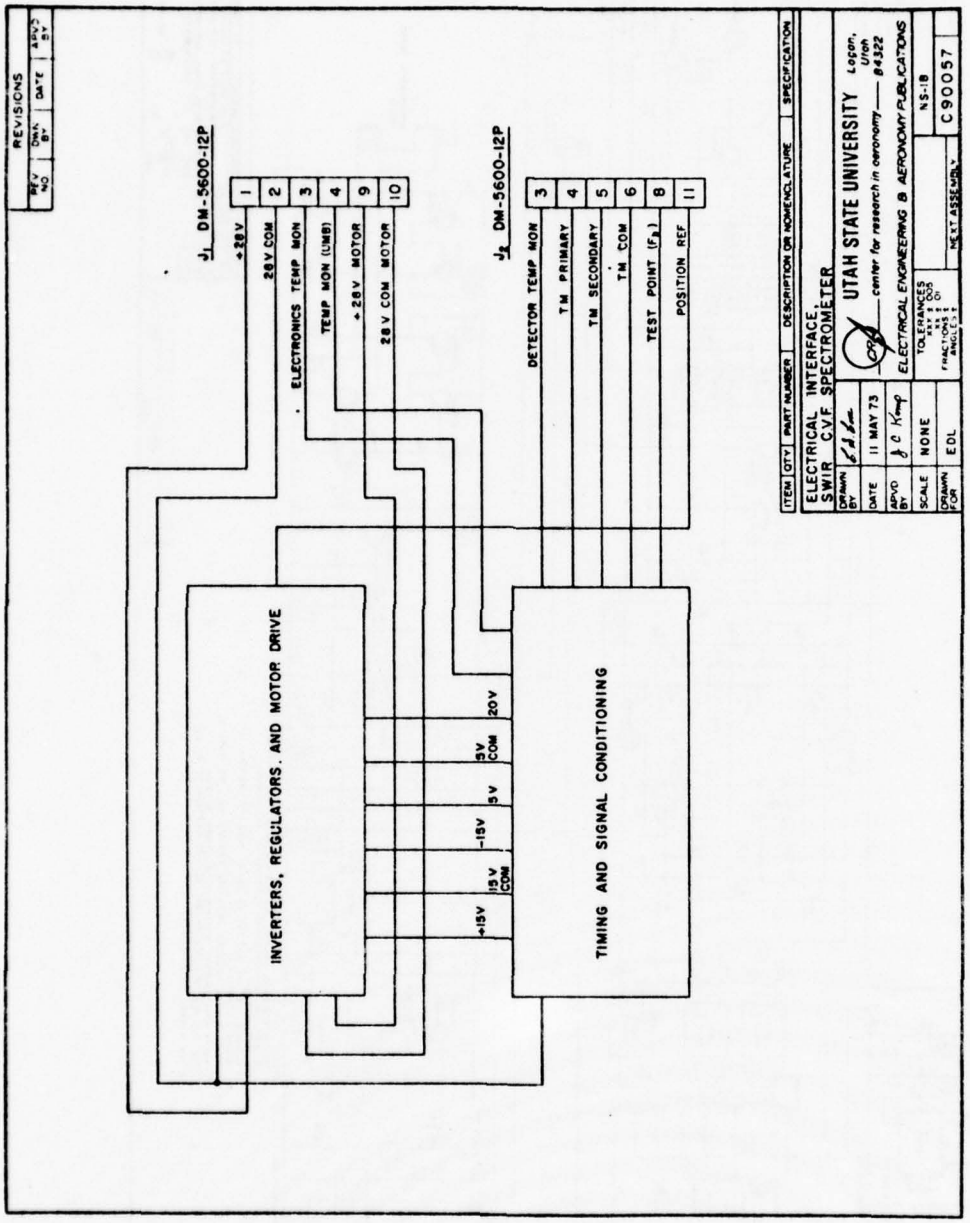


Figure A-49. CVF spectrometer electrical interface.

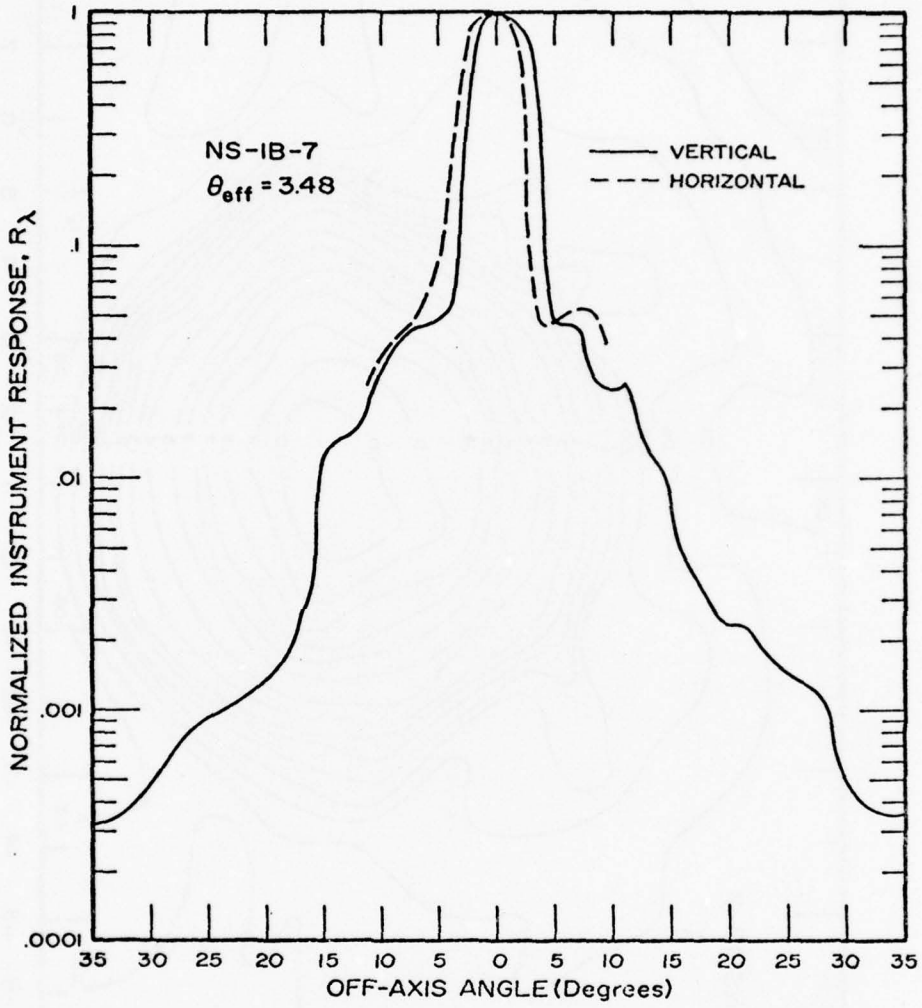


Figure A-50. CVF spectrometer ortho-normal field of view (see Figure A-38).

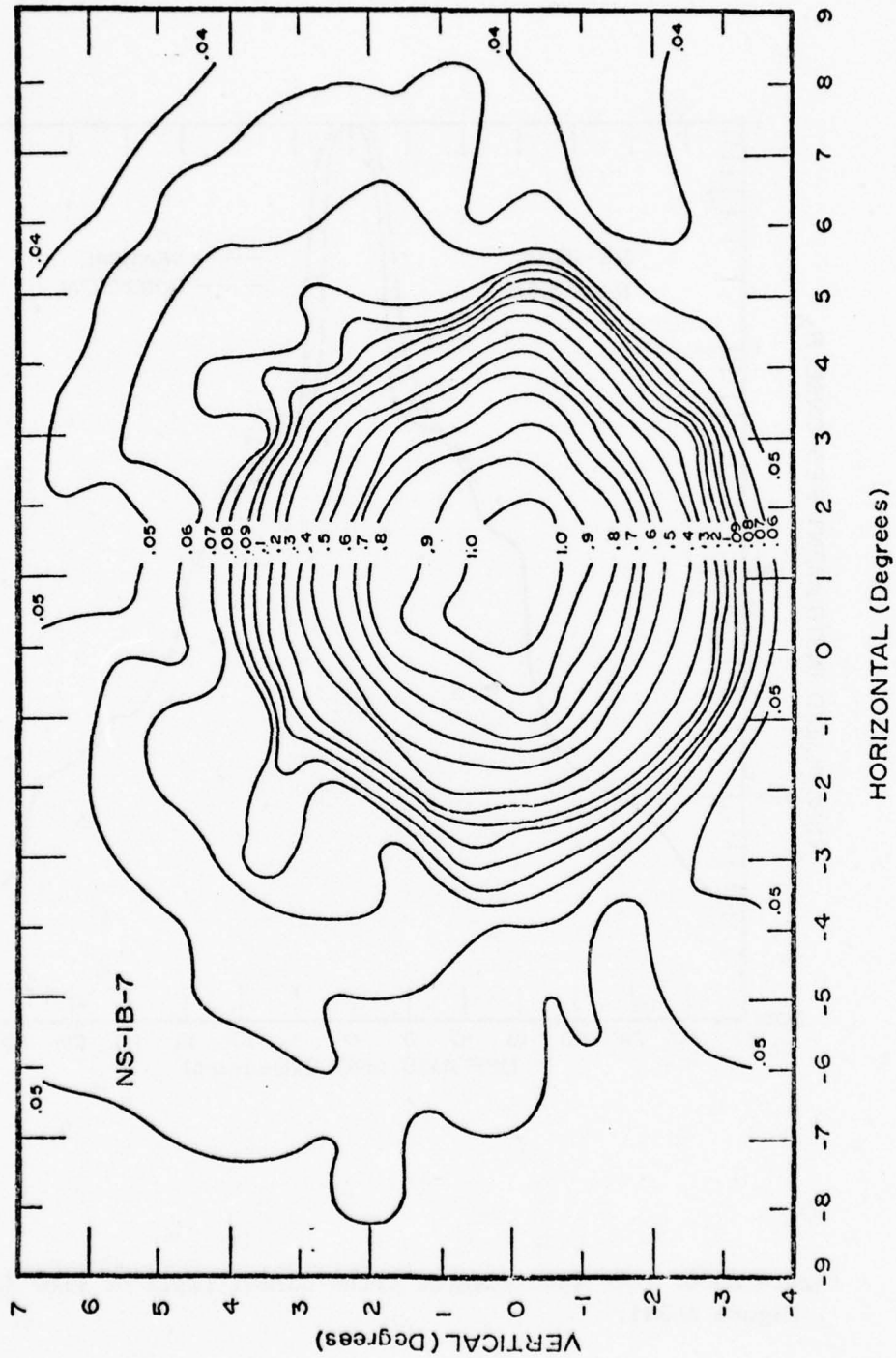


Figure A-51. CVF spectrometer polar field of view (see Figure A-38).

TABLE A-14

CVF SPECTROMETER POSITION REFERENCE, WAVELENGTH AND PERCENT SCAN, ϕ

Reference Position No.	Wavelength (μm) Long-wave Segment	Short-wave Segment	Percent Scan ϕ
1	5.59		10.1
2	5.21		15.9
3	4.93		20.4
4	4.59		26.0
5	4.31		30.4
6	3.96		36.2
7	3.69		40.6
8	3.35		46.1
9	3.08	3.40	50.4
10		3.20	56.1
11		3.05	60.5
12		2.86	66.0
13		2.71	70.4
14		2.51	76.2
15		2.39	79.8
16		2.18	82.1
17		2.03	90.4
18		1.84	96.0
19		1.70	1 00.1
20		1.59	1 03.3

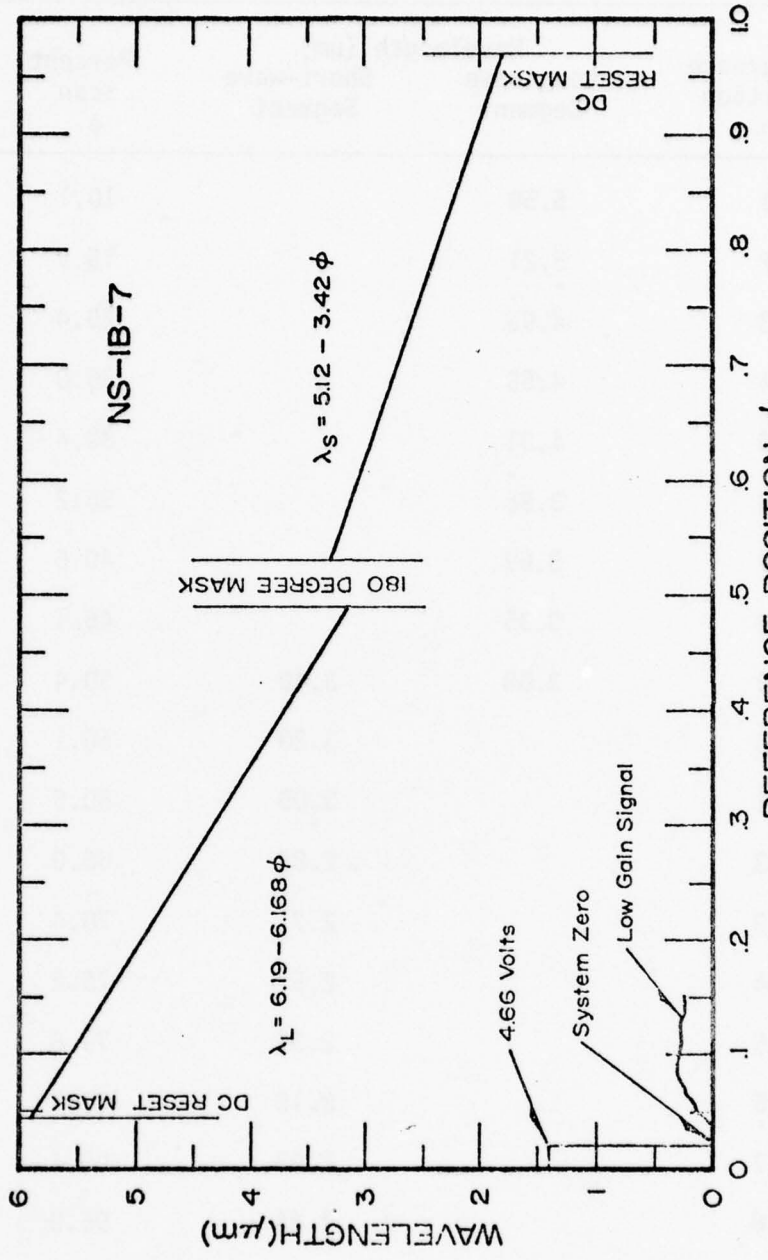


Figure A-52. CVF spectrometer absolute spectral scan position.

TABLE A-15

CIRCULAR VARIABLE FILTER SPECTRAL DATA

Theta	Lambda θ	Pct HBW	VHBW	Theta'	Lambda' θ	Deviation
0.	3.0410	1.3684	0.0632	0.	3.0044	1.2201
5.	3.0747	1.5065	0.0750	5.	3.0891	-0.4645
30.	3.4797	1.5310	0.0994	30.	3.5126	-0.9363
60.	3.9978	1.5591	0.1275	60.	4.0207	-0.5695
90.	4.5426	1.4990	0.0674	90.	4.5289	0.3021
120.	5.0610	1.5182	0.0867	120.	5.0371	0.4747
150.	5.5760	1.5054	0.0739	150.	5.5453	0.5539
175.	5.9704	1.3134	0.1181	175.	5.9688	0.0273
180.	6.0170	1.0830	0.3485	180.	6.0535	-0.6020
Average HBW = 1.4316						
0.	1.6846	1.6146	0.0975	0.	1.6311	3.2816
5.	1.6661	1.3385	0.1766	5.	1.6765	-0.6221
30.	1.8742	1.5954	0.0783	30.	1.9035	-1.5426
60.	2.1533	1.5558	0.0337	60.	2.1760	-1.0433
90.	2.4323	1.5582	0.0411	90.	2.4484	-0.6593
120.	2.7276	1.5068	0.0103	120.	2.7208	0.2505
150.	3.0035	1.4916	0.0236	150.	2.9933	0.3416
175.	3.2318	1.4605	0.0566	175.	3.2203	0.3569
180.	3.2623	1.5327	0.0195	180.	3.2657	-0.1044
Average HBW = 1.5171						

Column Explanations

Theta = Angular position on filter in degrees
Lambda θ = Bandpass center wavelength in microns, at position Theta
HBW = Bandpass width at the halfpower points in percent of Lambda
VHBW = (Average HBW) - HBW
Theta' = Angular position for purposes of best fit straight line
Lambda'θ = Center wavelength values for best fit straight line,
Lambda'θ = K * Theta'
Deviation= (Lambda θ - Lambda'θ) * 100/Lambda θ

Ambient to 77°K shift factor = 0.9842

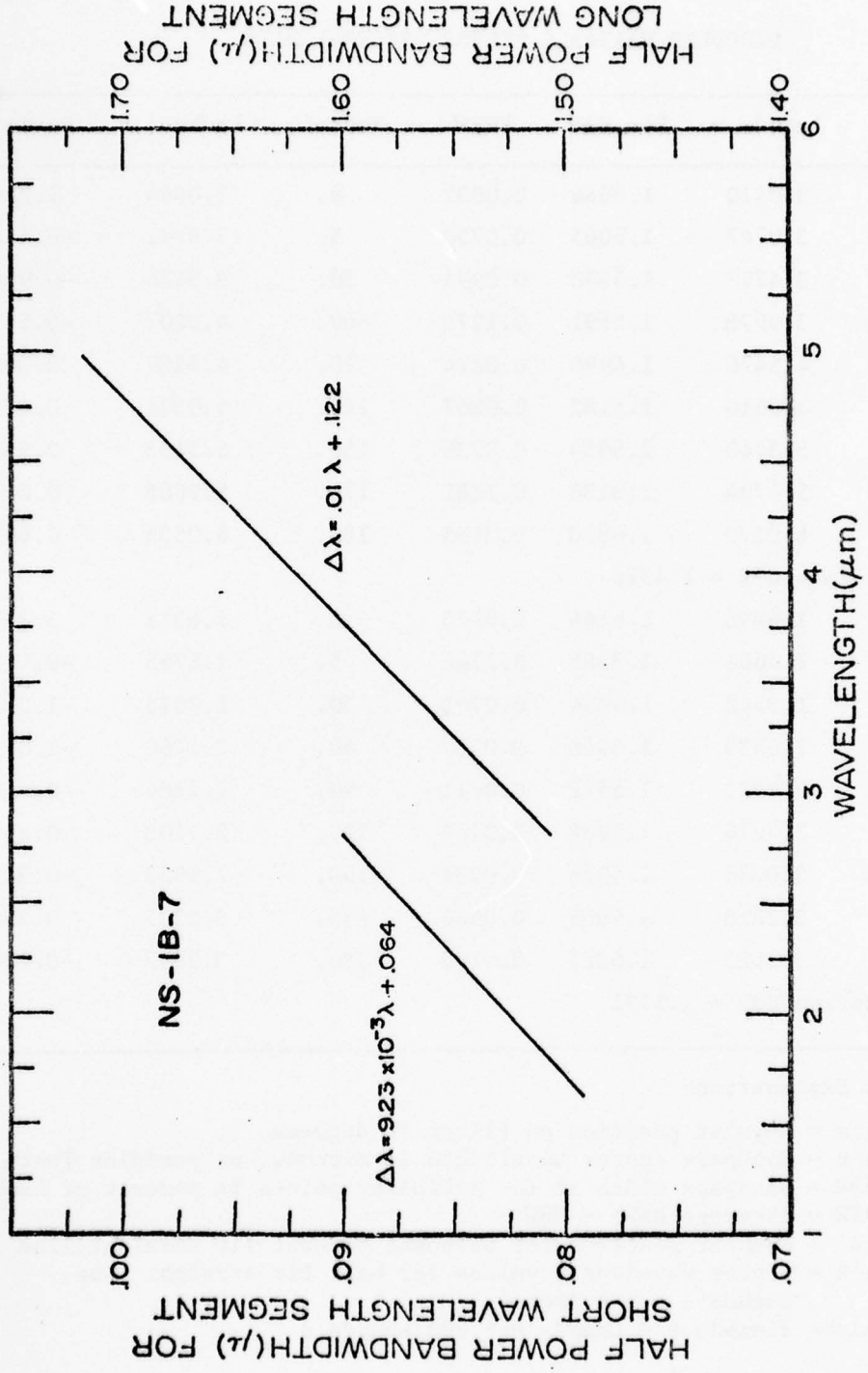


Figure A-53. CVF spectrometer optical resolution.

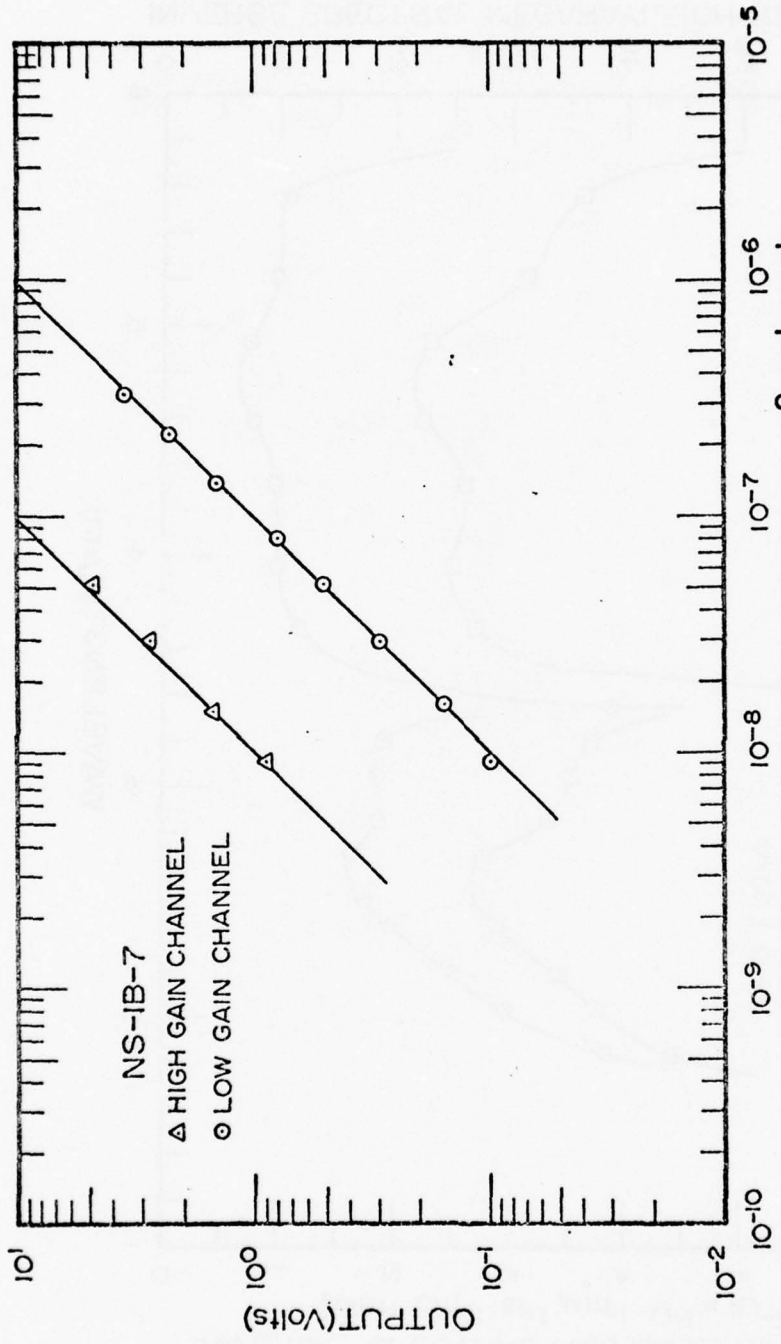


Figure A-54. CVF spectrometer 4.3 μm extended source calibration.

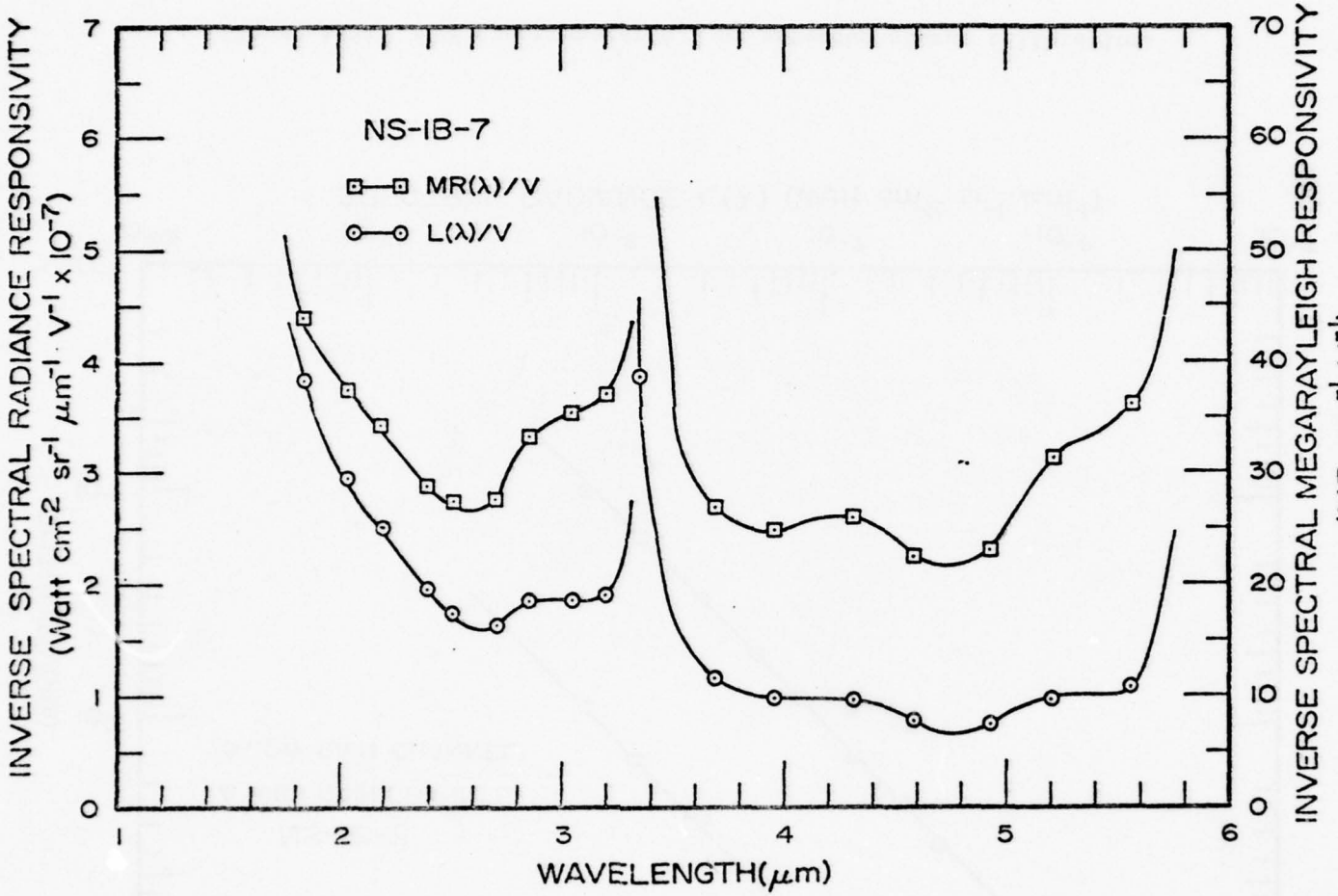


Figure A-55. CVF spectrometer absolute inverse spectral radiant responsivity.

TABLE A-16

BLACK BRANT 18.219-1 PHOTOMETER SPECIFICATIONS

Parameter	PM-1-7 Link #2 Channel #12	PM-1-24 Link #2 Channel #11	PM-1-25 Link #2 Channel #8	PM-1-26[3] Link #2 Channel #10	PM-1-28 Link #2 Channel #9	PM-1-30[2] Link #1 Channel #6
H.V. Mon (volts)	1.84	2.16	1.95	1.28	1.61	1.73
Temp. Mon (volts)[1]	1.96	2.25	1.92	1.95	1.99	2.77
Filter λ(Å)	5200	5200	3466	3914	5577	3914
Filter λo (actual)	5201.25	5203.00	3462.00	3919.10	5575.80	3916.90
Filter $\Delta\lambda$ (Å)	26.5	10.0	21.0	18.4	17.5	19.1
Filter Tr pk (%)	75.8	48.3	10.0	13.9	53.3	14.1
Full angle Fiele of View (°)	5.00	5.20	5.01	5.05	5.00	5.20
Offset (volts)	0.18	0.00	0.00	-0.05	0.15	0.05
Cal. Pulse (volts)	0.80	2.40	2.50	1.10	2.10	2.40
Conversion	.32v-.06	.215v-0.0	.75v-0.0	23.50v+.47	17.19v-2.58	2.90-.23
(Volts-kR)	$v \leq 2.75$	$v \leq 2.70$	$v \leq 2.63$	$v \leq 2.67$	$v \leq 2.68$	$v \leq 2.75$
Conversion	3.24v-8.56	2.279v-5.613	8.75v-20.91	245.49v-592.46	188.28v-462.48	33.73v-83.67
(Volts-kR)	$v > 2.75$	$v > 2.70$	$v > 2.63$	$v > 2.67$	$v > 2.68$	$v > 2.75$

Notes: 1. Ambient room temperature of +26° C
2. Forward looking
3. Side looking

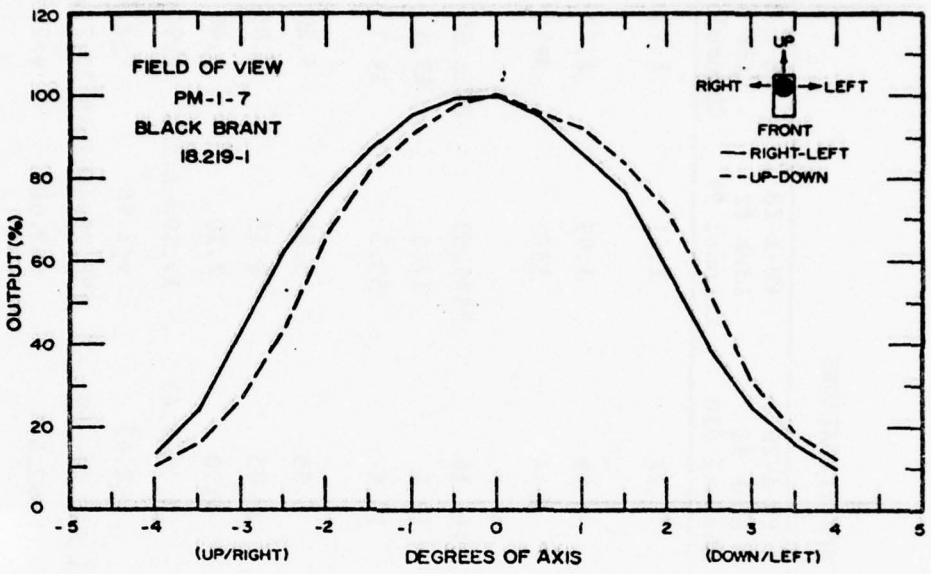


Figure A-56. Photometer field of view - PM-1-7.

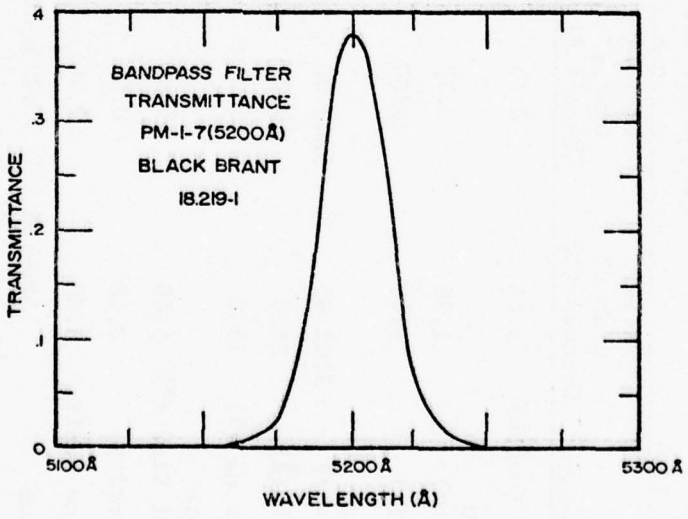


Figure A-57. Photometer bandpass filter transmittance - PM-1-7.

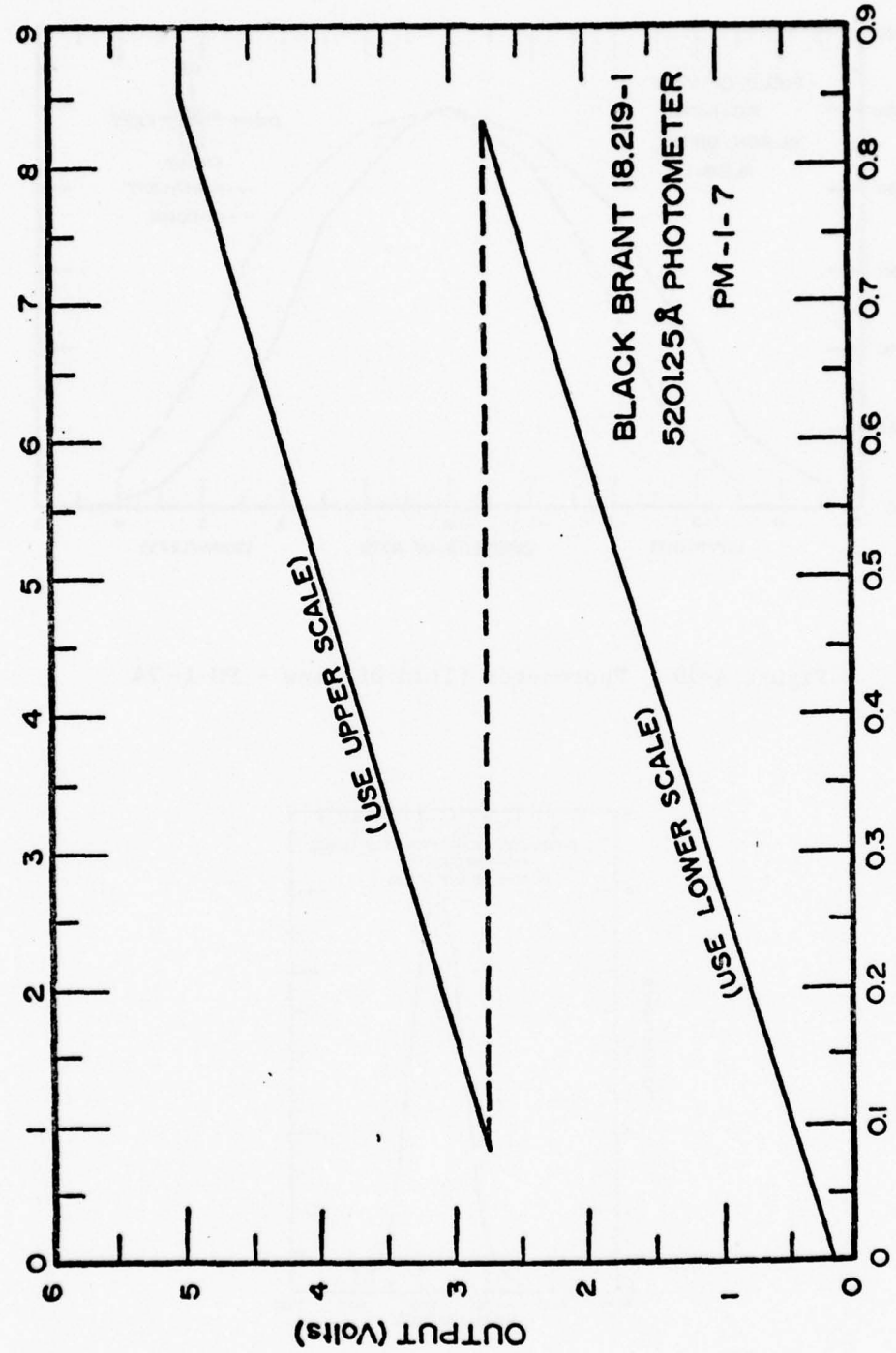


Figure A-58. Photometer responsivity - PM-1-7.

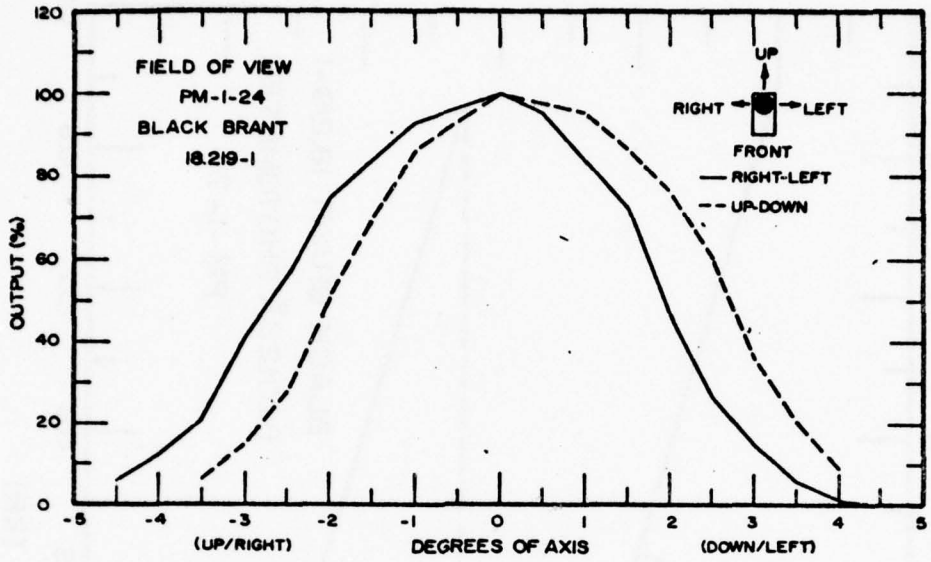


Figure A-59. Photometer field of view - PM-1-24

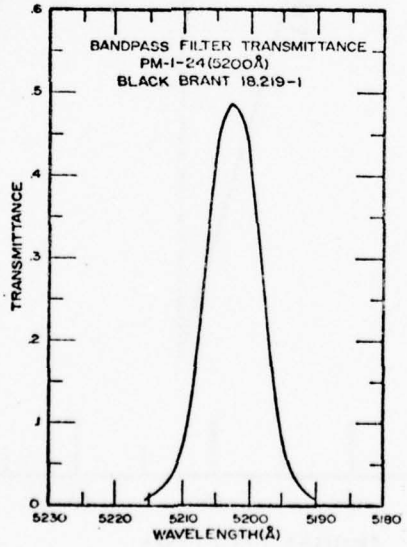


Figure A-60. Photometer bandpass filter transmittance - PM-1-24 .

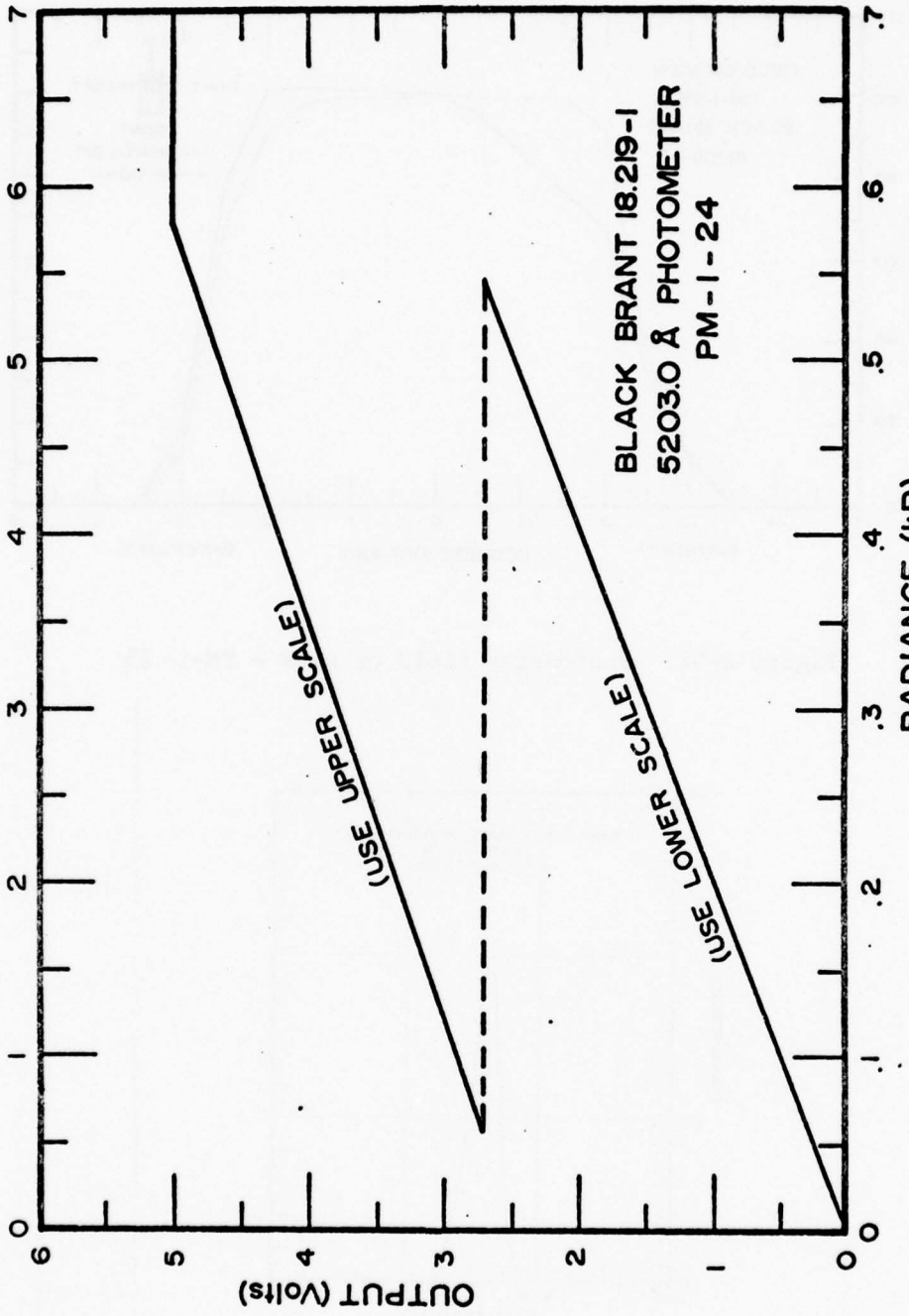


Figure A-61. Photometer responsivity - PM-1-24.

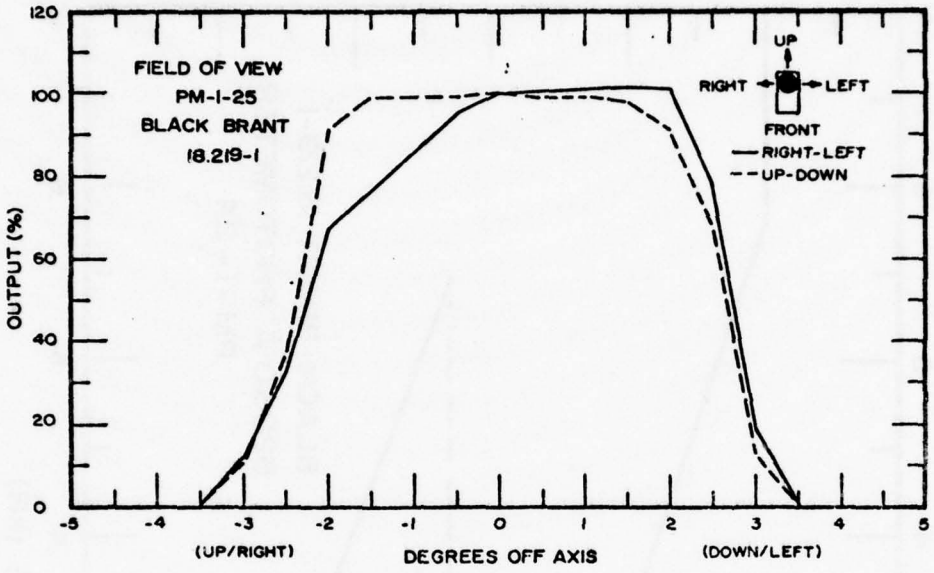


Figure A-62. Photometer field of view - PM-1-25.

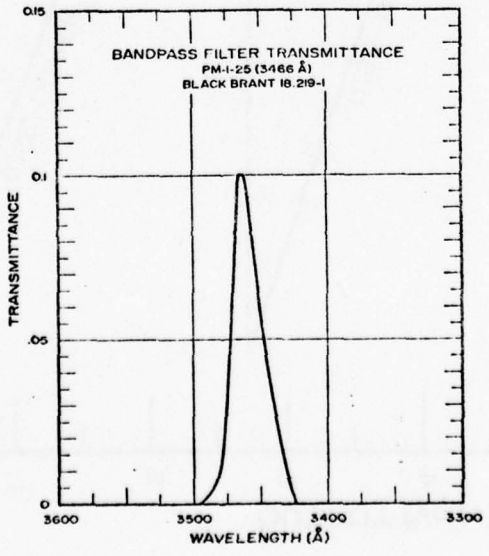


Figure A-63. Photometer bandpass filter transmittance - PM-1-25.

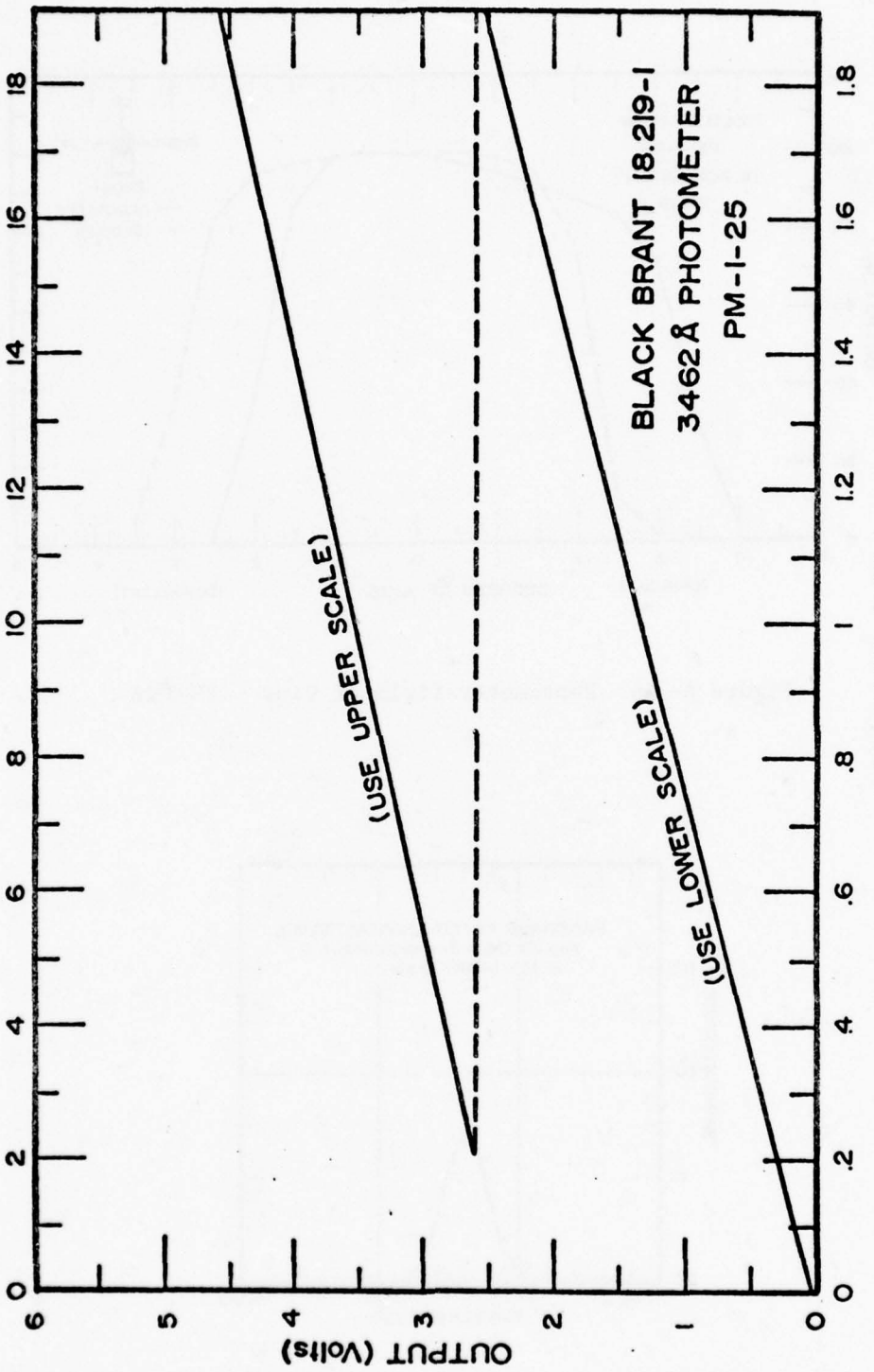


Figure A-64. Photometer responsivity - PM-1-25.

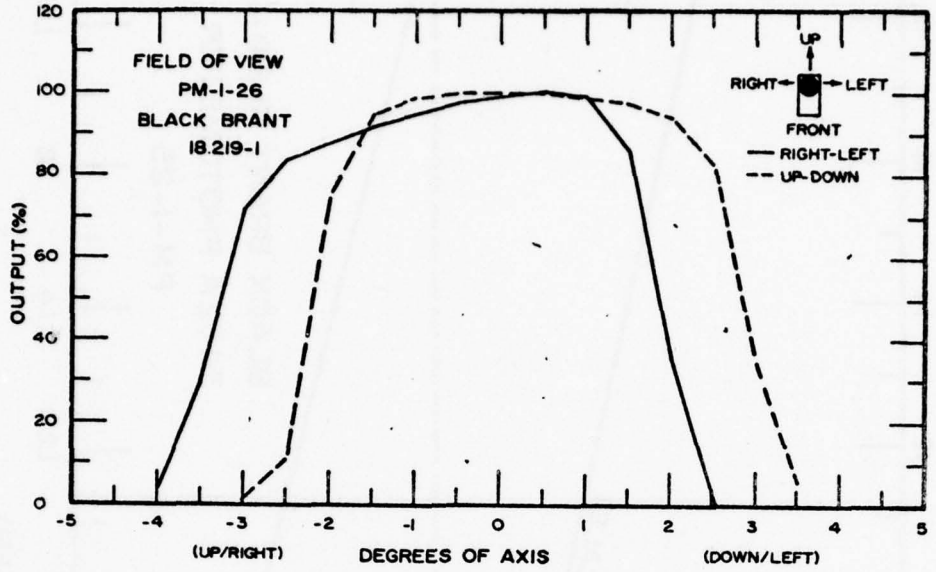


Figure A- 65 Photometer field of view - PM-1 26 .

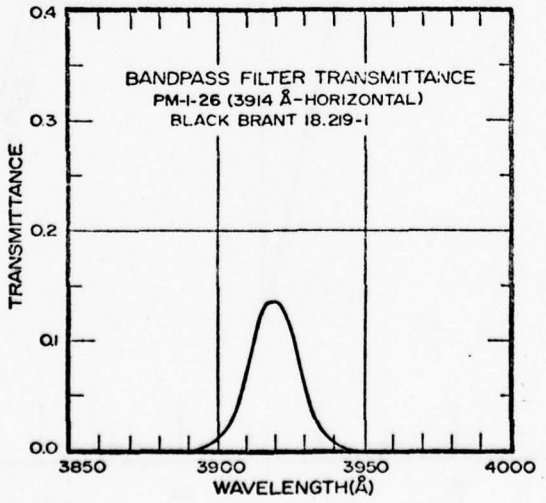


Figure A-66. Photometer bandpass filter transmittance - PM-1- 26.

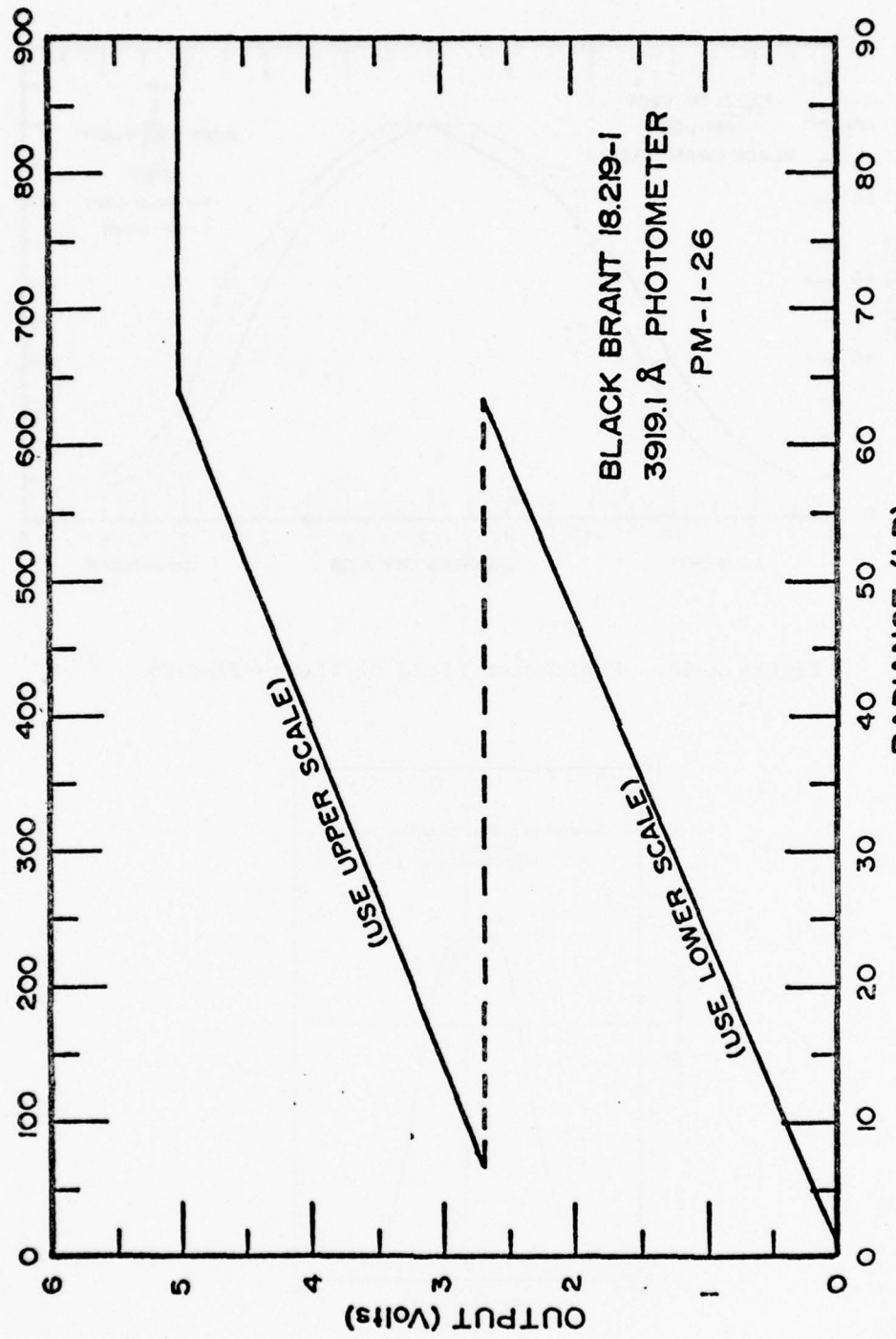


Figure A-67. Photometer responsivity - PM-1-26.

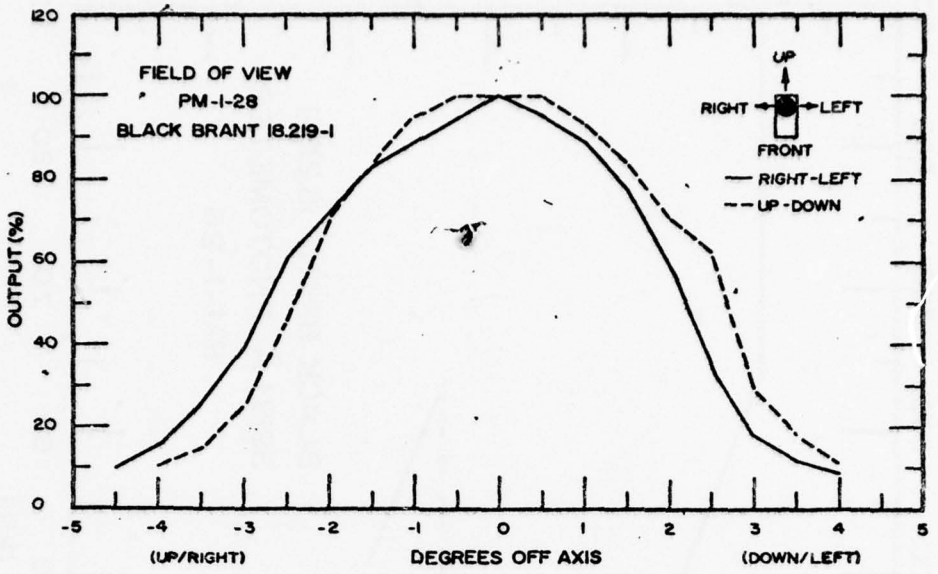


Figure A-68. Photometer field of view - PM-1-28.

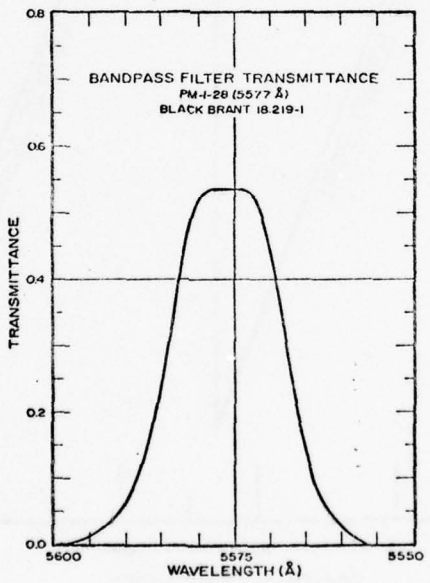


Figure A-69. Photometer bandpass filter transmittance - PM-1-28.

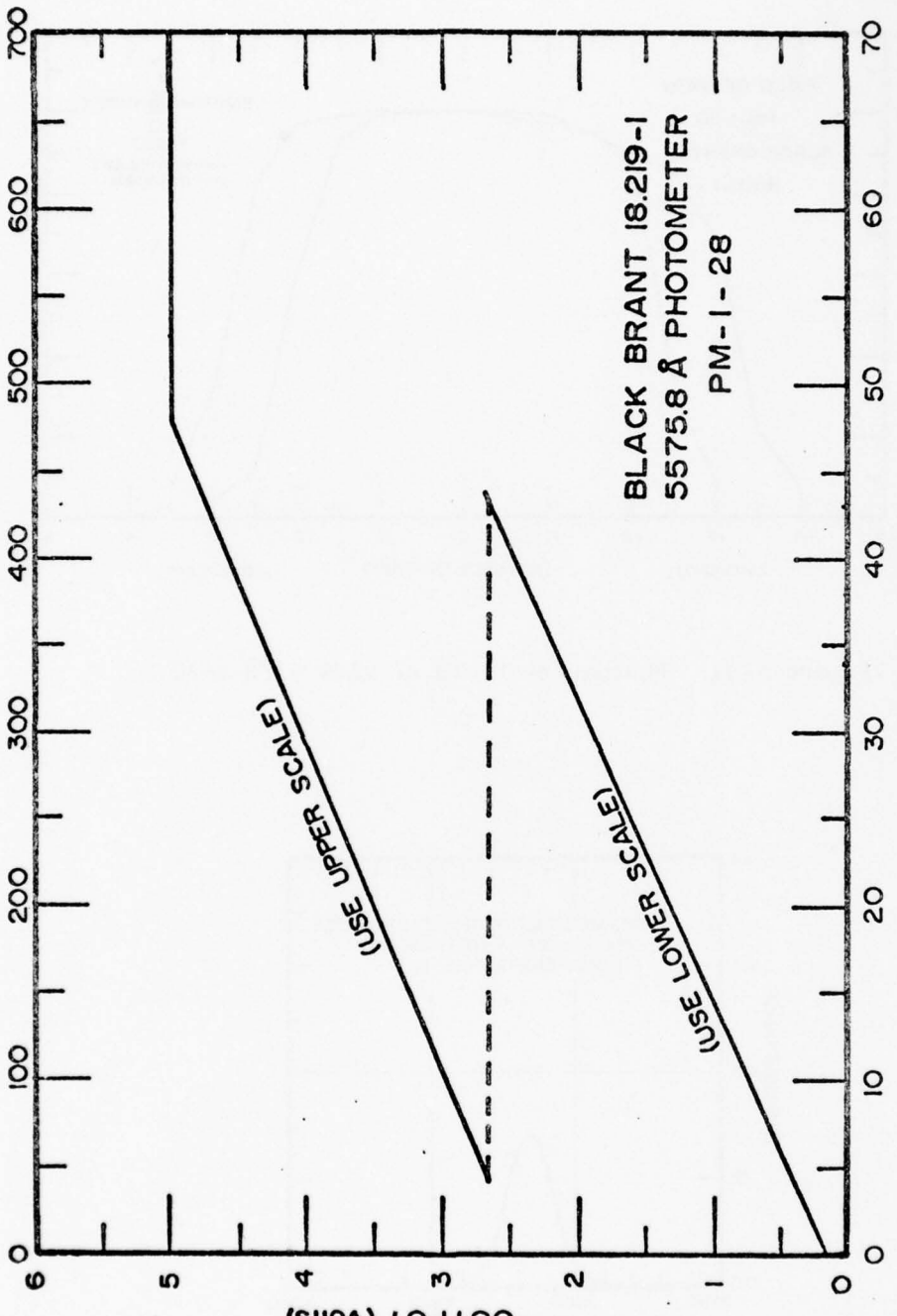


Figure A-70. Photometer responsivity - PM-1-28.

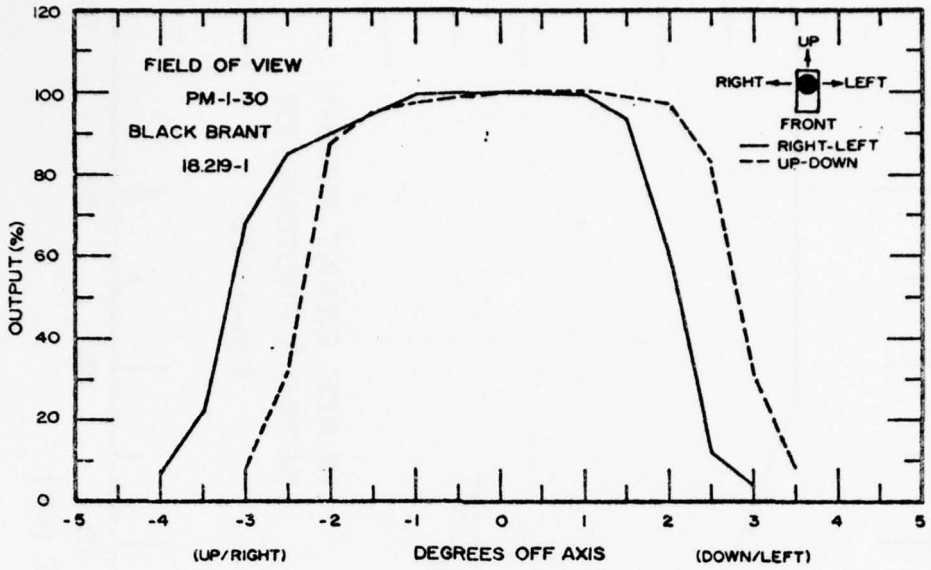


Figure A-71. Photometer field of view - PM-1-30.

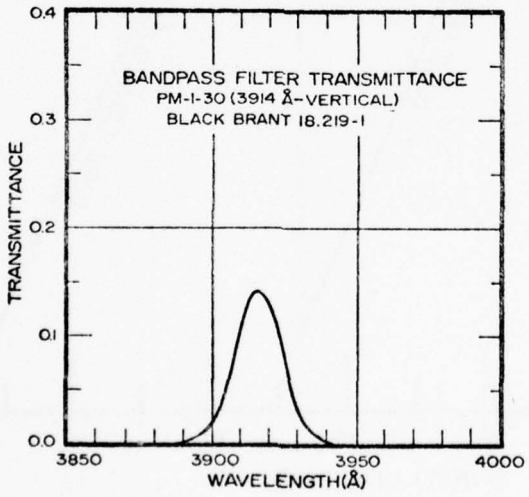


Figure A-72. Photometer bandpass filter transmittance - PM-1-30.

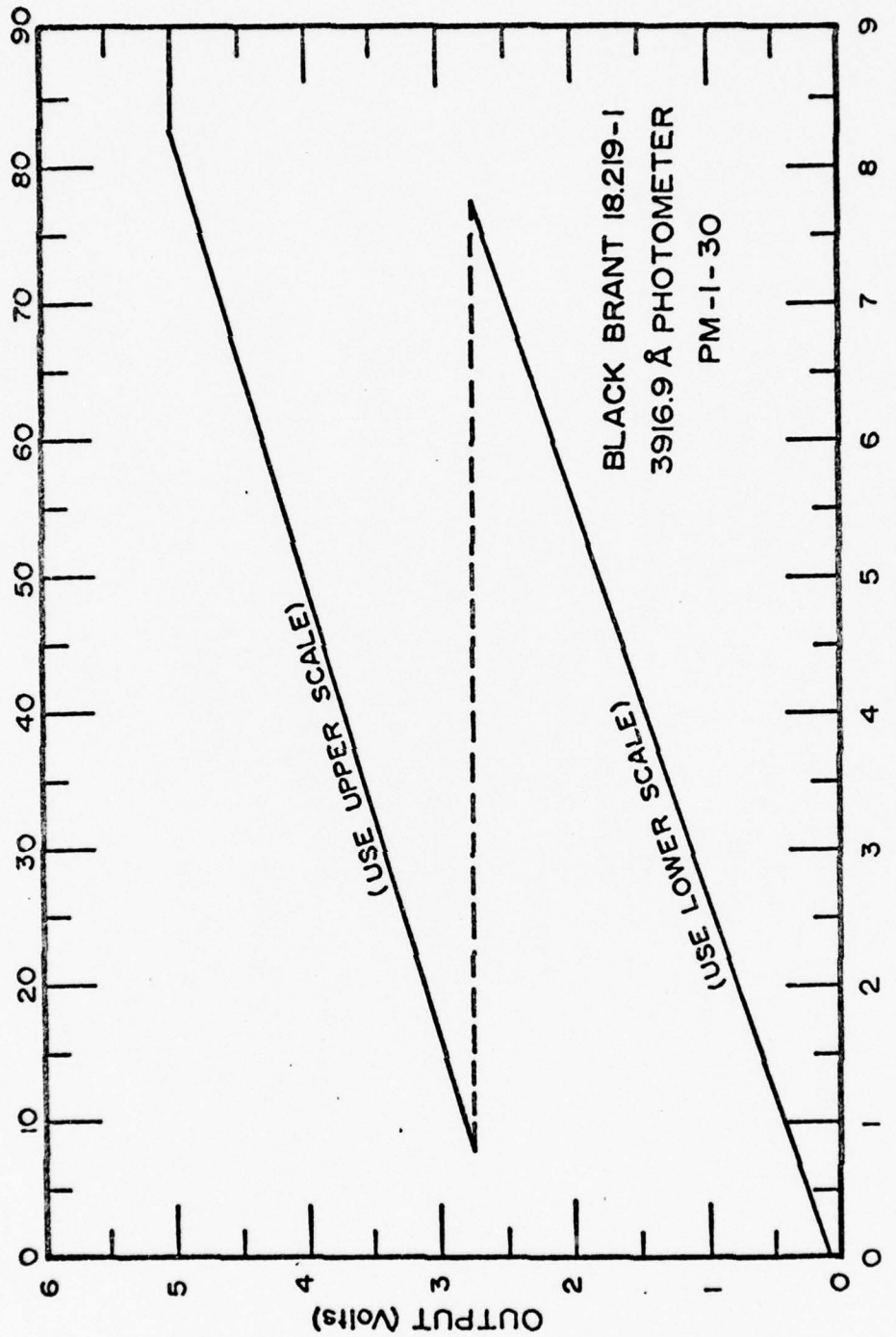


Figure A-73. Photometer responsivity - PM-1-30.

APPENDIX B

PAYLOAD TELEMETRY AND

TRAJECTORY TECHNICAL DATA

BLACK BRANT 18.219-1

Preceding Page BLANK - FILMED

TABLE B-1

TELEMETRY TECHNICAL DATA, LINK 1 (2251.5 MHz)
BLACK BRANT 18.219-1

IRIG Channel	Frequency (KHz)	Channel Description
19	93	Particle Counters
18	70	Electron Spectrometer
17	52.5	Langmuir Probe
16	40	IR Spectrometer-Low
15	30	Plasma Frequency Probe
13	14.5	IR Spectrometer-High
12	10.5	Radiometer (2.8 μm Horizontal)
11	7.35	1x60 Commutator (NRZ)
10	5.4	Radiometer (4.3 μm Horizontal)
9	3.9	Radiometer (5.3 μm Vertical)
8	3.0	ACS Roll
7	2.3	Radiometer (4.3 μm Vertical)
6	1.7	Photometer (3914 A Vertical)
5	1.3	ACS Yaw
4	.96	ACS Pitch
3	.73	LP Sweep Monitor
2	.56	TM Voltage Monitor

Transmitter: Vector Model T-105-S
FM/FM Modulation
$\pm$ 125 KHz Deviation
5.0 Watts RF Power

Antenna: Ball Bros. AN16-B

Subcarrier: Vector Model TS-41
Input Signal: 0-5 volts
All Channels
In-flight Calibration

TABLE B-2

TELEMETRY TECHNICAL DATA, LINK 2 (2279.5 MHz)
BLACK BRANT 18.219-1

IRIG Channel	Frequency (KHz)	Channel Description
19	93	RPA A_o TM
18	70	AMP MS 1
17	52.5	AMP MS 2
16	40	MS Collector Current
15	30	ESA Sweep Monitor
14	22	MS Calibration
13	14.5	ESA Spectral Data
12	10.5	Photometer (5200 A wide band)
11	7.35	Photometer (5200 A narrow band)
10	5.4	Photometer (3914 A)
9	3.9	Photometer (5577 A)
8	3.0	Photometer (3466 A)
7	2.3	Scintillator
6	1.7	RPA Mode Monitor
5	1.3	RPA Sweep Monitor
4	.96	Magnetometer
3	.73	ES Sweep

Transmitter:	Vector Model T-105-S FM/FM Modulation $\pm$ 125 KHz Deviation 5.0 Watts RF Power	Subcarrier:	Vector Model TS-41
		Input Signal:	0-5 Volts All Channels
Antenna:	Ball Bros. AN16-B	In-flight Calibration	

TABLE B-3

BLACK BRANT
1x60 COMMUTATOR ASSIGNMENTS
(TM LINK 1 IRIG CHANNEL 11)

Segment	Data
1	+28 Volt Monitor (Main Battery)
2	Primary Pyro Battery Monitor
3	Secondary Pyro Battery Monitor
4	ACS Pressure Monitor
5	ESA Door Monitor
6	Vertical Photometer Door
7	Radiometer Door
8	Nosetip
9	Radiometer Pop Cover
10	ES Slide
11	0 Volts
12	0 Volts
13	2.4 Volt Magnetometer Bias
14	EDS High Voltage Monitor
15	PC High Voltage Monitor (Delayed)
16	PC High Voltage Monitor (Geiger)
17	RPA Temperature
18	0 Volts
19	CVF Spectrometer Electronics Temp.
20	CVF Spectrometer Detector Temp.
21	Radiometer Electronics Temp. (Vertical)
22	Radiometer Detector Temp. (Vertical)
23	Radiometer Detector Temp. (Horizontal)
24	Radiometer Electronics Temp. (Horizontal)
25	0 Volts
26	3914 A Photometer Temp. (Vertical)

TABLE B-3 (cont.)

Segment	Data
27	3914 A Photometer High Voltage (Vertical)
28	5200 A Photometer Temp (Wide Band)
29	5200 A Photometer High Voltage (Wide Band)
30	5200 A Photometer Temp (Narrow Band)
31	5200 A Photometer High Voltage (Narrow Band)
32	0 Volts
33	3914 A Photometer Temp.
34	3914 A Photometer High Voltage
35	5577 A Photometer Temp.
36	5577 A Photometer High Voltage
37	3466 A Photometer Temp.
38	3466 A Photometer High Voltage
39	0 Volts
40	ESA +28 Volts Delayed
41	ESA +28 Volts Standby
42	ESA Cover
43	0 Volts
44	ESA +15 Volt Monitor
45	ESA -15 Volt Monitor
46	ESA PM High Voltage
47	ESA Post Accelerator High Voltage
48	ESA Temperature
49	0 Volts
50	MS 0.1 Volt Collector Current
51	MS Mass Calibration
52	MS Emission Control
53	MS High Voltage Monitor
54	MS RF Sweep
55	MS Bias Monitor (Mode)

TABLE B-3 (Cont.)

Segment	Data
56	0 Volts
57	+5 Volts
58	+5 Volts
59	+5 Volts
60	0 Volts

Data Channels: 0.0 - +5.0 volts
Frame Sync Pulse: +5.0 volts
Switch Action: Make Before Break

TABLE B-4

ADDITIONAL TRACKING AND RECOVERY SYSTEMS
BLACK BRANT 18.219-1

System	Description
Beacon	Vega Model 312-S 300 Watts peak RF power Transfrequency 2890 MHz Rec frequency 2800 MHz Delay 2.5 sec Antenna NMSU 6.061
L-Band Transponder (Recovery)	Bendix ATC Model TR-641A 240 watts peak RF power Trans frequency 1090 MHz Rec frequency 1030 MHz Code 6700
X-Band Recovery Beacon	Motorola Model SST-181X-E 400 watts peak RF power Trans frequency 9375 MHz Code 2 Rec frequency 9310 MHz Single Pulse Code 1
Range Receiver (Tracking)	Vector Model RAH-1113 462 MHz tone ranging

TABLE B-5

MAGNETIC ASPECT SENSOR CALIBRATION DATA

Field in Milligauss	Output Signal in Volts DC
600	4.78
550	4.59
500	4.39
450	4.19
400	3.99
350	3.80
300	3.60
250	3.40
200	3.20
150	3.00
100	2.80
50	2.60
0	2.40 (bias level)
- 50	2.20
-100	2.00
-150	1.80
-200	1.60
-250	1.40
-300	1.20
-350	1.00
-400	0.80
-450	0.60
-500	0.40
-550	0.20
-600	0.00

Note: Direction of magnetic field for voltage signals above bias level (magnetometer mounted at 45° - see Figures 2 and 4)

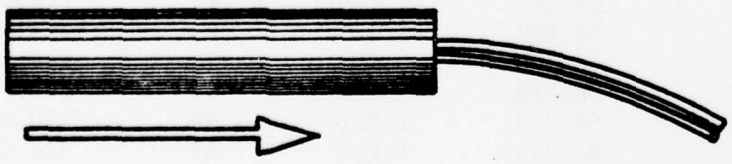


TABLE B-6

BLACK BRANT 18.219-1 TRAJECTORY LISTING

Time (Sec)	Altitude (km)	Velocity (km/sec)	Time (Sec)	Altitude (km)	Velocity (km/sec)
16	5.293	.699	59	70.710	1.553
17	6.013	.773	60	72.239	1.544
18	6.828	.843	61	73.759	1.535
19	7.679	.891	62	75.270	1.526
20	8.609	.970	63	78.263	1.508
21	9.594	1.032	65	79.746	1.499
22	10.658	1.107	66	81.219	1.489
23	11.787	1.182	67	82.682	1.479
24	12.997	1.262	68	84.134	1.469
25	14.290	1.351	69	85.576	1.459
26	15.671	1.438	70	87.009	1.450
27	17.140	1.531	71	88.433	1.441
28	18.704	1.625	72	89.848	1.431
29	20.356	1.708	73	91.254	1.422
30	22.085	1.780	74	92.650	1.412
31	23.873	1.822	75	94.031	1.397
32	25.681	1.823	76	95.403	1.392
33	27.483	1.812	77	96.770	1.385
34	29.270	1.801	78	98.127	1.376
35	31.045	1.789	79	99.475	1.366
36	32.808	1.779	80	100.143	1.362
37	34.562	1.769	81	102.143	1.347
38	36.306	1.757	82	103.463	1.338
39	38.040	1.747	83	104.774	1.328
40	39.765	1.741	84	106.075	1.319
41	41.485	1.739	85	107.367	1.310
42	43.201	1.731	86	108.648	1.299
43	44.905	1.717	87	109.917	1.287
44	46.595	1.704	88	111.173	1.275
45	48.276	1.694	89	112.415	1.263
46	49.946	1.682	90	113.647	1.254
47	51.603	1.669	91	114.870	1.246
48	53.247	1.658	92	116.088	1.239
49	54.880	1.648	93	117.300	1.233
50	56.503	1.639	94	118.506	1.226
51	58.118	1.630	95	119.705	1.218
52	59.725	1.621	96	120.893	1.208
53	61.323	1.611	97	122.071	1.199
54	62.912	1.602	98	123.239	1.189
55	64.493	1.593	99	124.398	1.179
56	66.063	1.583	100	125.547	1.170
57	67.622	1.573	101	126.686	1.160
58	69.171	1.563	102	127.817	1.152

TABLE B-6 (cont.)

Time (Sec)	Altitude (km)	Velocity (km/sec)	Time (Sec)	Altitude (km)	Velocity (km/sec)
103	128.939	1.143	148	169.704	.738
104	130.051	1.134	149	170.393	.729
105	131.153	1.125	150	171.078	.721
106	132.247	1.116	151	171.750	.713
107	133.331	1.107	152	172.413	.703
108	134.406	1.098	153	173.067	.695
109	135.473	1.089	154	173.712	.686
110	136.529	1.080	155	174.346	.676
111	137.576	1.070	156	174.972	.668
112	138.614	1.061	157	175.588	.659
113	139.642	1.052	158	176.194	.651
114	140.661	1.043	159	176.791	.644
115	141.669	1.034	160	177.379	.634
116	142.668	1.025	161	177.958	.624
117	143.658	1.016	162	178.529	.617
118	144.638	1.006	163	179.091	.608
119	145.609	.997	164	179.642	.599
120	146.570	.988	165	180.185	.592
121	147.522	.979	166	180.719	.583
122	148.465	.970	167	180.242	.575
123	149.398	.961	168	181.755	.568
124	150.323	.952	169	182.260	.560
125	151.238	.943	170	182.755	.551
126	152.143	.934	171	183.241	.543
127	153.039	.925	172	183.718	.535
128	153.925	.916	173	184.185	.528
129	154.803	.907	174	184.644	.520
130	155.671	.897	175	185.532	.502
131	156.530	.889	176	185.093	.511
132	157.379	.879	177	185.964	.494
133	158.219	.870	178	186.387	.486
134	159.050	.861	179	186.801	.476
135	159.871	.852	180	187.205	.467
136	160.683	.844	181	187.599	.462
137	161.485	.836	182	187.986	.456
138	162.278	.827	183	188.362	.488
139	163.062	.817	184	188.727	.439
140	163.838	.809	185	189.083	.432
141	164.603	.800	186	189.431	.426
142	165.359	.791	187	189.771	.419
143	166.106	.782	188	190.100	.410
144	166.843	.773	189	190.419	.403
145	167.572	.765	190	190.728	.395
146	168.292	.755	191	191.027	.388
147	169.002	.747	192	191.319	.380

TABLE B-6 (Cont.)

Time (Sec)	Altitude (km)	Velocity (km/sec)	Time (Sec)	Altitude (km)	Velocity (km/sec)
193	191.603	.374	238	194.814	.294
194	191.879	.367	239	194.664	.299
195	192.146	.359	240	194.503	.305
196	192.401	.351	241	194.334	.309
197	192.644	.345	242	194.158	.312
198	192.879	.342	243	193.975	.314
199	193.107	.340	244	193.786	.317
200	193.329	.335	245	193.591	.323
201	193.543	.326	246	193.390	.329
202	193.744	.314	247	193.182	.335
203	193.932	.302	248	192.967	.343
204	194.107	.296	249	192.740	.353
205	194.274	.296	250	192.500	.363
206	194.435	.296	251	192.244	.373
207	194.595	.294	252	191.974	.380
208	194.750	.291	253	191.691	.383
209	194.896	.286	254	191.402	.384
210	195.029	.279	255	191.109	.384
211	195.147	.273	256	190.814	.387
212	195.249	.268	257	190.515	.394
213	195.337	.263	258	190.207	.407
214	195.416	.259	259	189.885	.421
215	195.487	.258	260	189.547	.432
216	195.553	.255	261	189.195	.442
217	195.613	.253	262	188.833	.449
218	195.669	.252	263	188.465	.453
219	195.717	.253	264	188.093	.455
220	195.758	.254	265	187.715	.460
221	195.791	.254	266	187.328	.467
222	195.814	.256	267	186.928	.475
223	195.827	.258	268	186.518	.484
224	195.829	.258	269	186.099	.492
225	195.821	.258	270	185.673	.498
226	195.802	.258	271	185.239	.505
227	195.774	.258	272	184.796	.517
228	195.734	.257	273	184.340	.532
229	195.689	.257	274	183.872	.545
230	195.633	.259	275	183.393	.553
231	195.567	.262	276	182.906	.557
232	195.492	.264	277	182.412	.559
233	195.407	.268	278	181.913	.563
234	195.311	.272	279	181.404	.571
235	195.203	.277	280	180.886	.581
236	195.085	.283	281	180.357	.589
237	194.995	.289	282	179.820	.599

TABLE B-6 (cont.)

Time (Sec)	Altitude (km)	Velocity (km/sec)	Time (Sec)	Altitude (km)	Velocity (km/sec)
283	179.273	.612	328	144.921	1.013
284	178.712	.627	329	143.940	1.022
285	178.139	.639	330	142.950	1.030
286	177.557	.646	331	141.952	1.038
287	176.968	.651	332	140.944	1.048
288	176.371	.653	333	139.926	1.058
289	175.769	.655	334	138.899	1.067
290	175.160	.662	335	137.862	1.075
291	174.541	.673	336	136.818	1.081
292	173.912	.683	337	135.766	1.088
293	173.272	.693	338	134.706	1.096
294	172.623	.705	339	133.637	1.107
295	171.962	.719	340	132.555	1.119
296	171.289	.731	341	131.463	1.132
297	170.606	.739	342	130.359	1.143
298	169.914	.743	343	129.244	1.152
299	169.217	.746	344	128.122	1.160
300	168.514	.751	345	126.991	1.166
301	167.801	.760	346	125.852	1.174
302	167.080	.770	347	124.706	1.180
303	166.348	.779	348	123.552	1.189
304	165.607	.788	349	122.387	1.201
305	164.857	.795	350	121.211	1.214
306	164.099	.807	351	120.021	1.227
307	163.328	.821	352	118.820	1.237
308	162.544	.833	353	117.611	1.244
309	161.751	.843	354	116.394	1.250
310	160.948	.852	355	115.170	1.259
311	160.136	.857	356	113.936	1.268
312	159.318	.863	357	112.692	1.280
313	158.491	.870	358	111.436	1.292
314	157.656	.878	359	110.169	1.303
315	156.812	.888	360	108.891	1.312
316	155.957	.900	361	107.476	1.320
317	155.091	.912	362	106.311	1.327
318	154.213	.925	363	105.008	1.336
319	153.323	.936	364	103.696	1.345
320	152.424	.945	365	102.376	1.352
321	151.516	.952	366	101.046	1.361
322	150.600	.959	367	99.708	1.370
323	149.676	.966	368	98.361	1.380
324	148.744	.974	369	97.003	1.390
325	147.802	.983	370	95.635	1.400
326	146.852	.992	371	94.258	1.407
327	145.892	1.002	372	92.874	1.415

TABLE B-6 (cont.)

Time (Sec)	Altitude (km)	Velocity (km/sec)	Time (Sec)	Altitude (km)	Velocity (km/sec)
373	91.479	1.425	418	25.191	.913
374	90.076	1.435	419	23.912	.797
375	88.661	1.446	420	23.524	.759
376	87.236	1.455	421	22.805	.682
377	85.803	1.463	422	22.161	.607
378	84.362	1.470	423	21.591	.537
379	82.913	1.479	424	21.087	.475
380	81.454	1.489	425	20.640	.426
381	79.985	1.499	426	20.235	.389
382	78.506	1.508	427	19.862	.361
383	77.019	1.516	428	19.514	.339
384	75.523	1.526	429	19.187	.319
385	74.017	1.535	430	18.880	.299
386	72.501	1.544	431	18.592	.280
387	70.977	1.554	432	18.322	.264
388	69.441	1.564	433	18.067	.250
389	67.897	1.572	434	17.825	.238
390	66.364	1.578	435	17.593	.230
391	64.787	1.587	436	17.367	.225
392	63.219	1.596	437	17.174	.220
393	61.642	1.604	438	16.930	.217
394	60.059	1.606	439	16.716	.214
395	58.475	1.607	440	16.506	.210
396	56.889	1.609	441	16.299	.206
397	55.300	1.611	442	16.096	.202
398	53.710	1.611	443	15.896	.199
399	52.119	1.609	444	15.699	.198
400	50.531	1.606	445	15.503	.198
401	48.947	1.600	446	15.305	.200
402	47.366	1.599	447	15.106	.201
403	45.783	1.603	448	14.906	.202
404	44.196	1.603	449	14.706	.200
405	42.613	1.593	450	14.509	.197
406	41.043	1.580	451	14.315	.193
407	39.484	1.567	452	14.126	.189
408	37.938	1.552	453	13.940	.185
409	36.410	1.527	454	13.758	.182
410	34.911	1.489	455	13.580	.179
411	33.457	1.436	456	13.403	.176
412	32.058	1.373	457	13.228	.175
413	30.725	1.303	458	13.504	.175
414	29.463	1.228	459	12.880	.175
415	28.277	1.151	460	12.706	.174
416	27.169	1.072	461	12.535	.169
417	26.141	.992	462	12.370	.163

TABLE B-6 (cont.)

Time (Sec)	Altitude (km)	Velocity (km/sec)	Time (Sec)	Altitude (km)	Velocity (km/sec)
463	12.212	.156			
464	12.059	.152			
465	11.907	.154			
466	11.752	.160			
467	11.590	.167			
468	11.421	.171			
469	11.250	.171			
470	11.082	.168			
471	10.916	.165			
472	10.752	.165			
473	10.587	.168			
474	10.420	.168			
475	10.255	.163			
476	10.100	.151			
477	9.958	.136			
478	9.830	.125			
479	9.710	.120			
480	9.591	.124			
481	9.464	.134			
482	9.326	.143			
483	9.182	.147			
484	9.036	.146			
485	8.893	.142			
486	8.755	.139			
487	8.622	.135			
488	8.492	.130			
489	8.371	.120			
490	8.266	.105			
491	8.184	.088			
492	8.128	.074			
493	8.096	-			
494	8.080	-			
495	8.072	-			
496	8.064	-			
497	8.049	-			
498	8.022	-			
499	7.981	-			
500	7.928	-			

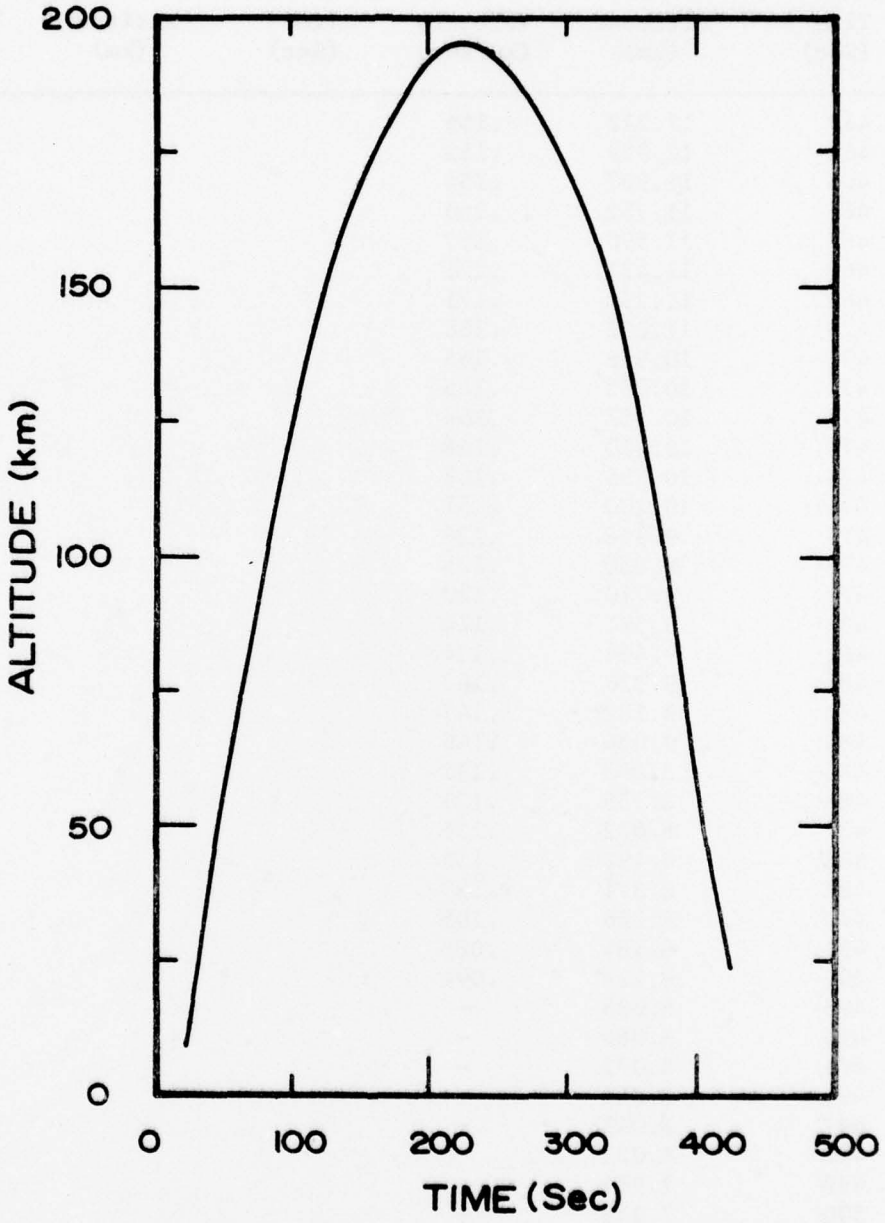


Figure B-1. Black Brant 18.219-1 trajectory.

APPENDIX C

DISTRIBUTION LIST

Preceding Page BLANK - NOT FILMED

DISTRIBUTION LIST

DEPARTMENT OF DEFENSE

Director
Defense Advanced Research Proj. Agency
Architect Building
1400 Wilson Blvd.
Arlington, VA 22209
(1) Attn LTC W.A. Whitaker
(1) Attn STO Capt. J. Justice

Defense Documentation Center
Cameron Station
Alexandria, VA 22314
(12) Attn TC

Director
Defense Nuclear Agency
Washington, D.C. 20305
(1) Attn DDST Warren W. Berning
(2) Attn STTL Tech Library
(1) Attn STSI Archives
(3) Attn RAAE Charles A. Blank
(1) Attn RAAE Harold C. Fitz, Jr.
(1) Attn RAAE Maj. John Clark

Director of Defense Research & Engineering
Department of Defense
Washington, D.C. 20301
(1) Attn AD/S&AS Daniel Brockway
(1) Attn DDS&SS Richard S. Ruffine

Commander
Field Command
Defense Nuclear Agency
Kirtland AFB, NM 87115
(1) Attn FCPR

Chief
Livermore Division FLD Command DNA
Lawrence Livermore Laboratory
P.O. Box 808
Livermore, CA 94550
(1) Attn FCPRL

Weapons Systems Evaluation Group
400 Army Navy Drive
Arlington, VA 22202
(1) Attn Document Control

DEPARTMENT OF ARMY

Commander
Harry Diamond Laboratories
2800 Powder Mill Road
Adelphi, MD 20783
(CNWDI-Inner Envelope: Attn: AMXDO-RBH)
(2) Attn AMXDO-NP

Director
U.S. Army Ballistic Research Labs
Aberdeen Proving Ground, MD 21005
(1) Attn AMXBR-CA Franklin E. Niles

Headquarters
U.S. Army Elct. Warfare Lab (ECOM)
Missile Electronic Warfare Tech Area
White Sands Missile Range, NM 88002
(1) Attn E. Butterfield

DEPARTMENT OF NAVY

Chief of Naval Research
Navy Department
Arlington, VA 22217
(1) Attn Code 427 CDR Ronald J. Oberle

Commander
Naval Electronics Laboratory Center
San Diego, CA 92152
(1) Attn Code 2200 1 Verne E. Hildebrand
(1) Attn Code 2200 Ilan Rothmuller

Director
Naval Research Laboratory
Washington, D.C. 20375
(1) Attn Code 7750 Paul Juluenne
(1) Attn Code 7750 Darrell F. Strodel
(1) Attn Code 2027 Tech Library
(1) Attn Code 7127 Charles Y. Johnson

(1) Attn Code 7701 Jack D. Brown
(1) Attn Code Douglas Strickland
(1) Attn Code 7750 Timoth P. Coffey
(1) Attn Douglas P. McNutt
(1) Attn Code 7750 Ellis Hyman

Commander
Naval Surface Weapons Center
White Oak, Silver Spring, MD 20910
(1) Attn Code 213 William L. Derksen
(1) Attn Code 1224 Navy Nuclear Programs Office

DEPARTMENT OF THE AIR FORCE

Commander
Aeronautical Systmes Division, AFSC
Wright-Patterson AFB, OH 45433
(1) Attn ASD-YH-EX LTC Robert Leverette

AF Cambridge Research Labs, AFSC
L.G. Hanscom Field
Bedford, MA 01730
(5) Attn OPR James C. Ulwick
(1) Attn LKB Kenneth S.W. Champion
(1) Attn OP John S. Garing
(1) Attn OPR Alva T. Stair

AF Weapons Laboratory, AFSC
Kirtland AFB, NM 87117
(1) Attn DYT Capt. David W. Goetz
(1) Attn SUL
(1) Attn DYT Maj. Don Mitchell

U.S. ENERGY RESEARCH AND DEV. ADMIN.

Los Alamos Scientific Laboratory
P.O. Box 1663
Los Alamos, NM 87545
(1) Attn Doc Con for Milton Peek

OTHER GOVERNMENT

Department of Commerce
Office of Telecommunications
Institute for Telecom Science
Boulder, CO 80302
(1) Attn Glenn Falcon
(1) Attn William F. Utlaut

NASA
600 Independence Avenue SW
Washington, D.C. 20546
(1) Attn M. Dubin
(1) Attn J. Holz

DEPARTMENT OF DEFENSE CONTRACTORS

Aerodyne Research Inc.
Tech/OPS Building
20 South Avenue
Burlington, MA 01803
(1) Attn F. Bien
(1) Attn M. Camac

Aerospace Corporation
P.O. Box 92957
Los Angeles, CA 90009
(1) Attn R.D. Rawcliffe
(1) Attn Harris Mayer
(1) Attn T. Taylor
(1) Attn R. Grove

General Electric Company
Tempo-Center for Advanced Studies
816 State Street (P.O. Drawer QQ)
Santa Barbara, CA 93102
(1) Attn Warren S. Knapp
(5) Attn Dasiac Art Feryok

General Research Corporation
P.O. Box 3587
Santa Barbara, CA 93105
(1) Attn John Ise, Jr.

Geophysical Institute
University of Alaska
Fairbanks, AK 99701
(All Class Attn: Security Officer)
(3) Attn Neil Brown (Uncl only)
(1) Attn T.N. Davis (Uncl only)

Honeywell incorporated
Radiation Center
2 Forbes Road
Lexington, MA 02173
(1) Attn W. Williamson

Institute for Defense Analyses
400 Army-Navy Drive
Arlington, VA 22202
(1) Attn Ernest Bauer
(1) Attn Hans Wolfhard

Lockheed Missiles and Space Company
3251 Hanover Street
Palo Alto, CA 94304
(1) Attn John Kumer
(1) Attn J.B. Reagan D/52-12
(1) Attn Billy M. McCormac Dept. 52-14
(1) Attn Martin Walt Dept. 52-10
(1) Attn Richard G. Johnson Dept. 52-12
(1) Attn Robert D. Sears Dept. 52-14

Mission Reasearch Corporation
735 State Street
Santa Barbara, CA 93101
(1) Attn P. Fischer
(1) Attn D. Archer

Photometrics, Inc.
442 Marrett Road
Lexington, MA 02173
(1) Attn Irving L. Kofsky

Physical Dynamics Inc.
P.O. Box 1069
Berkeley, CA 94701
(1) Attn Joseph B. Workman

Physical Sciences, Inc.
607 North Avenue, Door 18
Wakefield, MA 01880
(1) Attn Kurt Wray

R & D Associates
P.O. Box 9695
Marina Del Rey, CA 90291
(1) Attn Robert E. Lelevier
(1) Attn Forest Gilmore

R & D Associates
1815 N. Ft. Myer Drive
11th Floor
Arlington, VA 22209
(1) Attn Herbert J. Mitchell

Rand Corporation, The
1700 Main Street
Santa Monica, CA 90406
(1) Attn James Oakley

Science Applications, Inc.
P.O. Box 2351
La Jolla, CA 92038
(1) Attn Daniel A. Hamlin

Space Data Corporation
1331 South 26th Street
Phoenix, AZ 85034
(1) Attn Edward F. Allen

Stanford Research Institute
333 Ravenswood Avenue
Menlo Park, CA 94025
(1) Attn Walter G. Chestnut
(1) Attn M. Baron
(1) Attn Ray L. Leadabrand

Technology International Corporation
75 Wiggins Avenue
Bedford, MA 01730
(1) Attn W.P. Boquist

Utah State University
Logan, Ut. 84321
(1) Attn Doran Baker
(1) Attn Kay Baker
(1) Attn D. Burt
(1) Attn C. Wyatt

Visidyne, Inc.
19 Third Avenue
North West Industrial Park
Burlington, MA 01803
(1) Attn Oxcar Manley
(1) Attn J.W. Carpenter
(1) Attn William Reidy
(1) Attn T.C. Degges